OFF-AXIS ILLUMINATION FOR EXTENDING OPTICAL MICROLITHOGRAPHIC SYSTEM PERFORMANCE

Steve Brainerd
B.S., Rochester Institute of Technology, 1974

A thesis submitted to the faculty
of the Oregon Graduate Institute
of Science & Technology
in partial fulfillment of the
requirements for the degree
Master of Science
in Electrical Engineering

July, 1993

APPROVALS

This thesis "Off-Axis Illumination for Extending Optical Microlithographic System Performance" by Steve Brainerd has been examined and approved by the following Examination Committee:

Raj Solanki
Associate Professor
Thesis Advisor

Anthony E. Bell
Associate Professor

Delmer L. Fehrs
Principal Engineer
Tektronix Integrated Circuits Operation

ACKNOWLEDGMENTS

I would like to thank Micron Semiconductor in Boise Idaho for allowing me to do this work, ASM Lithography in Einhoven Holland for providing insight into the theory of off-axis illumination, and Linard Karklin of Silvaco for assisting in the SOLID simulations of the experimental results. The author would like to acknowledge the fact that the reticle used for the subresolution defocus proximity corrector evaluation was supported in part by DARPA-MTO contract MDA972-92-C-0054.

TABLE of CONTENTS

LIST OF FIGURES

LIST OF TABLES

ABSTRACT

OFF-AXIS ILLUMINATION FOR EXTENDING OPTICAL MICROLITHOGRAPHIC SYSTEM PERFORMANCE

Steve Brainerd

Supervising professor : Raj Solanki

Improvements in depth of focus and resolution for microlithographic projection printing systems can be achieved by illuminating the object (mask) with oblique or off axis rays. Three types of illumination as used on a waferstepper with a 0.48 numerical aperture objective lens were characterized for their effect on resolution, depth of focus, and proximity. The illumination types evaluated were partially coherent (sigma =0.64), off-axis quadrupole (inner sigma 0.26, outer sigma 0.70 and opening sigma = 0.26), and off-axis ring annular (inner sigma = 0.40 and outer sigma =0.70). All projected images were recorded in a modern high contrast positive photoresist. While this type of illumination offers significant performance gains, it is not without limitations. Two shortcomings are the loss of image irradiance and defocus proximity effects. This project will evaluate original methods to improve the later.

The results show that off-axis annular and quadrupole illumination improve the depth of focus for dense 0.36 to 0.50 micron linewidths as compared to partially coherent illumination by 45% and 56% respectively. The "defocus proximity effects" with off-axis illumination mentioned above is where the depth of focus for an exterior line on a dense line-space group is significantly less than an interior line. Three potential solutions evaluated for improving this exterior linewidth proximity defocus effect were: 1. The use of special sub-resolution compensating structures on the mask (object) features, 2. Contrast enhancement photoresist processing, and 3. Anti-reflective substrate coatings. The use of a modified reticle improved the depth of focus for an exterior line, while contrast enhancement and anti-reflective coatings did not offer any improvement. The experimental results were modeled using Silvacos SOLID 3.1 optical lithography simulator (Simulation of Optical LIthography in three Dimensions). Excellent correlation between the SOLID simulation model calibrated to the specific photoresist process used here and the experimental results was achieved.

I. INTRODUCTION

A. Previous work

The latest "hot" topic among semiconductor manufacturers is the use of off-axis illumination systems [2,4-7] to improve the resolution and depth of focus of fine microlithographic patterns in the half to sub half micron region. Since 1989 [8-24] there has been much published on the use of this technique for improving microlithographic performance. Each major waferstepper manufacturer and a few semiconductor companies have their own version of off-axis illumination. Nikon has SHRINC (Super High Resolution by Illumi-Nation Control) [19], Canon has CQUEST (Canon QUadrupole Effect for Stepper Technology) [16], Mitsubishi has PHOENEX (PHOtolithography ENhanced by modified EXposure) [23], and Samung has ATOM (Advanced Tilted illumination On Mask) [26] . Most authors publicize the depth of focus and resolution gains with off-axis illumination, but do not mention any adverse effects. Fehrs etal. in 1989 [11] discussed anomalous results, which were the premature over exposure of isolated features. They believed that this affect was caused by the reflection of un-diffracted light, which is traveling in the resist at 10° angles to the substrate instead of normal as with partially coherent illumination. There is a transition region from high resolution to low resolution (no pattern clear region). Off-axis illumination is designed to improve the high frequency features and hence the low frequencies are degraded. This effect is shown in the MTF curve in figure 1 [11]. The high frequency modulation improvement is due to the off-axis illumination allowing larger diffraction angles to be captured by the objective lens. The low frequency modulation degradation is due to optical path length differences between the zero and the ±1 orders required for image formation. Scattered or stray actinic radiation from these low resolution areas reduces the image contrast in the adjacent high resolution area, which significantly degrades the image quality. This image degradation for high resolution features adjacent to a large low resolution area in the defocus mode is shown for the exterior 0.5 micron lines of the dense line-space structure in figure 2. Figure 3 illustrates the different types of defocus proximity effects encountered with off-axis illumination systems. Workers at NEC [18] mentioned this edge linewidth defocus proximity effect with off-axis illumination and showed SEMs of it, but offered no solutions to the problem.

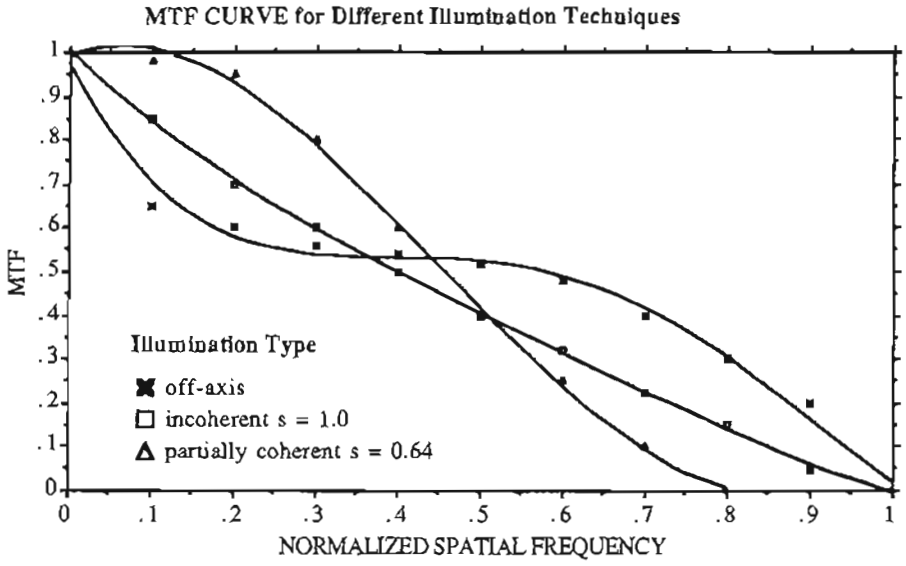

figure 1 MTF curves for various illumination techniques

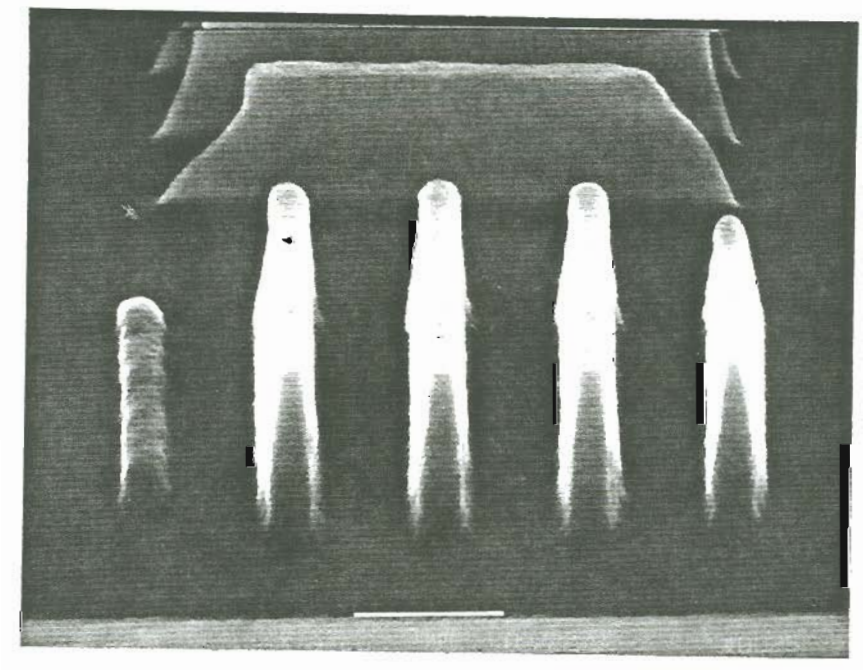

figure 2 SEM micrograph of 0.5 micron line space pairs at -1.5 micron defocus with annular illumination showing the exterior linewidth proximity effect.

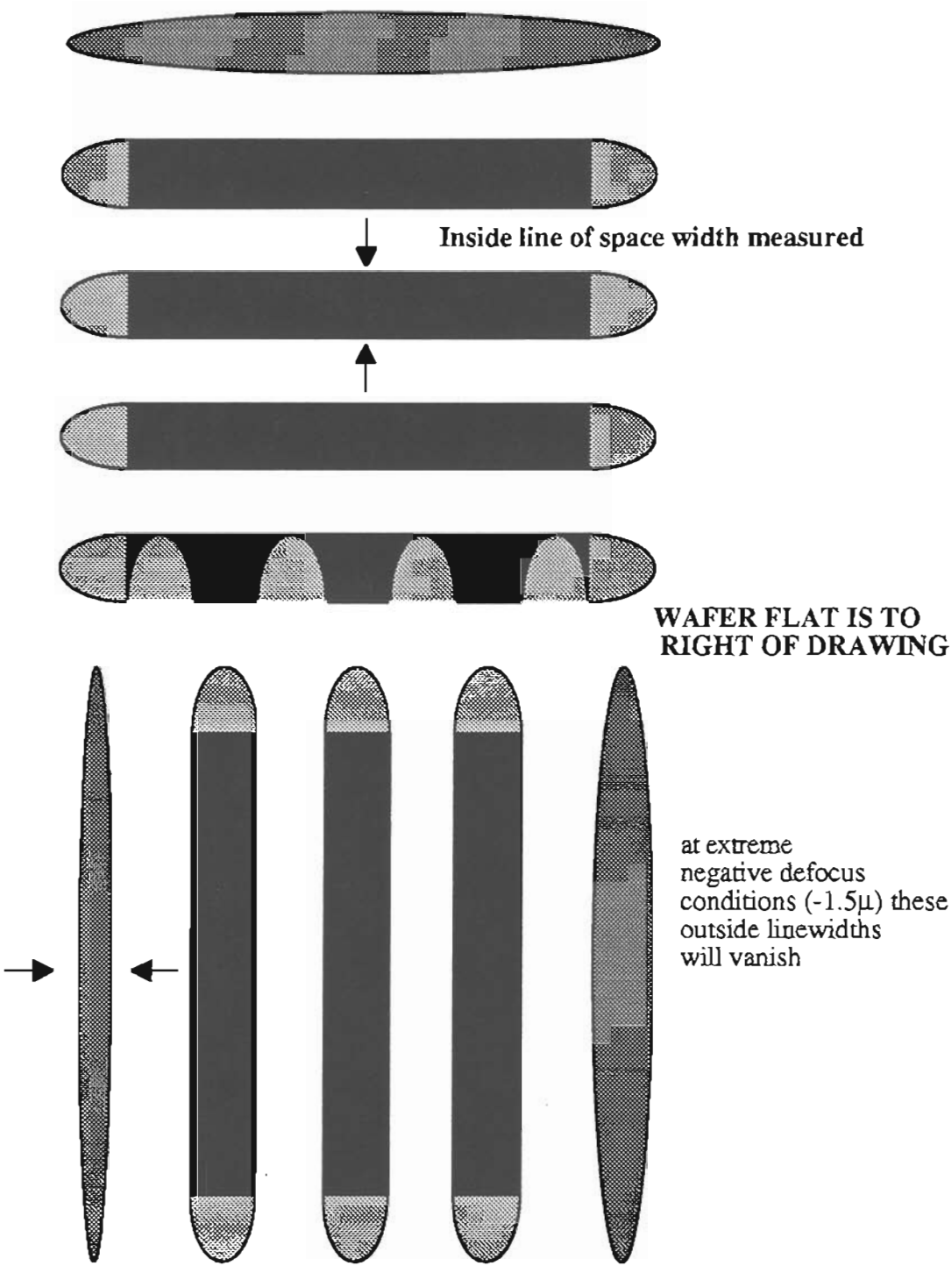

figure 3 Off-axis illumination defocus proximity effects on line and space pairs.

The effect of these defocus proximity effects on the interior and exterior linewidth depth of focus deviation is illustrated in figures 4 and 5 for dense 0.50 micron line-space pairs. With off-axis illumination the exterior line CD size decreases very rapidly with defocus, while the interior linewidths CDs remain constant. This exterior linewidth CD defocus trend is similar to an isolated features CD-defocus relationship. With partially coherent illumination the depth of focus for the interior and exterior linewidths are basically equivalent. It was observed that the magnitude of this exterior linewidth degradation with defocus was related to the proximity and size of adjacent structures. Structures in close proximity to these exterior linewidths caused the CDs to be less affected by defocus than structures further away.

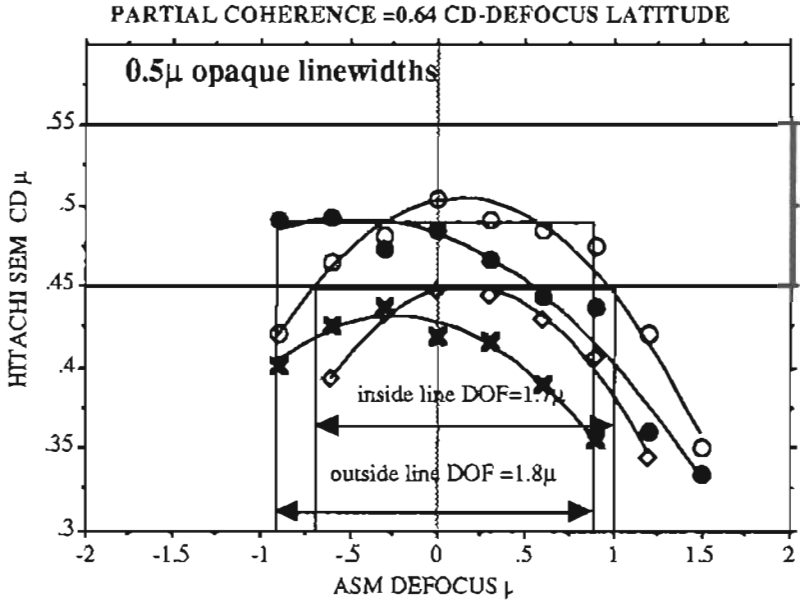

figure 4 Exposure-defocus latitude for partially coherent illumination

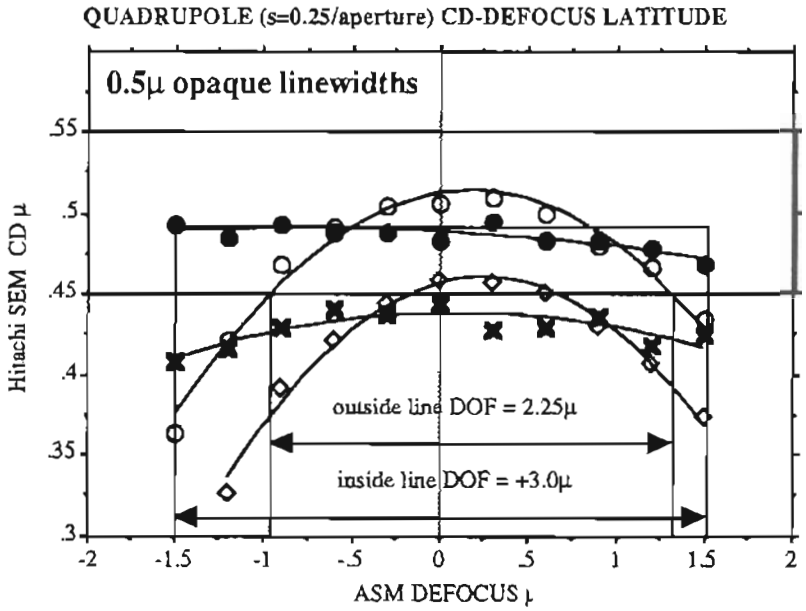

figure 5 Exposure-defocus latitude for quadrupole illumination.

B. Types of illumination

The two types of illumination we are most concerned with in microlithography are partially coherent [27-29] and off-axis. These illuminate the entrance pupil in different ways altering the Fraunhofer diffraction pattern in the Fourier transfer plane. This "filtering" or modification of the transform pattern has a very significant effect on the resulting image.

Partially coherent illumination is concerned with spatial rather than temporal coherence and is achieved by under filling the entrance pupil in a Koehler type illumination system. Koelher illumination is where the exposure source is projected through the condenser lens and focused in the entrance pupil plane of the objective lens. This under filling of the entrance pupil is achieved by reducing the source diameter typically with aperture stops. This partially coherent illumination filters or blocks the diffracted light orders from the objects high frequency features, which increase the image contrast on the low and medium frequency features. This contrast improvement is

achieved because the scattered low modulation diffracted light from the high frequency features is absent. Figure 1 shows this contrast enhancement for the low to medium frequency features and figure 6 shows a projection optical system with partially coherent illumination.

Off-axis or dark field illumination is where the illumination rays strike the object at an oblique angle. This is accomplished by blocking the normally incident zero order beam. For features smaller than the diffraction limited frequency as defined by the maximum diffraction angle accepted by the objective lens, only zero order or un-modulated light is transmitted through the lens. This unmodulated energy just adds to the modulated energy in the aerial image, reducing the image contrast. Off-axis illumination effectively blocks this light by shifting the zero order light to be in the position of the maximum ±1 order diffracted beam accepted by the lens. This allows a larger ±1 order diffraction angle beam to be accepted by the lens. Image formation now occurs by the interference of two beams being the zero order and either the +1 or -1 diffracted beam. This effectively increases the resolution. The depth of focus is also significantly increased with this two beam image formation because there is less or theoretically no phase (optical path length) difference between the interfering image formation beams in the defocus mode.

C. Theory

Figure 6 shows a projection system with normal partially coherent or 3 beam illumination. In the projection system described here we are concerned with the phase or spatial purity and not its bandwidth or temporal qualities of the radiation. The temporal coherence is achieved by using monochromatic illumination. Partially coherent illumination is achieved by using a Koelher type setup, where the exposure source is imaged through the condenser lens in the entrance pupil of the projection lens. The degree of coherence is given by: sigma s = source image diameter/(entrance pupil diameter). Incoherent illumination sigma = 1.0 and coherent sigma = 0.0. Radiation of a given wavelength incident on the reticle or object plane will be diffracted. This diffraction pattern will enter the entrance pupil, where it will be filtered by the partially coherent illumination. The source image in the entrance pupil is the effective source size for image reconstruction. If the source is a point, then the illumination is said to be spatially coherent. The entrance pupil is the Fourier transform plane of the object, which means that this plane contains all the information about the diffracted object required to reconstruct it in the image plane. The image is built up by the interference of filtered diffraction patterns.

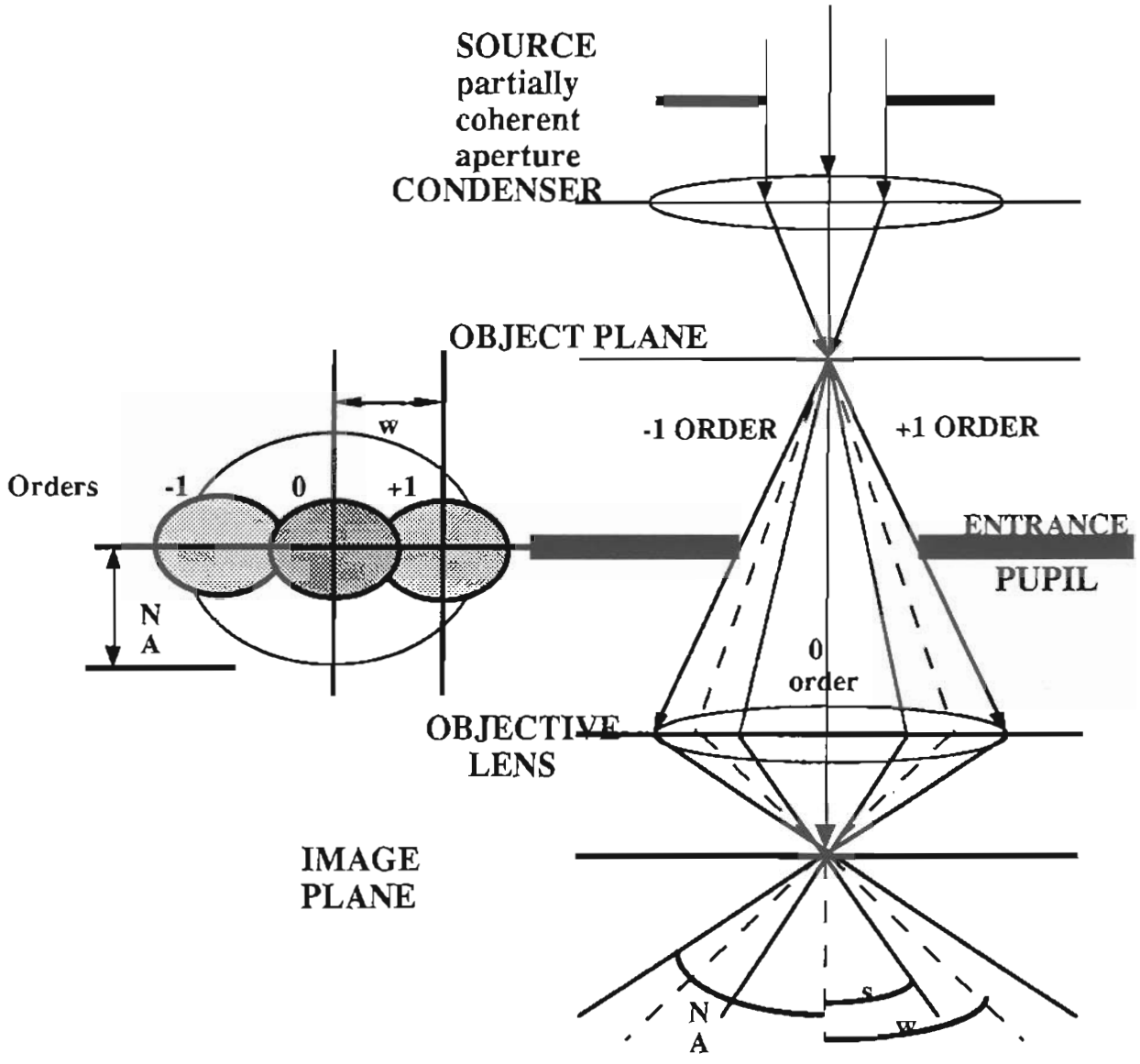

figure 6 Conventional or 3 beam partially coherent illumination

All diffracted points in the entrance pupil resulting from object slit openings of width "a" spaced on 2a separations forming a grating pattern will have a phase correlation based on the diffraction equation:

$$m\lambda = a\sin(w)$$

λ is the actinic illumination wavelength ; w is the diffraction angle (1)

(where m is the diffraction order 1,3,5 etc..). As the slit opening is made smaller the diffraction angle w increases until these diffracted orders are no longer captured by the entrance pupil and objective lens due to their physical diameters. The exact reconstruction for a given frequency is defined when the MTF or contrast is 1.0 or 100% modulation as shown in figure 1. The modulation or contrast of the image is determined by the cross section of the first diffracted order with the entrance pupil. Optimal contrast is achieved when the first order diffracted beams fall completely inside the entrance pupil diameter. The image modulation goes to zero if the first order falls just outside the entrance pupil. This limiting feature size is defined as the cutoff frequency or diffraction limited resolution. The objective lens diameter is defined by the numerical aperture NA , which is given as:

$$NA = n\sin(w) = \frac{D}{2f} = \frac{\lambda}{2RES}$$

D= objective lens diameter; f =objective lens focal length

RES = limiting resolution for coherent illumination

w = maximum diifraction angle accepted by projection lens resulting from the RES feature (2)

For the periodic grating structure evaluated here with a coherent illumination resolution RES the diffraction angle is given by the equation:

$$\sin(w) = \frac{m\lambda}{2RES}$$

RES = limiting resolution for coherent illumination

w = diifraction angle resulting from the RES feature (3)

The spatially coherent illumination resolution limit can be represented by letting w equal the maximum diffraction angle accepted by projection lens with numerical aperture NA and combining equations 2 and 3 as given in the well known equation 4 below.

$$RES_{sc\ cutoff} = \text{spatially coherent resolution} = \frac{0.5\lambda}{NA} = \frac{\lambda}{2\sin(w)} \qquad (4)$$

For spatially coherent illumination, these diffraction patterns will image as separate points in the entrance pupil. The image of this grating pattern is reconstructed by the interference between the zero order and all fully transmitted diffraction orders. This is typically described as image formation by 3 beam (0, -1, and +1 diffracted orders) interference. For spatially coherent illumination the image is an exact reconstruction of the object up to the limiting coherent cut-off frequency (when MTF = 0) given by:

$$\upsilon_c = \frac{NA}{\lambda}$$

λ is the actinic illumination wavelength ; NA is the objective lens numerical aperture (5)

The illumination is described as spatially incoherent when the effective source is infinite in extent, but more practically when the source image size is the exact size of the entrance pupil. For spatially incoherent illumination the limiting cut-off frequency given by:

$$\upsilon_c = \frac{NA}{2\lambda}$$

λ is the actinic wavelength; NA is the ojective lens numerical aperture (6)

If this projected source image diameter is increased, but made smaller than the entrance pupil diameter, then the illumination is said to be partially coherent. With incoherent illumination features smaller than the coherent cut-off frequency will only transmit low modulation light through the lens. This low modulated energy from the high frequency features diffracted light just acts as scattered light, which reduces the image contrast for larger features. Thus by filtering or blocking this low modulation light from these high frequency features diffracted orders with more coherent illumination, the image contrast and modulation is increased for features below the partially coherent cutoff frequency as shown in figure 1. For partially coherent illumination the limiting cutoff resolution [24] depends on the degree of coherence and is given by:

$$RES_{pc\ cutoff} = \text{partially coherent resolution} = \frac{0.5\lambda}{NA(1+s)}$$

where s is the degree of partial coherence (7)

When the illumination is made more coherent the absolute resolution of the optic system is decreased, but the contrast or modulation of the medium frequencies are increased. This contrast increase can result in a slight effective resolution increase for certain feature frequencies and shapes. It has been shown that square clear apertures or contacts depth of focus can be increased by increasing the coherence of the illumination [31].

Depth of focus is given by the expression:

$$DOF = \frac{k2\lambda}{NA^2}$$

where k1 and k2 are factors dependent on the photoresist process

λ is the actinic illumination wavelength; NA is the objective lens numerial aperture (8)

with CD, image quality, and sidewall angle requirements defining the practical tolerances. These image structure parameters are degraded in the defocus mode by a loss in image contrast caused by the optical path length differences between the 0 and ±1st order diffracted rays. Since image formation with partially coherent illumination occurs from the interference of the 3 diffract order beams, there is always a contrast loss in the de-focus mode. This contrast loss is due to the phase difference between the two first order beams with respect to the 0 order.

For features smaller than the cut-off frequency only zero order or un-modulated light is transmitted through the lens. This is due to the large diffraction angles for ±1 orders falling outside the entrance pupil for these small features. This un-modulated energy just adds to the modulated energy in the aerial image, reducing the image contrast. The image contrast and modulation for medium frequency features is increased by blocking this high frequency un-modulated 0 order light with annular or oblique illumination. These medium frequency features are between the incoherent

and coherent cutoff frequencies as shown in figure 1. This increased modulation significantly increases the resolution of the system. The illumination effectively moves the 0 order light causing it to be incident on the object at an oblique angle. The diffracted first orders are also shifted by this off-axis oblique illumination angle, which allows the lens to capture this 0 order and one 1st order as shown in figure 7a. Image formation will occur from the interference of the 0 diffracted order and one first order. This type of image formation is called 2 beam interference. Off-axis illumination allows the objective lens to capture larger diffraction angle beams than partially coherent illumination, resulting in a higher resolution capabilities for the projection system.

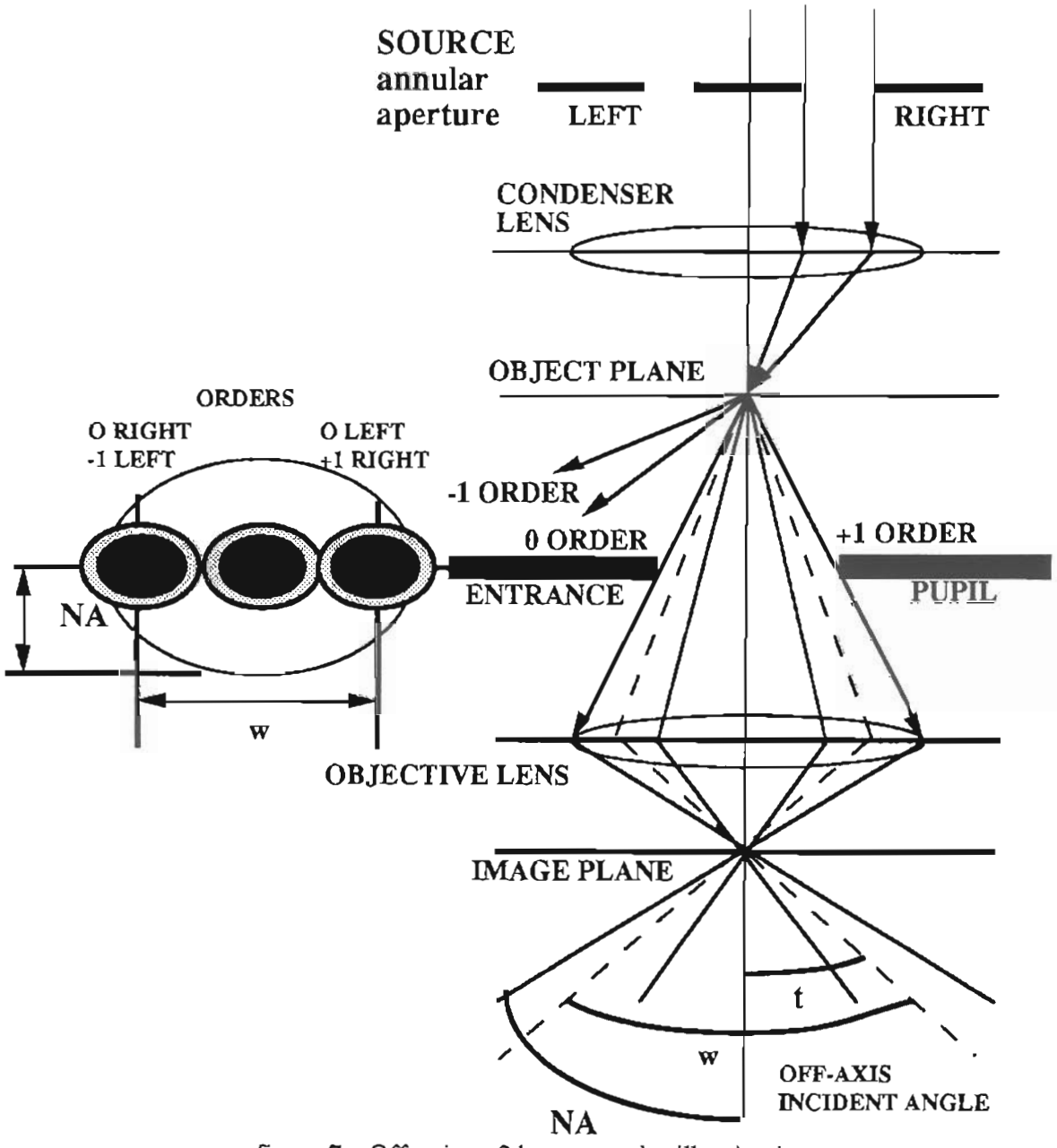

figure 7a Off-axis or 2 beam annular illumination

The off axis illumination limiting resolution is given by equation 9 below:

$$\text{Off–axis RES}_{\text{cutoff}} = \frac{0.5\lambda}{NA(1+s)+\theta}$$

θ = off–axis illumination incident angle on reticle (9)

When the source is at the edge of the entrance pupil [Theta = NA(1+s)] the off-axis illumination resolution limit can be represented as:

$$\text{Off–axis resolution} = \frac{0.25\lambda}{NA} = \frac{\lambda}{4\sin(w)} \quad (10)$$

The theoretical resolution limit for an off-axis illumination system is twice that of a coherent system as given by equation 10 and because the captured diffraction angle is doubled as shown in figure 7b. Comparing typical partially coherent systems (s = 0.70 and 0.40) with off-axis illumination, the theoretical resolution is increased 20 to 40%. The resolution improvement factor of off-axis illumination over partially coherent illumination can be given as:

$$\text{Resolution improvement factor for off–axis illumination } X = \frac{2}{(1+s)}$$

X =number of times resolution with off–axis illumination is improved over partially coherent

s = sigma = degree of partial coherence (11)

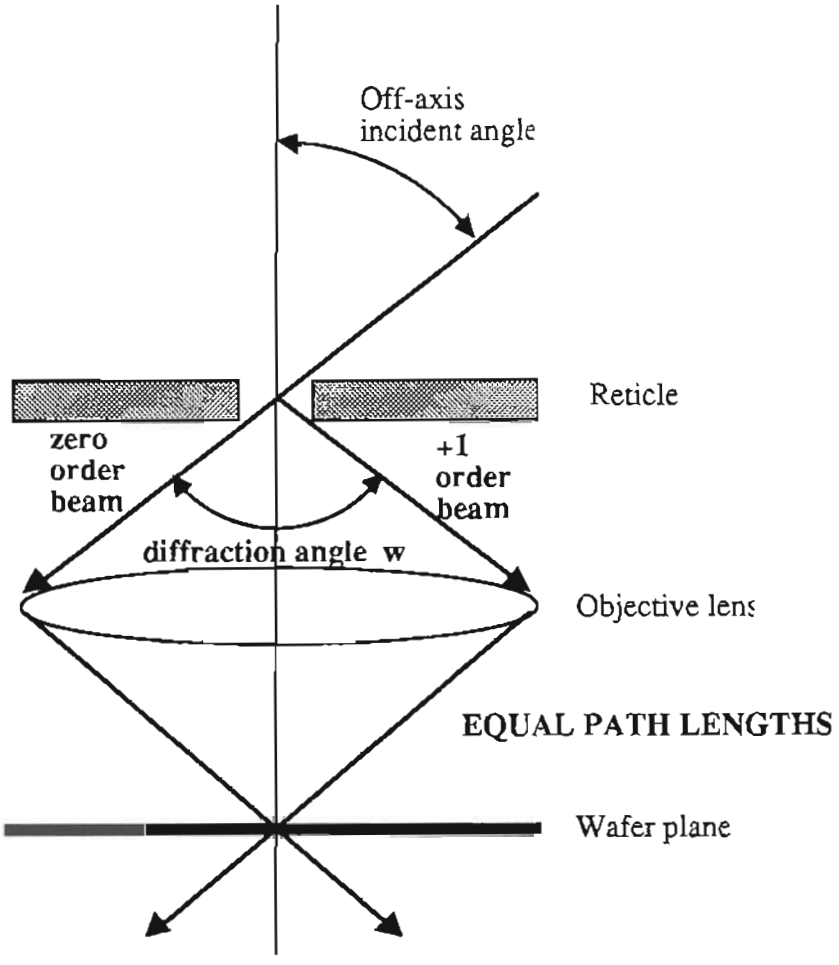

figure 7b off-axis illumination theoretical 2X coherent resolution improvement beam paths

For feature sizes below the coherent cut-off frequency the contrast or image modulation is reduced, because the optical path lengths for the zero order and the 1st order are not equal even at best focus as shown in figure 7c.

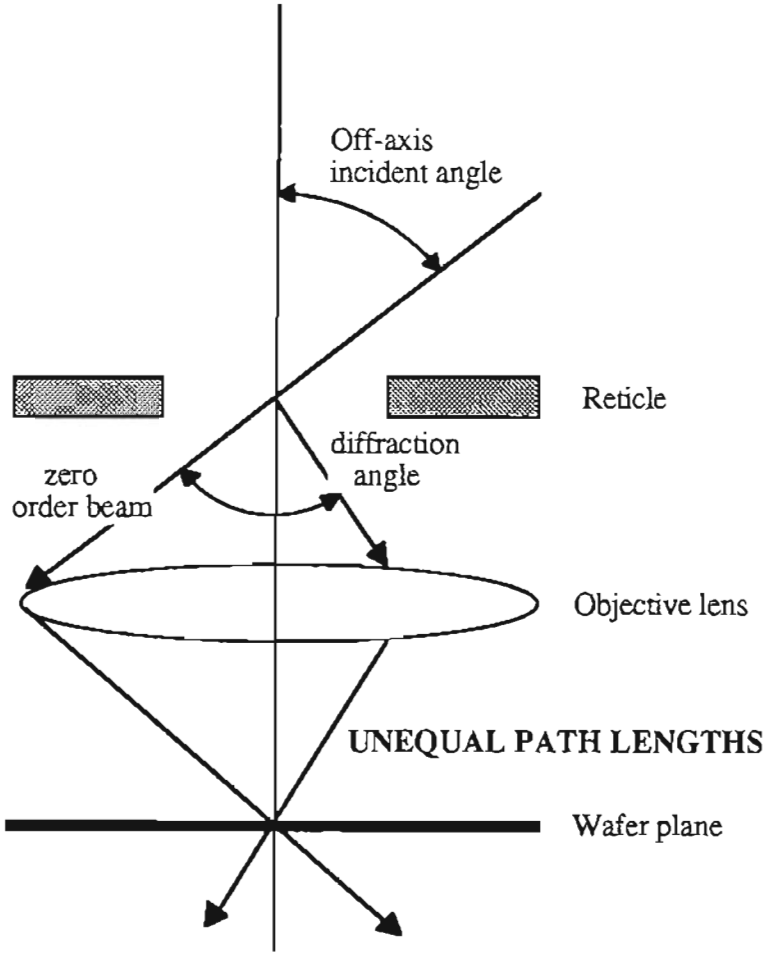

figure 7c Annular illumination reduced contrast for large feature sizes due to unequal path lengths

This means that the off-axis illumination oblique angle incident on the reticle will determine the optimal resolution for the system. Optimal resolution here refers to that minimum equal line and space pair that has the highest contrast and greatest depth of focus, resulting from equivalent path lengths for the 0 and ±1 diffracted orders in the 2 beam interference image formation case. The relationship between illumination incident angle theta and optimal resolution is given as:

$$\text{Off–axis resolution} = \frac{\lambda}{2(NA + \sin\theta)}$$

θ is the off–axis illumination incident angle on the reticle (object plane)

(12)

Thus the illumination obstruction apertures can be tuned to a particular frequency or minimum critical dimension. The optimum incident illumination angle for a given feature size "a" as shown in figure 7b is given as:

$$\text{Optimum off–axis illumination incident angle } \theta = \arcsin\left(\frac{\lambda}{a}\right) = \frac{w}{2}$$

θ is the off–axis illumination beam incident angle on the reticle (object plane)

a is the feature size and w is the resulting diffraction angle (13)

This means for a given feature size the optimum off-axis illumination incident angle is equal to one half the features diffraction angle. The design of the actual illumination obstruction aperture opening locations is typically given in entrance pupil coordinates or relative sizes. The optimal off-axis illumination opening location using figure 7a conventions is given by:

$$\text{Fraction of Entrance Pupil diameter for Off–axis aperture opening} = \left(\frac{\sin(w/2)}{NA}\right)$$

NA is the projection lens numerical aperture
a is the feature size and w is the resulting diffraction angle (14)

The theoretical partially coherent illumination resolution limit with the system employed here (NA = 0.48, sigma = 0.64, and an illumination wavelength of 0.365 microns) was 0.23 microns, while off-axis was 0.19 microns. The actual practical partially coherent illumination resolution limit was 0.35 microns, while the annular off-axis was 0.30 microns. This is a 14% resolution improvement.

Another important feature of off-axis illumination is that the depth of focus is improved due to less phase different between the two beam image formation in the de-focus mode. When the image focal plane is shifted in the z axis, the optical path lengths for the two interfering beams involved in

image formation are effectively equivalent. This means that the image contrast is not de-graded in the de-focus mode and thus the depth of focus for off-axis illumination is significantly greater than partially coherent illumination. This depth of focus improvement using off-axis illumination is its greatest benefit.

A better way to explain this depth of focus improvement with off-axis illumination is taken from W.N. Partlo etal with GCA [25]. Refer to figure 7d for an illustration of this argument. After diffracting through the reticle, the -1 order of the left illumination beam travels the same path as the zero order of the right illumination beam (this occurs for the +1 order of the right beam and the zero order of the left beam). Even though there are four beams interfering at the image plane, both pairs behave exactly the same. The effect is that of a single pair of beams. Any two beams interfering to form a sinusoidal intensity pattern have infinite depth of focus [32]. Since the incident angle of each beam is symmetric about the optical axis, the position of the maximum and minimum in the intensity pattern does not shift as the z-position (defocus) is changed.

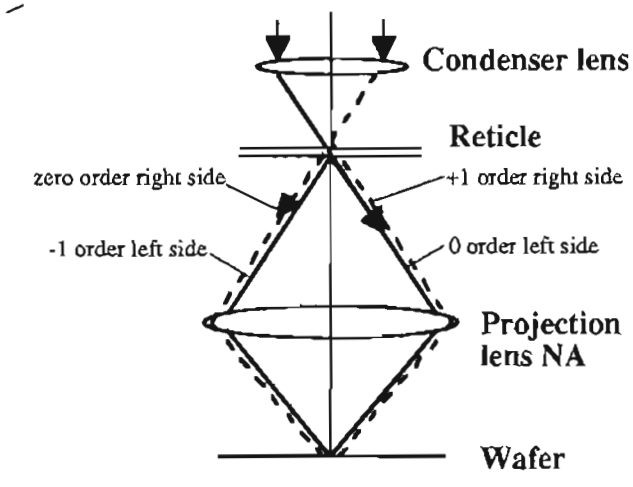

figure 7d Depth of focus gain with 2 beam off-axis illumination diffracted beam paths .

II. PHYSICAL MODEL

A. Aperture design and waferstepper setup

The illumination was modified by filtering the source illumination with special aperture blades. The particular apertures used are illustrated in figures 8 - 10. The blades were fabricated out of spring steel. The aperture patterns were generated by a computerized electric wire cutting technique. These apertures were inserted in the integrator block as shown in figure 11. The zoom lens was adjusted to achieve maximum image plane irradiance and irradiance uniformity across the illumination field. The partially coherent aperture (figure 8) had a fill factor of s = 0.64, which is the standard for this projection optical system.

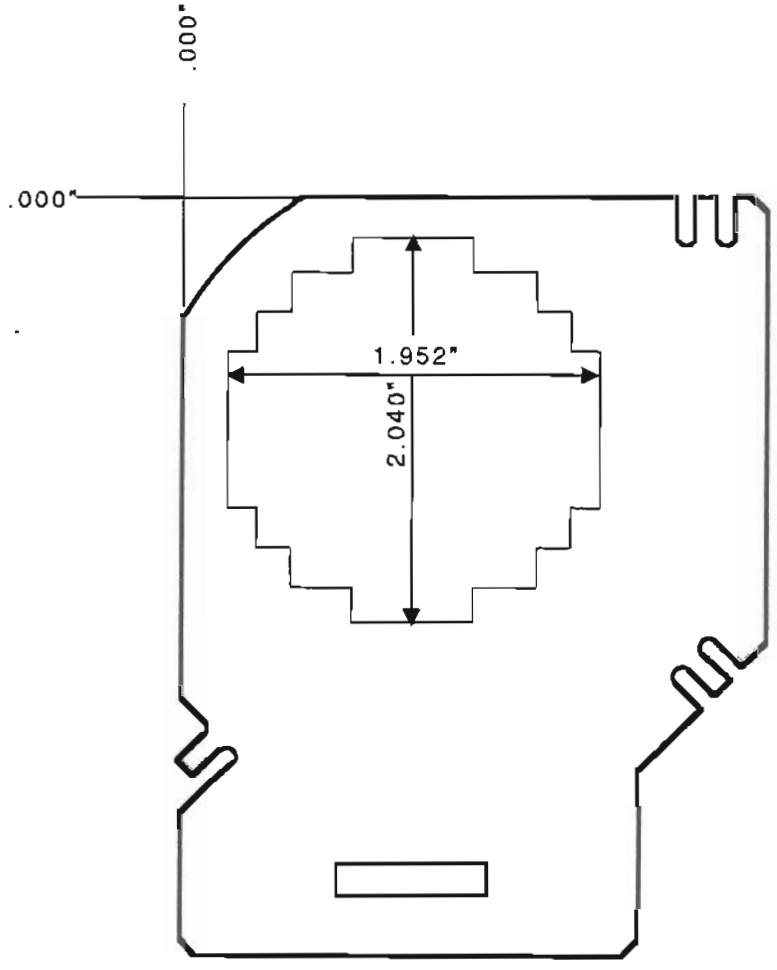

figure 8 Partially coherent illumination aperture (sigma =0.64)

The resolution improvement one could achieve with off-axis illumination as tested on the projection system here was restricted by the physical illuminator design. The maximum off-axis illumination incident angle was limited by the physical diameter of the integrator lens, which had a 0.70 partial coherence sigma value. The first off-axis illumination type evaluated was an annular design. The inner diameter for this annular aperture had a 0.40 partial coherence sigma value with a 11.80º incident angle. The outer diameter had a 0.70 partial coherence sigma value with a 20.5º incident angle. This inner-outer aperture diameter requirement and the photoresist process contrast reduces the theoretical off-axis resolution limit.

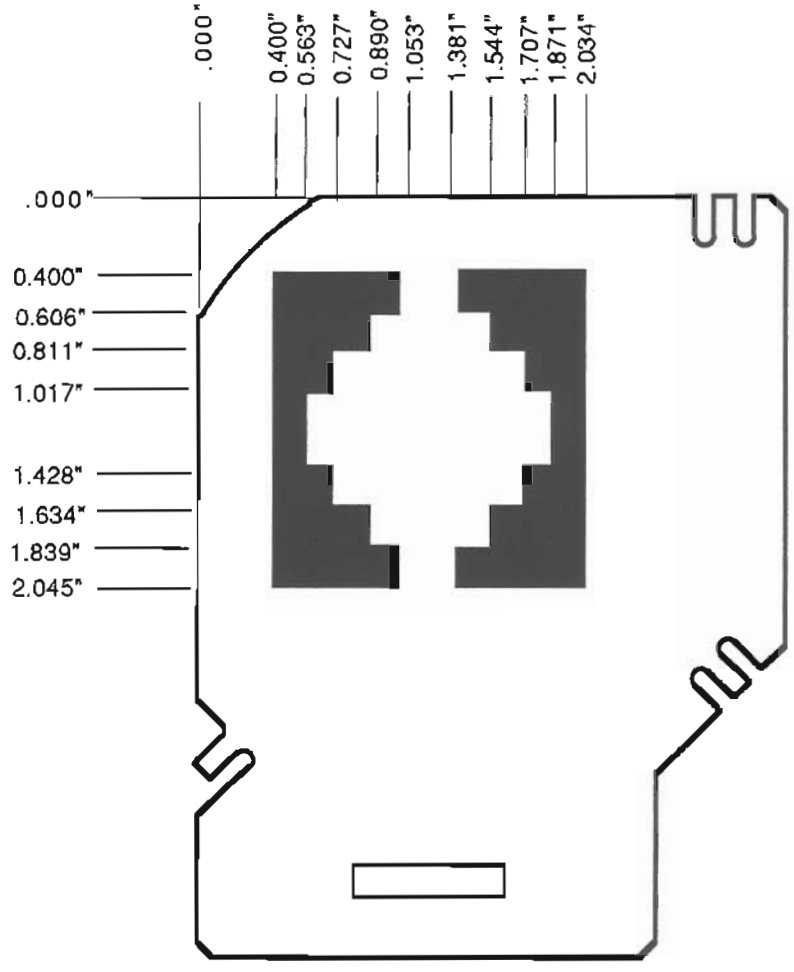

figure 9 Annular illumination aperture (inner sigma =0.40, and an outer sigma =0.70)

The second off-axis illumination type evaluated was the quadrupole type as shown in figure 10a. This design consists of four aperture opening spaced symmetrically around the optic axis. This is basically a modified annular design with only the corners of the annular ring open. The quadrupole design is optimized for only vertical and horizontal oriented patterns, as the diffraction angle directions for both orientations is optimal in the corners of a square annulus as shown in figure 10b. The quadrupole design has the best depth of focus and resolution for the vertical and horizontal features, but is inferior to the annular and partially coherent illuminations for oblique or 45º oriented features. This design is similar to both Nikons SHRINC (Super High Resolution by Illumi-Nation Control) [19] and Canons CQUEST (Canon QUadrupole Effect for Stepper Technology) [16]. The design here used 0.26 sigma openings with a 0.70 sigma exterior edge distance from the optic axis.

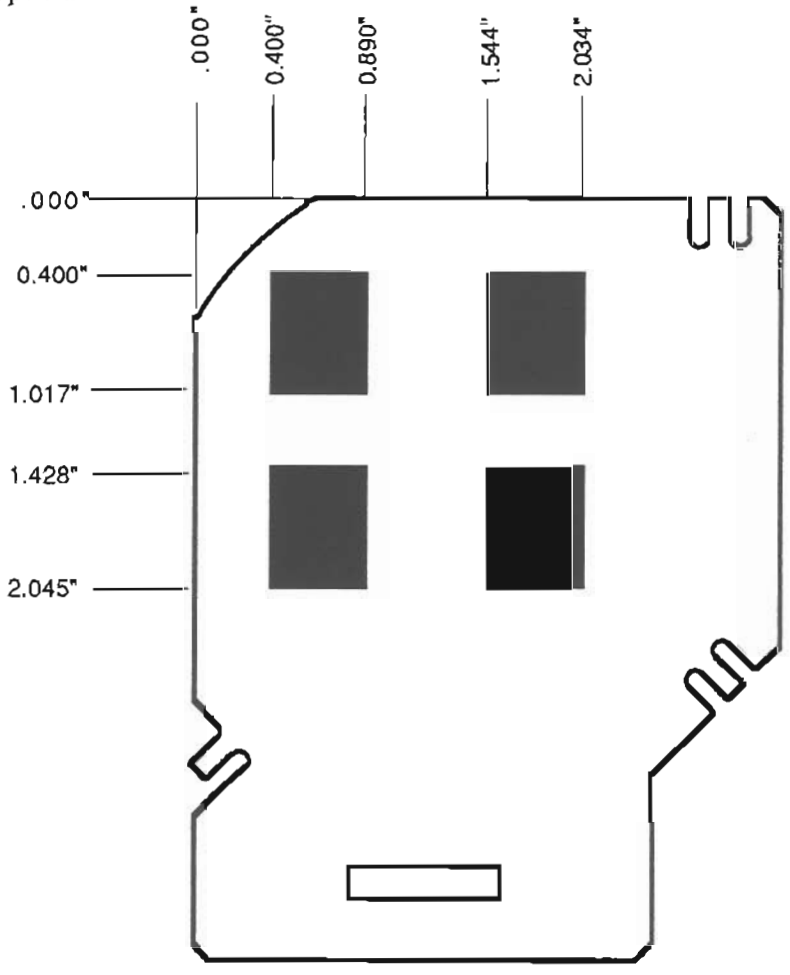

figure 10a Quadrupole off-axis illumination aperture (sigma = 0.26 per opening)

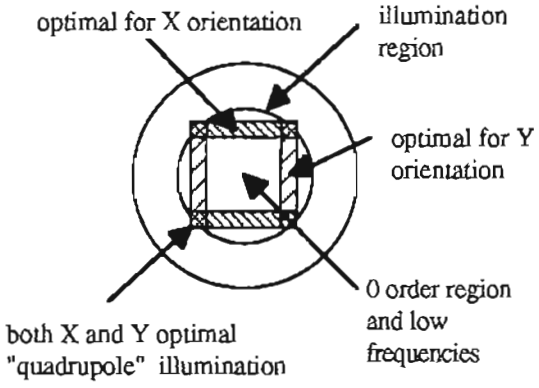

figure 10b Optimal quadrupole illumination regions for feature frequency and orientation.

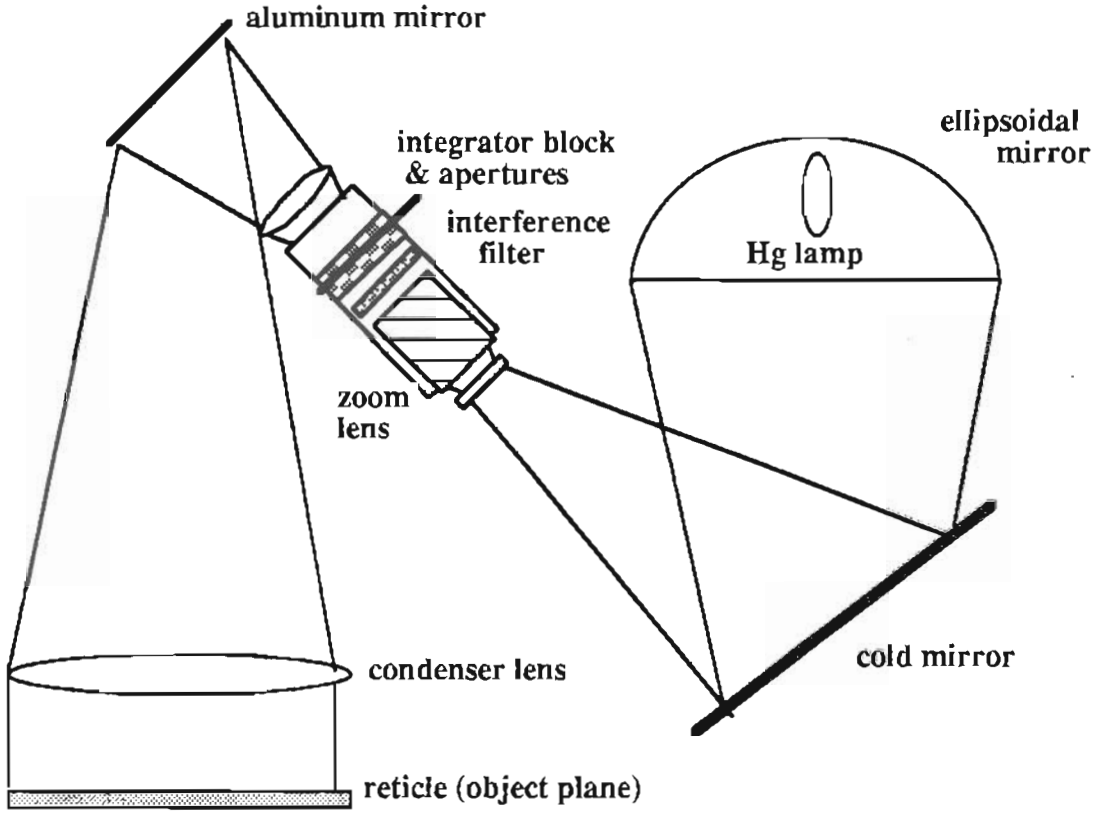

figure 11 Experimental illumination system

B. Photoresist process description

1. Standard high contrast

A modern high contrast i-line (365nm wavelength) sensitive positive photoresist used for all tests. The photoresist applied to bare planar silicon substrates by spin coating. The spin speed in RPM determines the final coating thickness. These photoresist coated wafers received a hotplate post-spin bake to remove any excess solvent and to stabilize the photo-speed. The wafers were exposed to the pattern shown in figure 12 using an advanced waferstepper capable of varying the illumination using apertures as shown in figures 8 - 10. Following exposure the wafers received a post-exposure hotplate bake (PEB),which is designed to slightly diffuse the unexposed photo-active compound in the photoresist matrix into the exposed regions. This post-exposure bake improves the pattern size (CD) control by reducing variations caused by previous processing. The wafers were subsequently developed in a 2.38% solution of tetra-methyl ammonium hydroxide (TMAH). Once the pre-set development time is complete, the wafers are rinsed with de-ionized water and spun dry. An exact processing description can not be given here as it is proprietary to Micron.

2. Super high contrast

The positive photoresist coated wafers processed as defined above were coated with MicroSi's WS365 contrast enhancement material (CEM). A barrier coating material is applied to the photoresist coated wafers by spinning the wafers at 1000 RPM. This material is solution of water and poly-vinyl alcohol which is designed to prevent inter-mixing between the CEM and the positive photoresist. The WS365 contrast enhancement material is subsequently spun coated to a thickness of 2000Å. The wafers were exposed to the pattern shown in figure 12 using an advanced waferstepper. The exposure times had to be increased 100% when this CEM material was used.

Following exposure the wafers received a de-ionized water rinse to remove the CEM material prior to the post-exposure hotplate bake (PEB). After post-exposure bake, the wafers were subsequently developed in a 2.38% solution of tetra-methyl ammonium hydroxide (TMAH). Once the pre-set development time is complete, the wafers are rinsed with de-ionized water and spun dry.

3. Anti-reflective substrate process

The bare silicon substrates prior to coating the positive photoresist were spin coated with Brewers i-line ARC-XLT anti-reflective coating material. Different reflectivities were achieved by varying the spin speed. After coating the anti-reflective material the wafers received a 210ºC hotplate bake for 60 seconds. The substrate reflectivity was subsequently measured at 365nm wavelength. The 897i photoresist was then applied to these coated wafers using the process described above.

C. Measurement procedures

All photoresist pattern (CD or critical dimension) measurements were made on a Hitachi model S6000 scanning electron microscope (SEM) metrology system. All positive photoresist linewidth dimensions were measured in microns. The depth of focus was defined as that focal plane range where the nominal linewidth measured at 0.0 micron defocus varies only by ±10%.

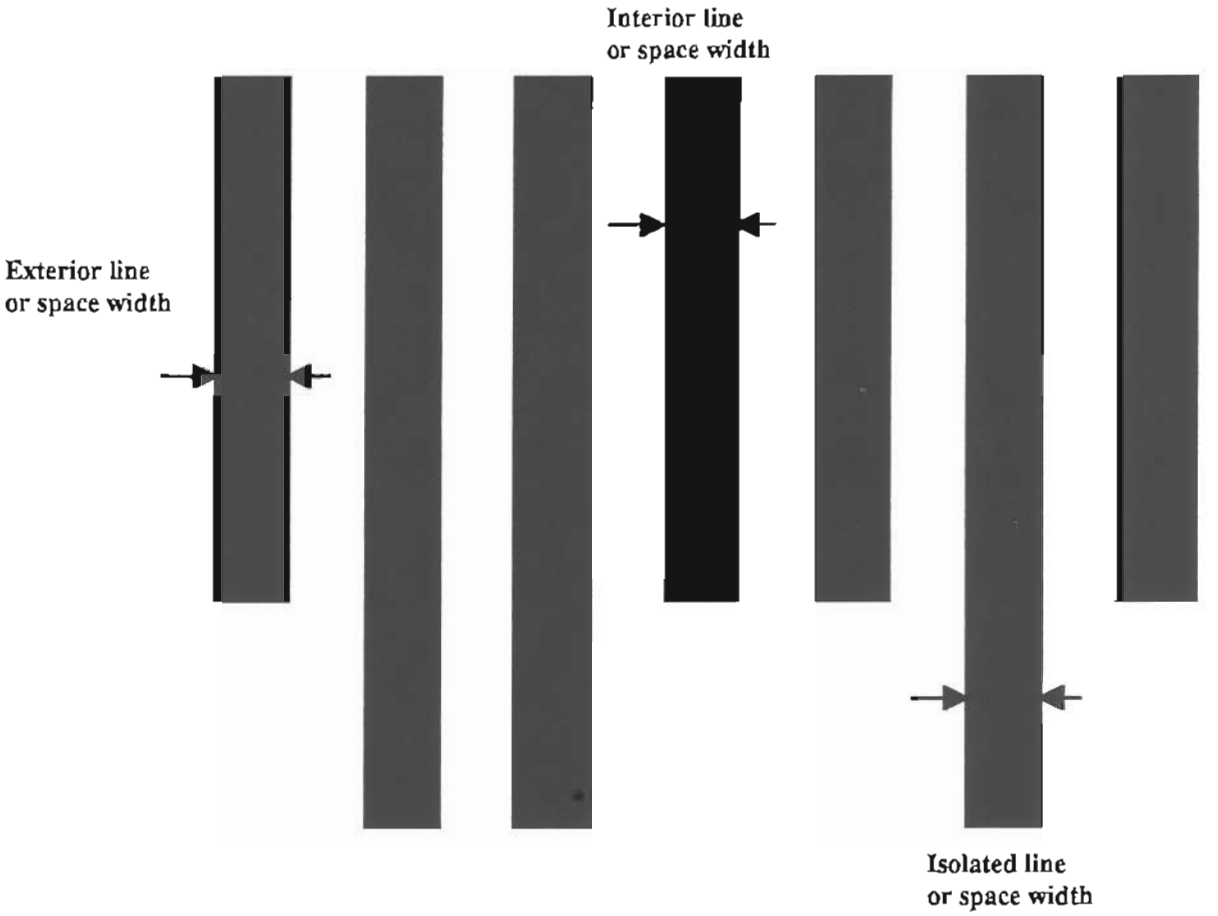

figure 12 Hitachi S6000 SEM CD measurement locations

III. EXPERIMENTAL RESULTS

The depth of focus data presented here was generated with partially coherent (sigma =0.64), quadrupole (inner sigma 0.26, outer sigma 0.70 and opening sigma = 0.26), and annular (inner sigma = 0.40 and outer sigma =0.70) illumination on a waferstepper with a 0.48 numerical aperture lens. Depth of focus was quantified as that focal plane range where the nominal linewidth at 0.0 micron defocus varies only by ±10%. The flatter the curve on these plots the greater the depth of focus. All CD measurements were taken at the center and one corner of a 15 x 15 mm field (lens). The feature types evaluated were isolated, dense, and dense oblique (45º) opaque positive photoresist linewidths. The nominal 1X reticle feature sizes evaluated were 0.36, 0.40,

and 0.50 microns. SEM micrographs were taken at a 65 degree tilt angle for each focus condition at an exposure dose that produced a 1:1 CD at 0.0 micron defocus. The SEM micrographs and CD measurement data show that off-axis illumination produces significant improvements in resolution, image quality and depth of focus as compared to partially coherent illumination. Figures 13 through 30 show plots of feature size vs defocus. These plots were used to determine the depth of focus for a particular feature size and orientation for each illumination condition. Table 1 summaries the depth of focus results. Plots of depth of focus vs linewidth shown in figures 31 through 33 graphically illustrate the results summarized in table 1. The photoresist image sidewall and height in the defocus mode for off-axis illumination is superior to partially coherent illumination as can be seen in the SEM micrographs. Off-axis annular illumination is a more flexible solution than quadrupole, because of its benefit to isolated and oblique (45º) features. This can be readily observed in table 1 and the SEM micrographs. There appears to be a positive 0.3 micron focal plane shift with the annular as compared to the quadrupole illumination .

			center of 15mm x 15mm field					corner of 15mm x 15mm field				
Feature type	Feature Location	line width (μm)	sigma = 0.64	Quad..	% Gain	Annul.	% Gain	sigma = 0.64	Quad..	% Gain	Annul.	% Gain
vertical	interior	0.36	0.9	2.1	133	1.5	67	0.6	2.25	275	2.1	250
vertical	interior	0.40	2.1	3.0	43	2.25	7	1.8	2.85	58	2.55	42
vertical	interior	0.50	3.0	3.0	0	3.0	0	2.85	3.0	5	3.0	5
vertical	exterior	0.36	0.9	1.2	33	1.5	67	0.6	0.9	50	1.2	100
vertical	exterior	0.40	2.1	2.85	36	2.1	0	1.8	2.25	25	1.8	0
vertical	exterior	0.50	2.55	2.4	6	2.4	-6	2.25	2.25	13	2.25	0
45°	interior	0.36	0.0	0.0	0	0.0	0	0.0	0.0	0	0.0	0
45°	interior	0.40	1.8	0.6	-67	1.2	-33	1.5	1.2	-20	1.8	20
45°	interior	0.50	2.55	2.85	12	2.85	12	2.55	2.25	-12	2.85	12
45°	exterior	0.36	0.0	0.0	0	0.0	0	0.0	0.0	0	0.0	0
45°	exterior	0.40	1.8	0.6	-67	1.2	-33	1.5	1.2	-20	1.5	0
45°	exterior	0.50	2.55	2.85	12	2.85	12	2.25	2.25	0	2.25	0
isolated		0.36	1.5	1.5	0	1.5	0	1.5	1.95	30	1.8	20
isolated		0.40	1.8	1.5	-17	1.5	-17	1.8	1.95	8	2.1	17
isolated		0.50	1.8	1.8	0	1.5	-17	2.55	1.95	-24	2.1	-18

Table 1 Effect of illumination type on depth of focus for various feature types

One drawback to off-axis illumination as evaluated on this "standard" system is the reduction in irradiance, which caused 61% decrease in available energy. Further modifying the illumination system with a higher output lamp and better illumination distribution could correct this problem. The irradiance and illumination uniformity results are outlined in table 2 below. The irradiance uniformity is for the illuminated image area, where 121 irradiance readings are taken across the 15

x 15mm image field. The % uniformity is defined as: [(high reading - low reading)/(high reading - low reading)] X 100.

ILLUMINATION	IRRADIANCE	% UNIFORMITY
partially coherent	420 mw/cm2	1.65%
quadrupole	165 mw/cm2	2.03%
annular	175 mw/cm2	1.70%

Table 2 Illumination irradiance and uniformity

Sections A through C below show plots of linewidth dimension as a function of defocus setting. The exposure doses were adjusted for both isolated and dense linewidths to obtain a processed photoresist dimension equivalent to the nominal 1X reticle dimension. The exposure dose for the isolated linewidth was higher than the dense to achieve the same photoresist dimension. This is due to a proximity effect resulting from less high frequency features diffracted light adding to the energy required to expose the isolated linewidth. This effect is more noticeable in the defocus mode as observed by the shape of the CD vs defocus curves for isolated and dense linewidths. S. Olsen etal [33] claimed making the illumination less coherent in a conventional system will reduce the isolated and dense linewidth difference. W.N. Partlo etal with GCA [25] showed that increasing the obstruction size (incident angle increased) on an annular illumination system will reduce this isolated and dense linewidth difference. These ideas were not tested here.

A. Isolated linewidths

Figures 13 through 18 illustrate the isolated linewidth depth of focus latitude for the three different illumination types. Center and corner of field CD data is presented.

1. Critical dimension vs defocus curves on -axis (center of field)

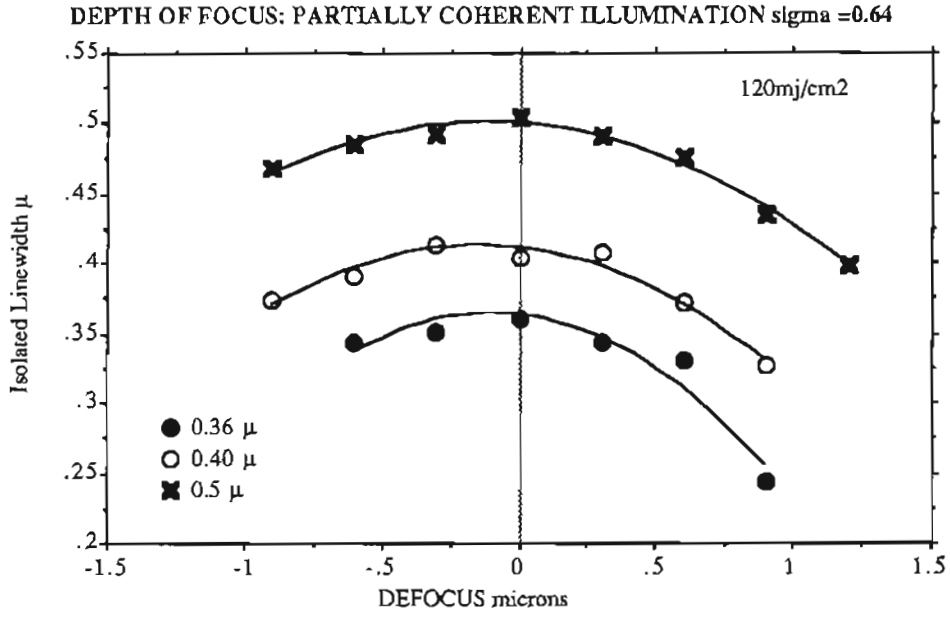

Figure 13 Depth of focus for isolated linewidths and partially coherent illumination

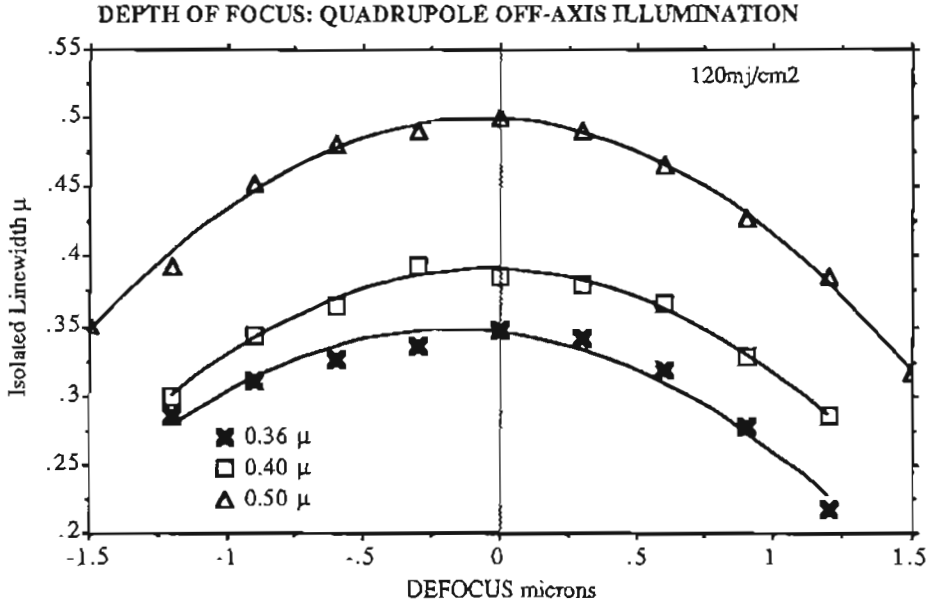

Figure 14 Depth of focus for isolated linewidths and quadrupole illumination.

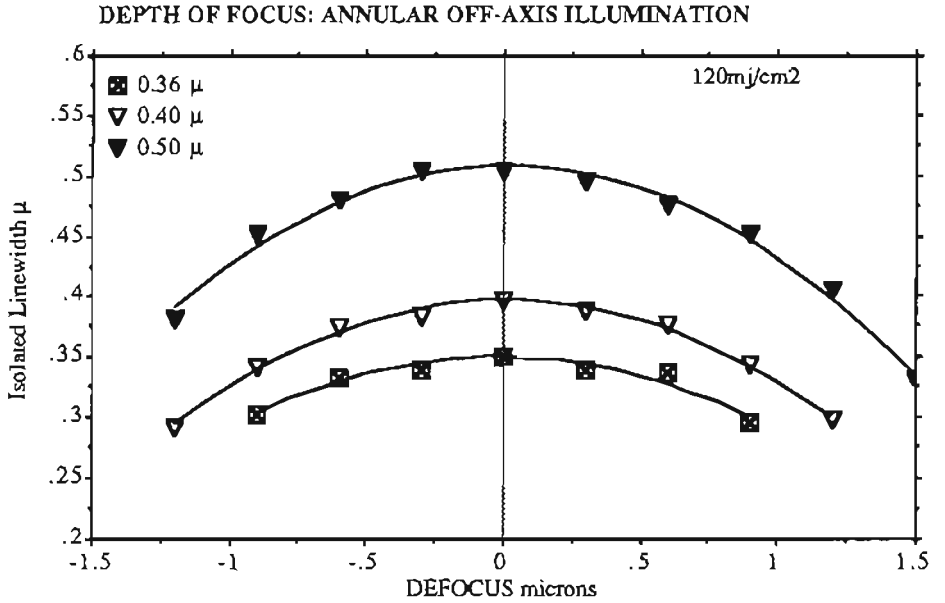

Figure 15 Depth of focus for isolated linewidths and annular illumination.

2. Critical dimension vs defocus curves off the optical axis (corner of field)

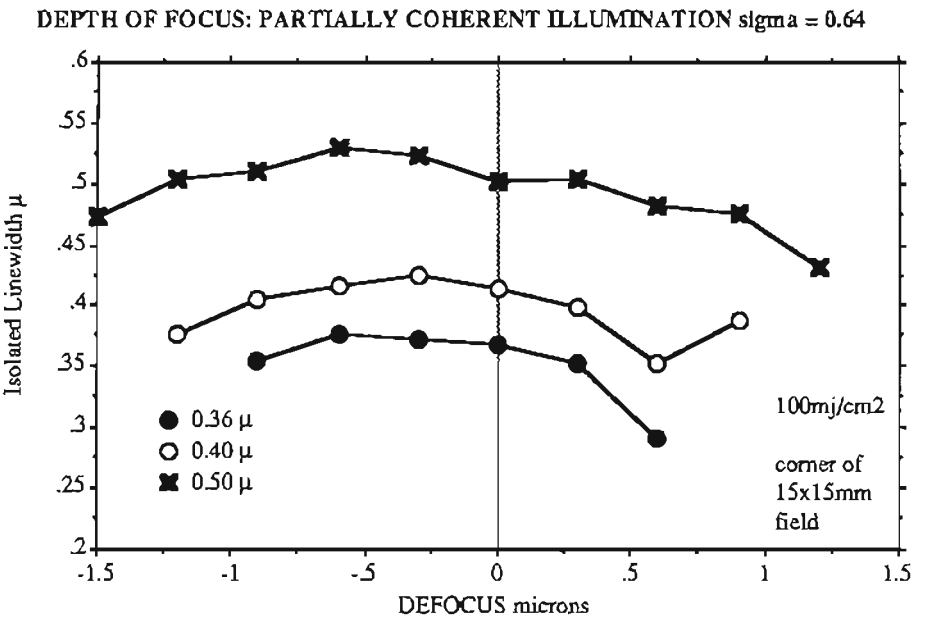

Figure 16 Depth of focus for isolated linewidths in the corner of the 15x15mm field and partially coherent illumination.

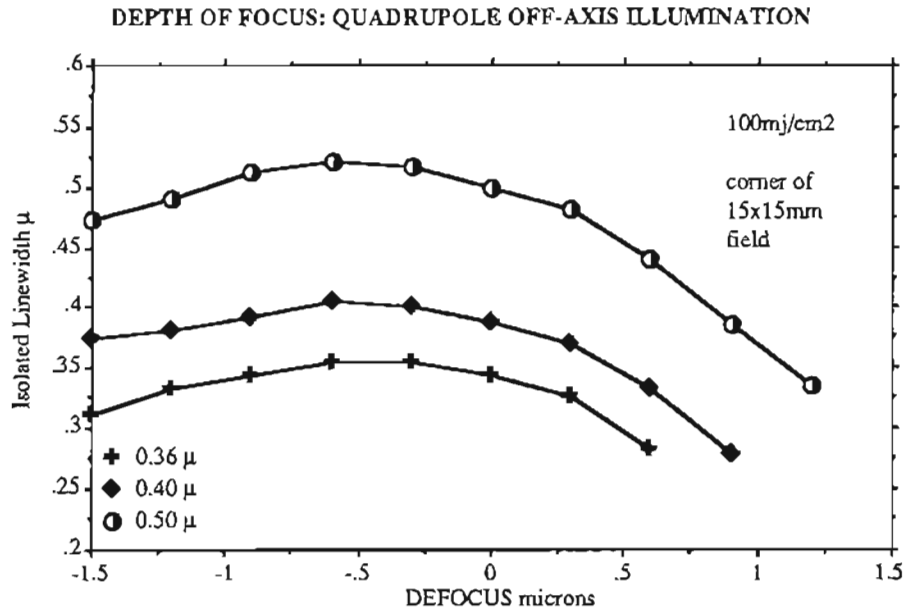

Figure 17 Depth of focus for isolated linewidths in the corner of the 15x15mm field and quadrupole illumination

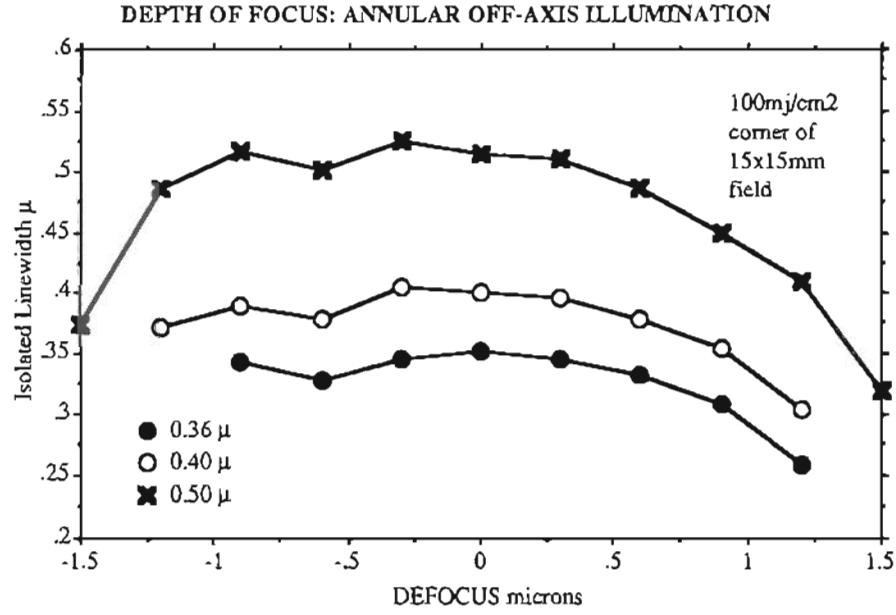

Figure 18 Depth of focus for isolated linewidths in the corner of the 15x15mm field and annular illumination

B. Dense linewidths (grating type features)

Figures 19 through 24 illustrate the interior dense linewidth depth of focus latitude for the three different illumination types. Center and corner of field CD data is presented.

1. Critical dimension vs defocus curves on axis (center of field)

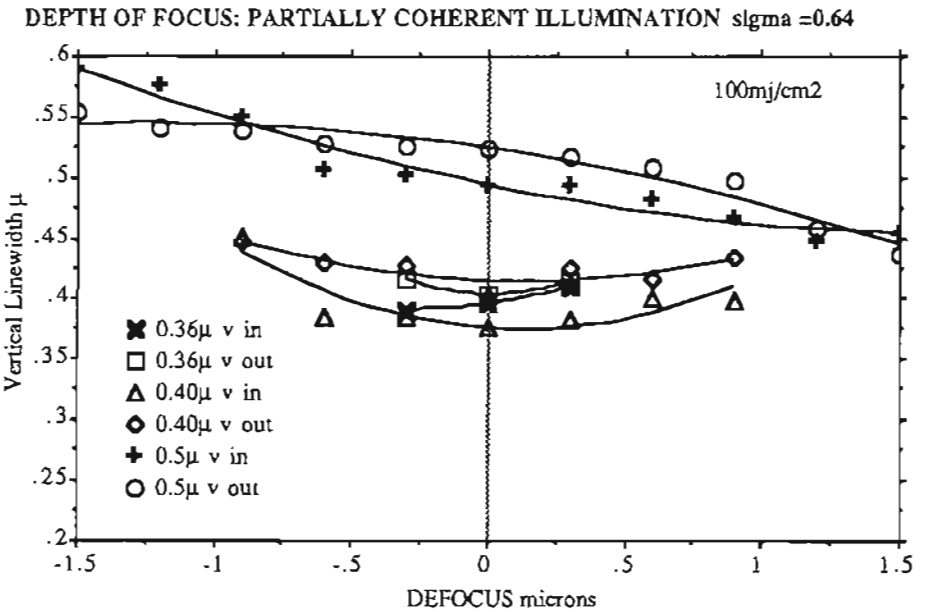

Figure 19 Depth of focus for dense vertical linewidths using partially coherent illumination.

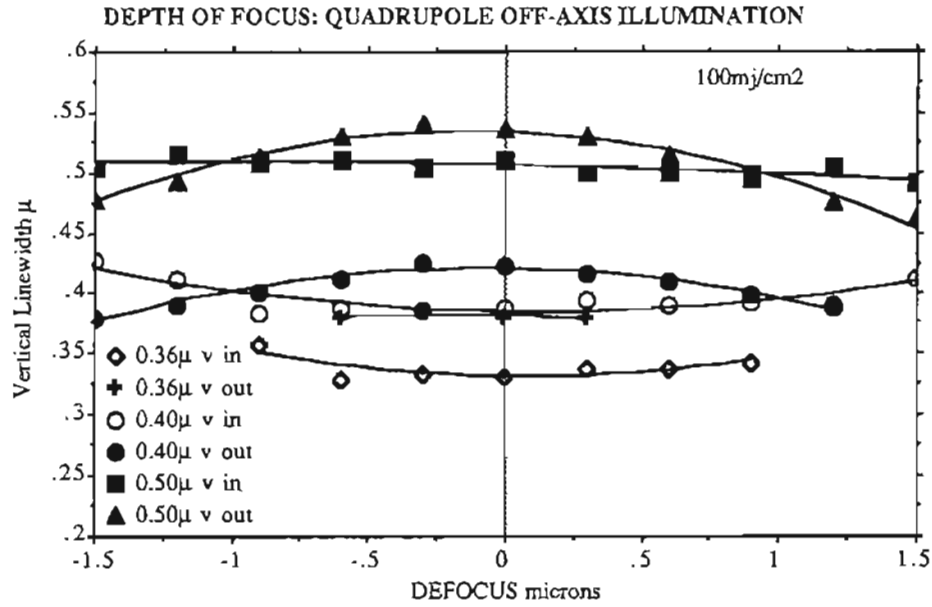

Figure 20 Depth of focus for dense vertical linewidths using off-axis quadrupole illumination.

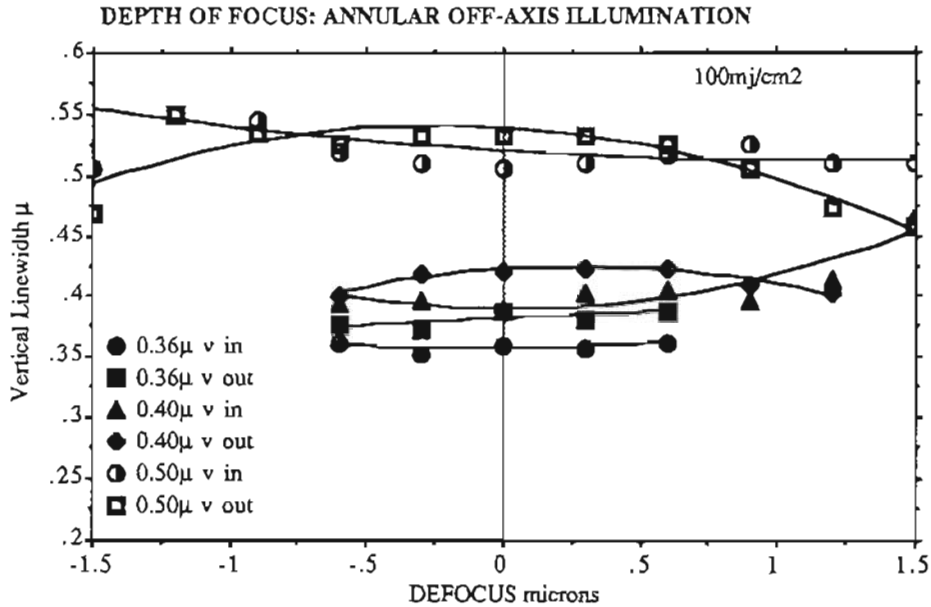

Figure 21 Depth of focus for dense vertical linewidths using off-axis annular illumination.

2. Critical dimension vs defocus curves off the optical axis (corner of field)

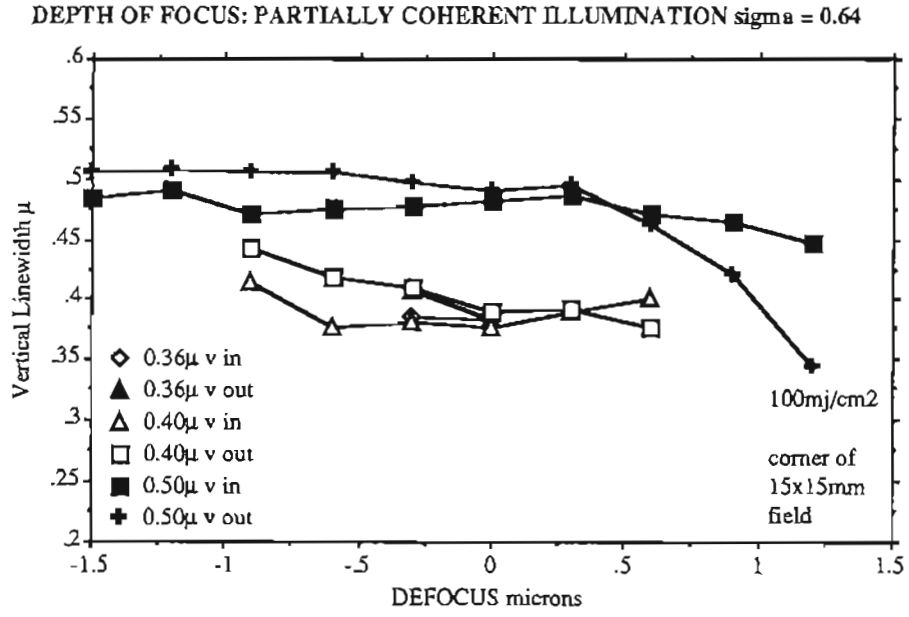

Figure 22 DOF for dense vertical linewidths in field corner and partially coherent illumination.

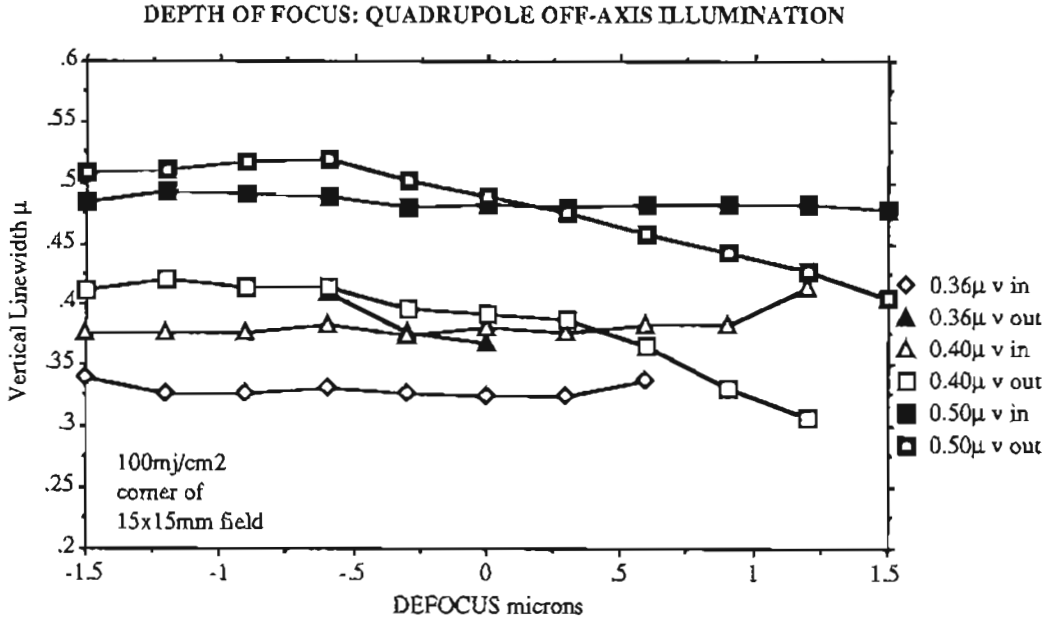

Figure 23 DOF for dense vertical linewidths in field corner and quadrupole illumination.

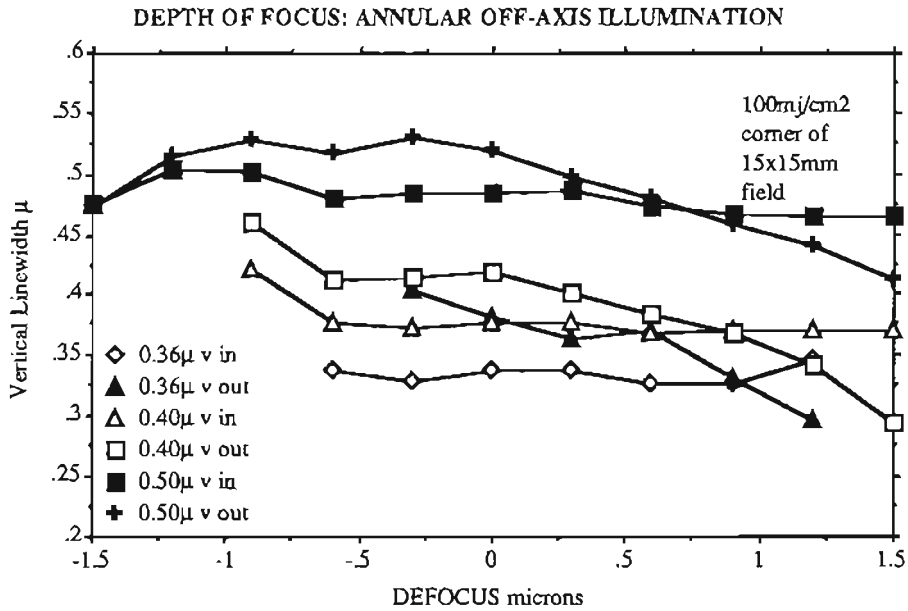

Figure 24 DOF for dense vertical linewidths in field corner and annular illumination.

C. Dense oblique (45º orientation to optical axis) linewidths

Figures 25 through 30 illustrate the interior dense 45º oriented linewidth depth of focus latitude for the three different illumination types. Center and corner of field CD data is presented.

1. Critical dimension vs defocus curves on axis (center of field)

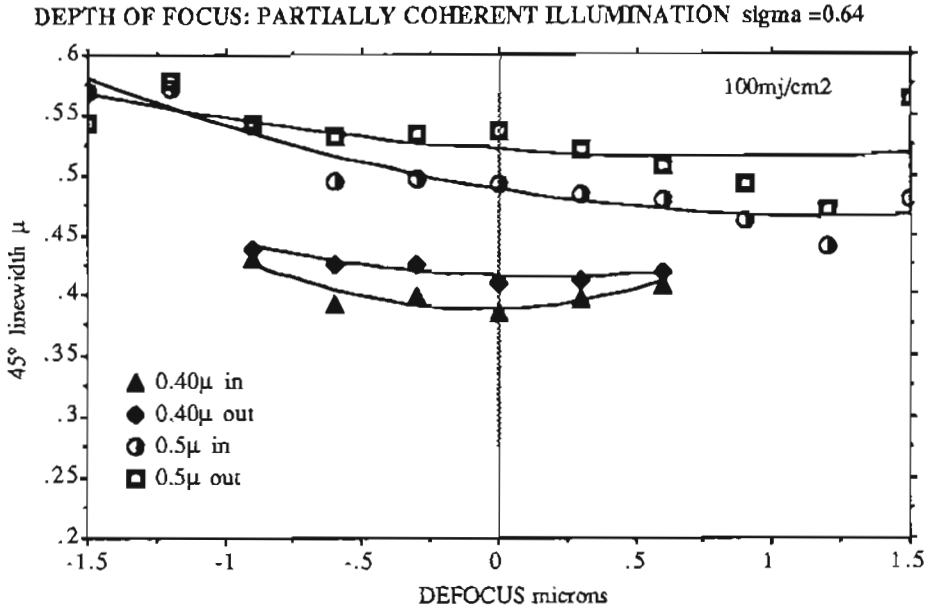

Figure 25 Depth of focus for dense 45º oriented linewidths and partially coherent illumination.

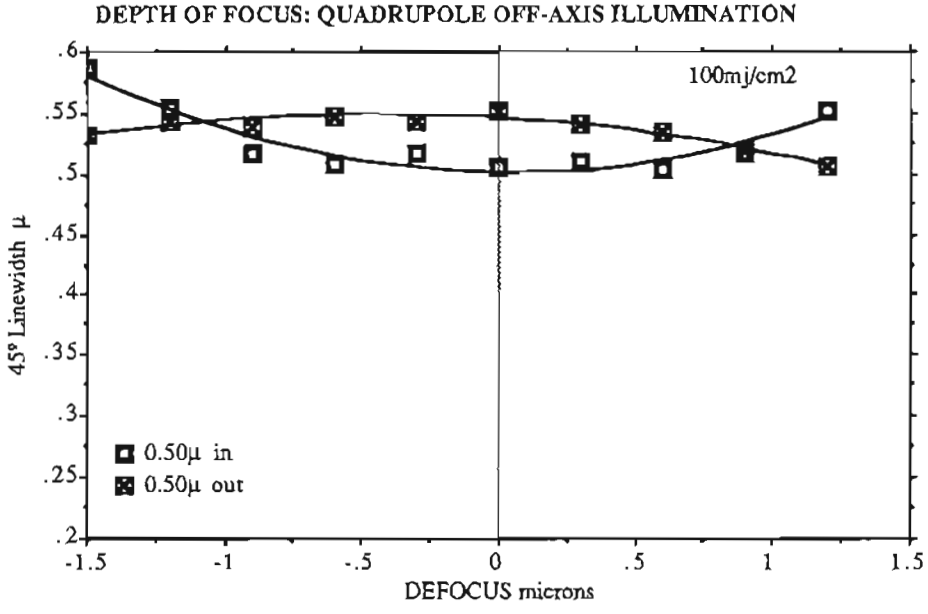

Figure 26 Depth of focus for dense 45º oriented linewidths and quadrupole illumination.

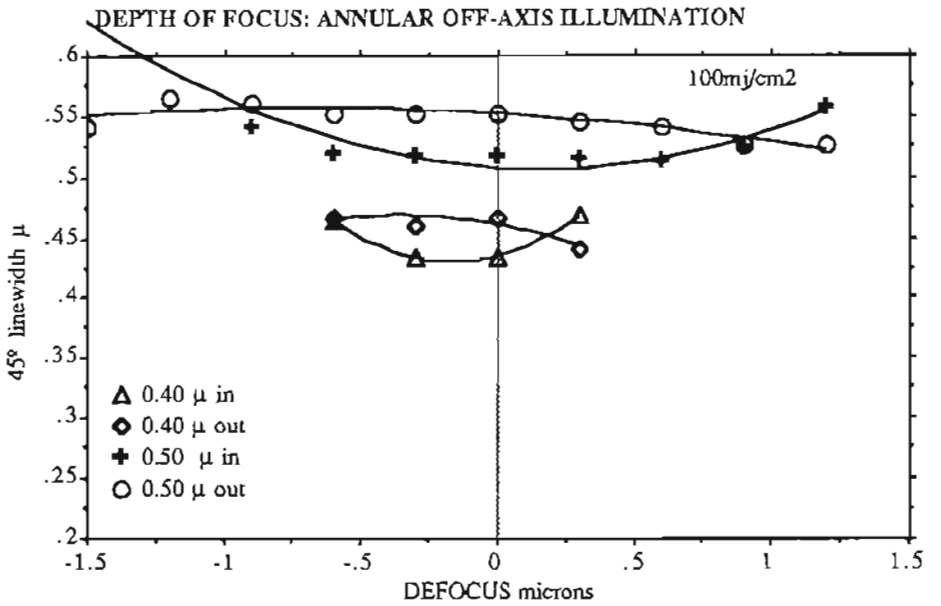

Figure 27 Depth of focus for dense 45º oriented linewidths and annular illumination.

2. Critical dimension vs defocus curves off the optical axis (corner of field)

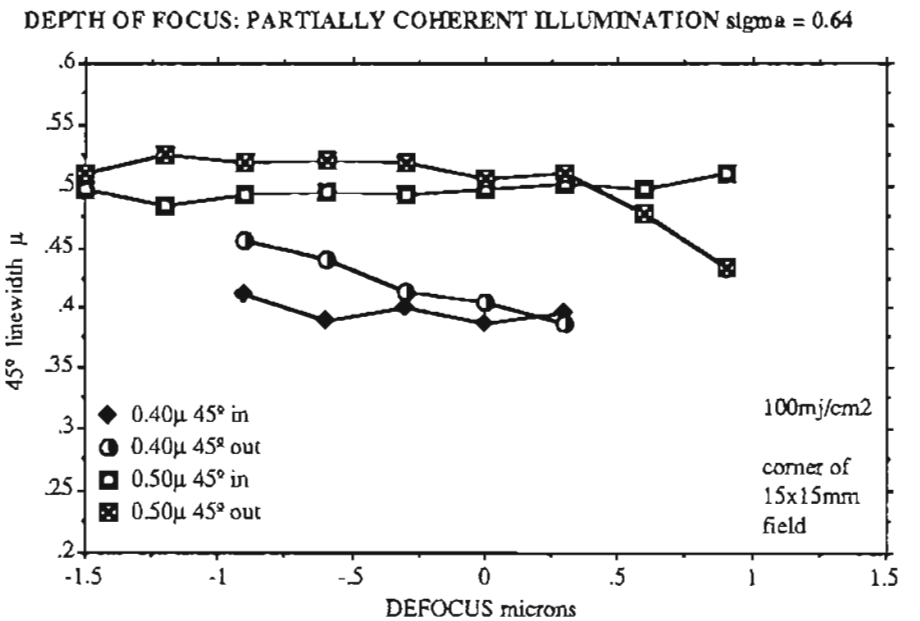

Figure 28 Depth of focus for dense 45º oriented linewidths in the corner of the 15x15mm field and partially coherent illumination.

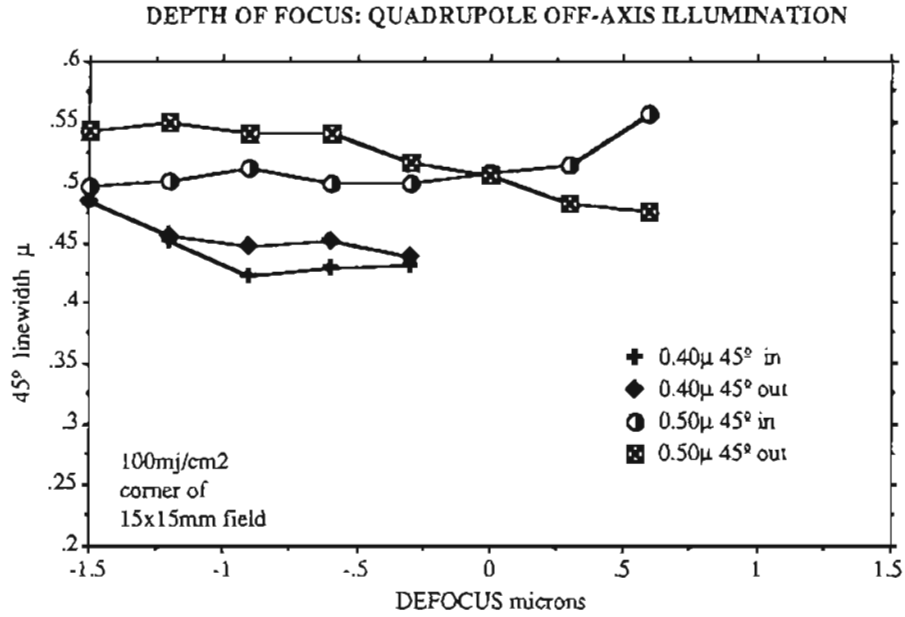

Figure 29 Depth of focus for dense 45º oriented linewidths in the corner of the 15x15mm field and quadrupole illumination.

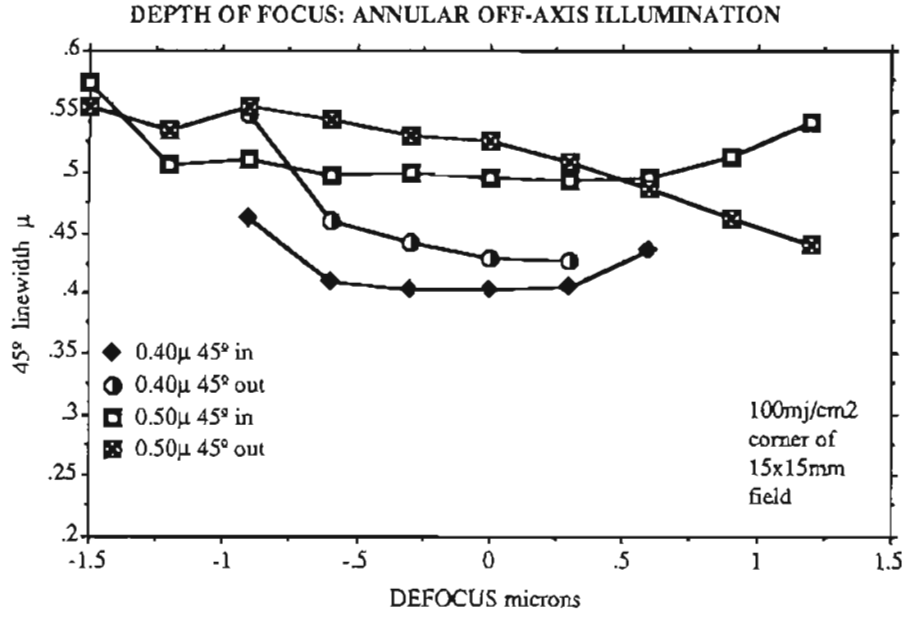

Figure 30 Depth of focus for dense 45º oriented linewidths in the corner of the 15x15mm field and annular illumination.

D. Depth of Focus vs linewidth Plots

Figures 31 through 33 illustrate the linewidth depth of focus CD dependence for the three different illumination types. Only corner of field CD data is presented.

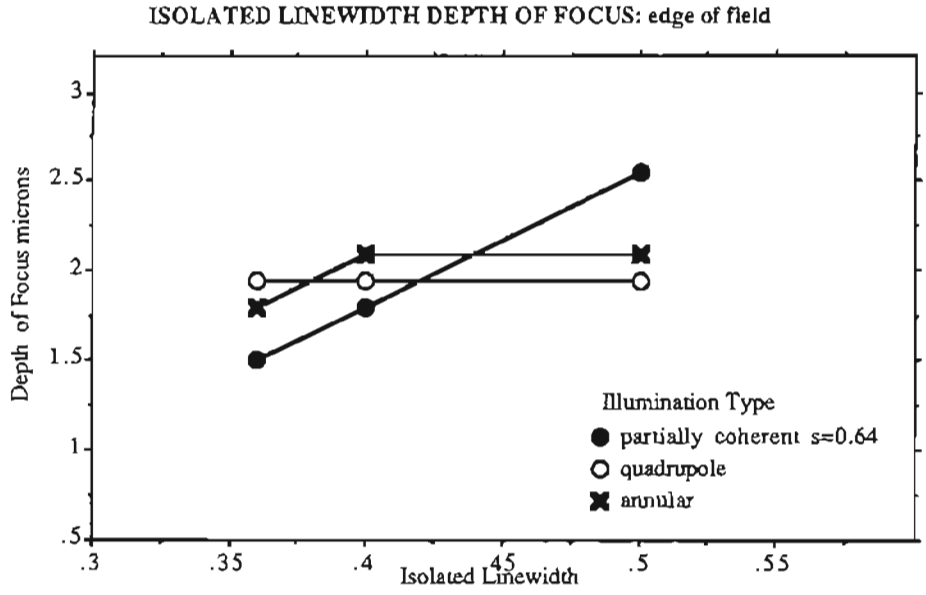

Figure 31 Depth of focus vs isolated (corner of field) linewidths

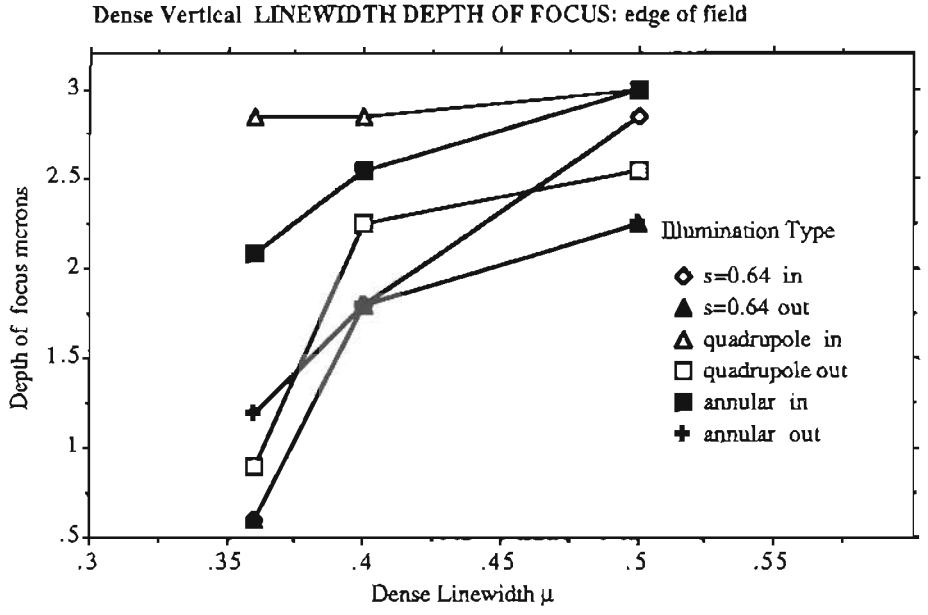

Figure 32 Depth of focus vs dense vertical (corner of field) linewidths

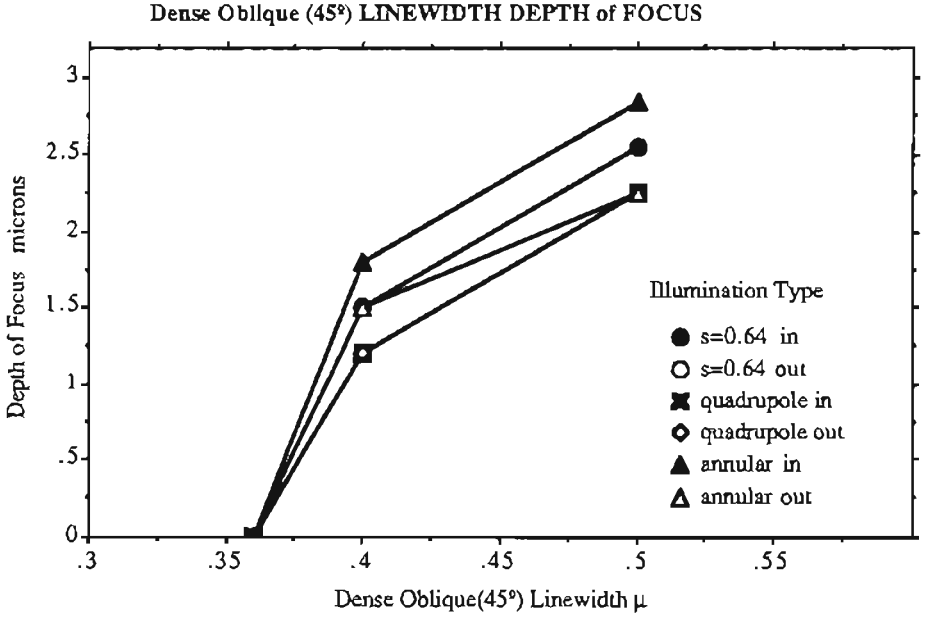

Figure 33 Depth of focus vs dense oblique (45º) (corner of field)linewidths.

E. Critical dimension linearity

Figures 34 and 35 illustrate the CD linearity for isolated and dense linewidths for the three different illumination types. Center of field CD data is presented.

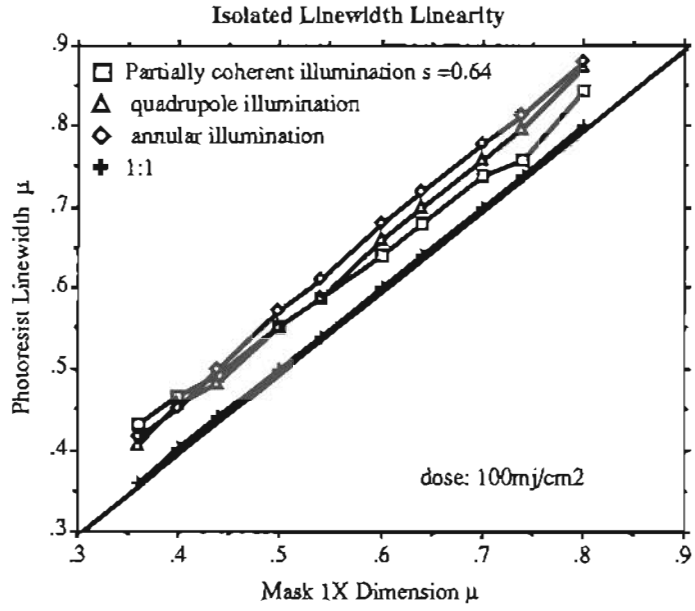

Figure 34 Linearity between mask size and photoresist for isolated patterns.

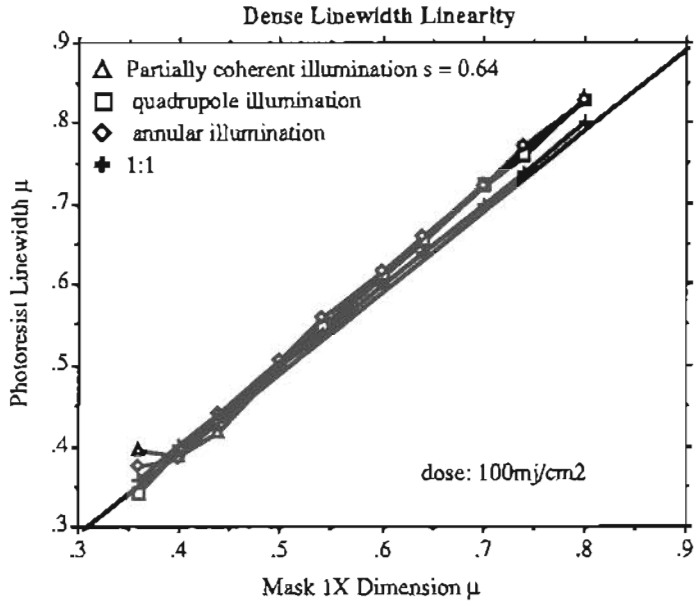

Figure 35 Linearity between mask size and photoresist for dense patterns.

F. Exposure dose latitude

The following plot show that the illumination type had no effect on the exposure latitude for the experimental conditions used in this evaluation. Matsumoto etal. [20] had reported a degradation in exposure latitude with off-axis illumination, which was not observed here.

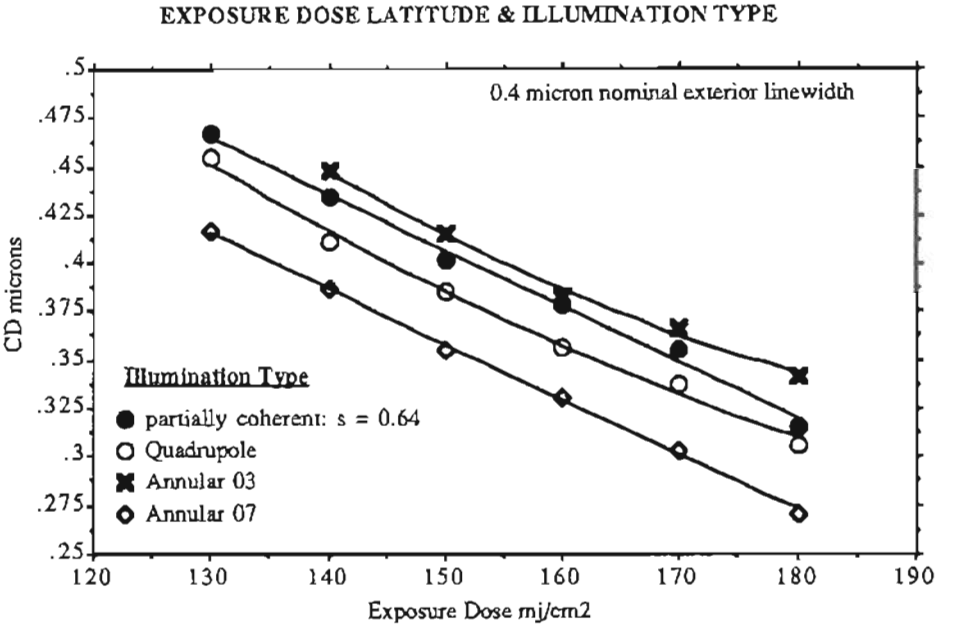

Figure 36. Exposure Dose CD latitude for exterior 0.4 micron linewidths.

G. SEM Micrograph cross-sections (15000X)

Scanning electron microscope micrographs were taken of 0.36, 0.40, and 0.50 micron equal line and space pairs. The exterior linewidth defocus proximity effects are shown for the negative defocus conditions. The dense interior and isolated CD difference proximity effect was observed for all illumination types evaluated.

-0.9μ Defocus
(wafer moved towards lens)

100 mj/cm2

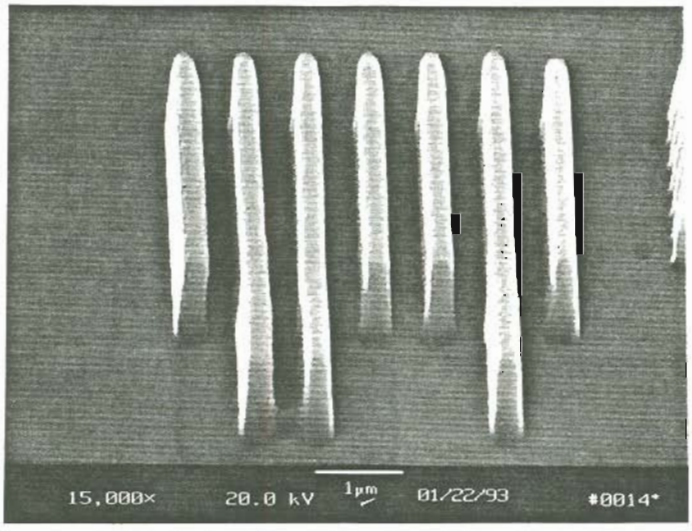

Off-Axis Illumination Quadrupole

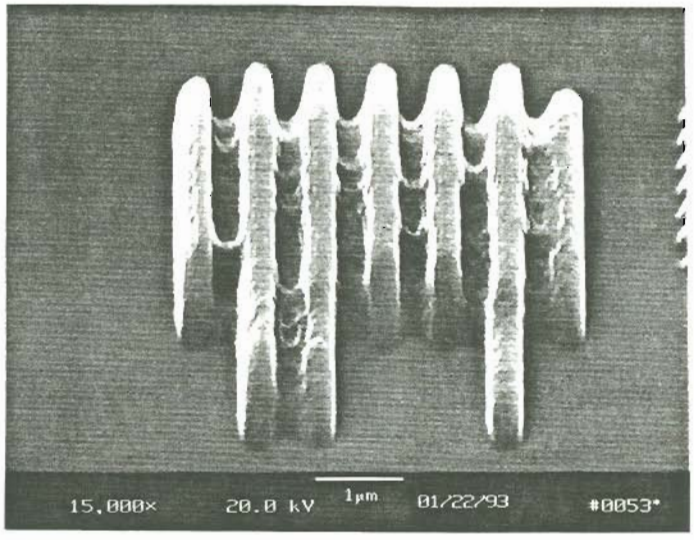

Partially coherent illumination
sigma =0.64

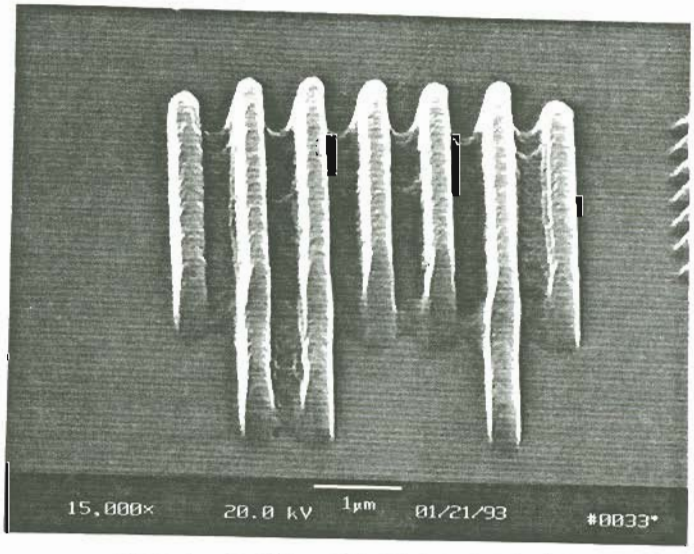

Off-Axis Illumination Annular

Figure 37. -0.90 micron Defocus condition for 0.36 micron linewidths.

0.0μ Defocus

100 mj/cm2

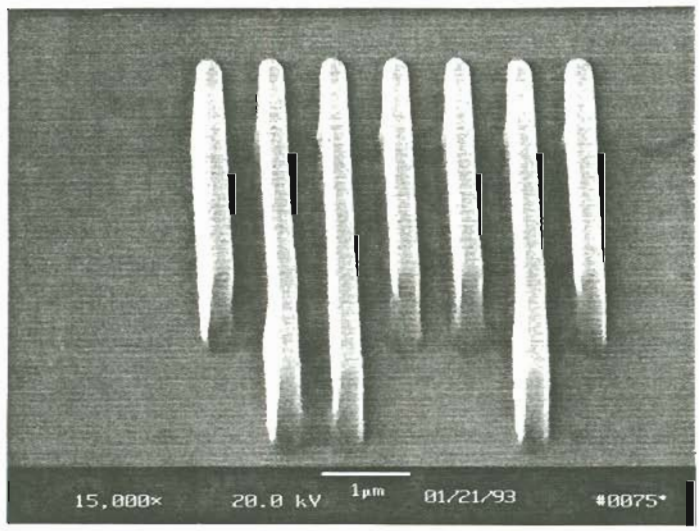

Off-Axis Illumination Quadrupole

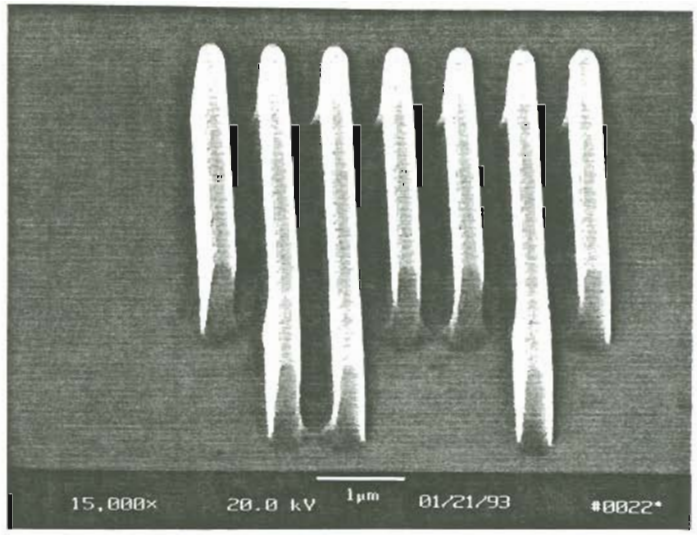

Partially coherent illumination
sigma =0.64

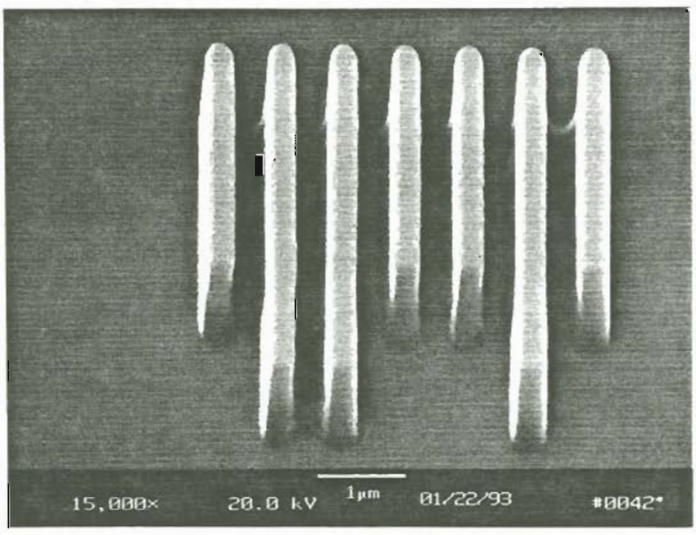

Off-Axis Illumination Annular

Figure 38. 0.00 micron Defocus condition for 0.36 micron linewidths.

+0.9μ Defocus
(wafer moved away from lens)

100 mj/cm2

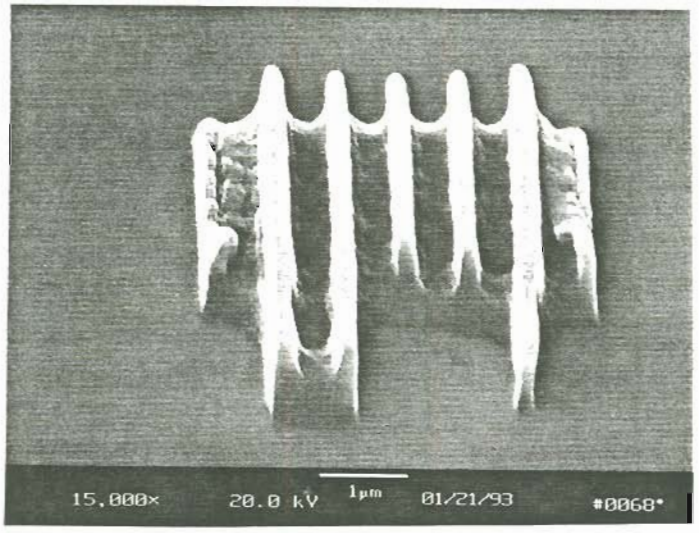

Off-Axis Illumination Quadrupole

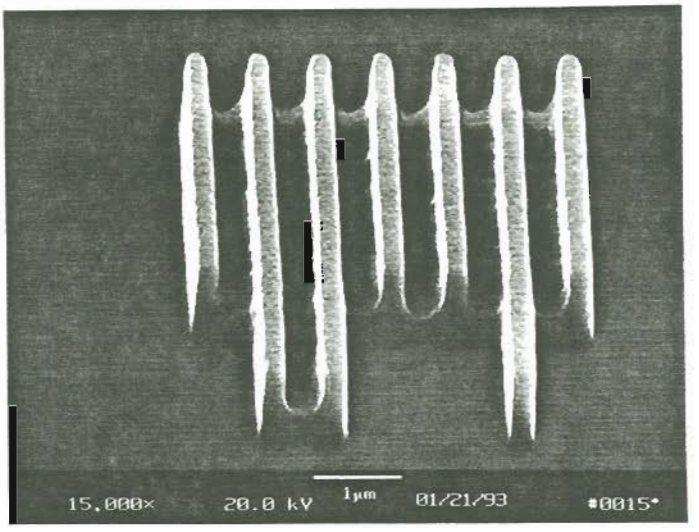

Partially coherent illumination
sigma =0.64

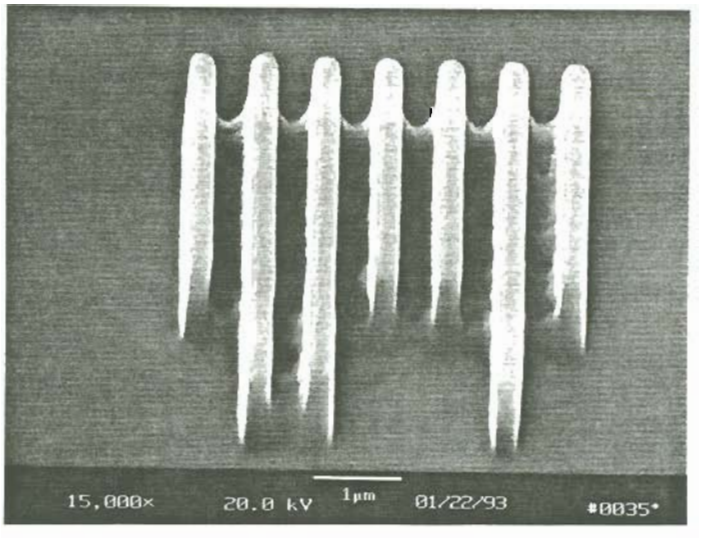

Off-Axis Illumination Annular

Figure 39. +0.90 micron Defocus condition for 0.36 micron linewidths.

-0.9μ Defocus
(wafer moved towards lens)

100 mj/cm2

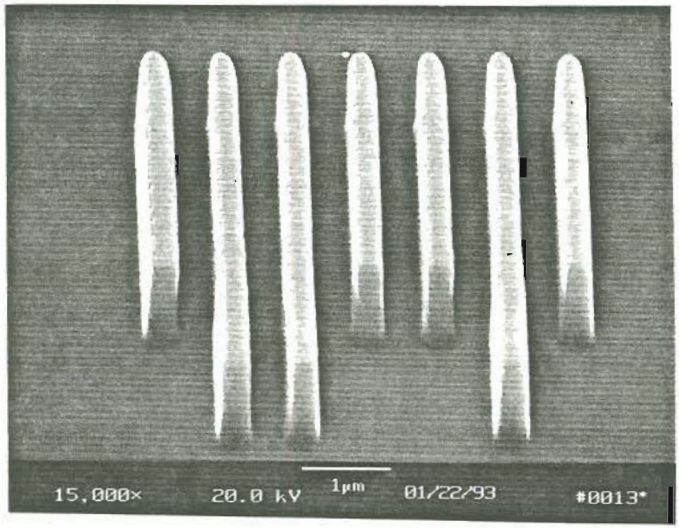

Off-Axis Illumination Quadrupole

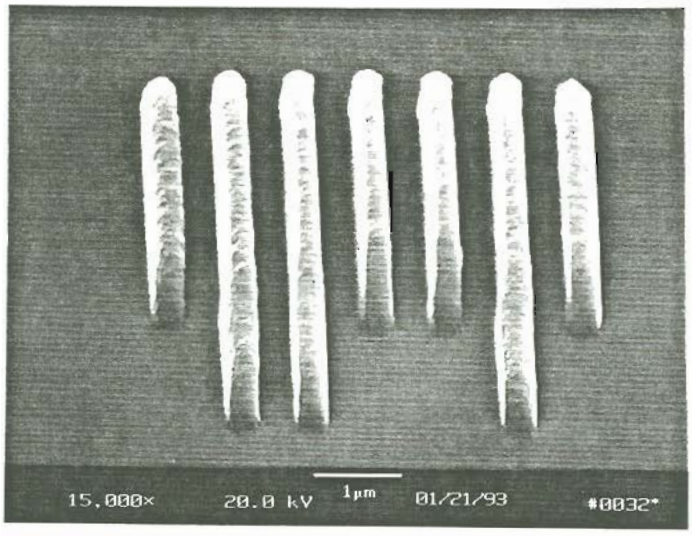

Partially coherent illumination
sigma =0.64

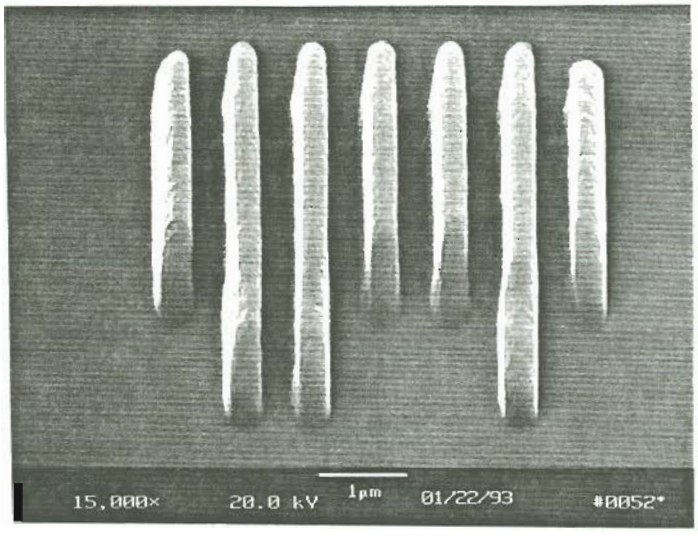

Off-Axis Illumination Annular

Figure 40. -0.90 micron Defocus condition for 0.40 micron linewidths.

0.0μ Defocus

100 mj/cm2

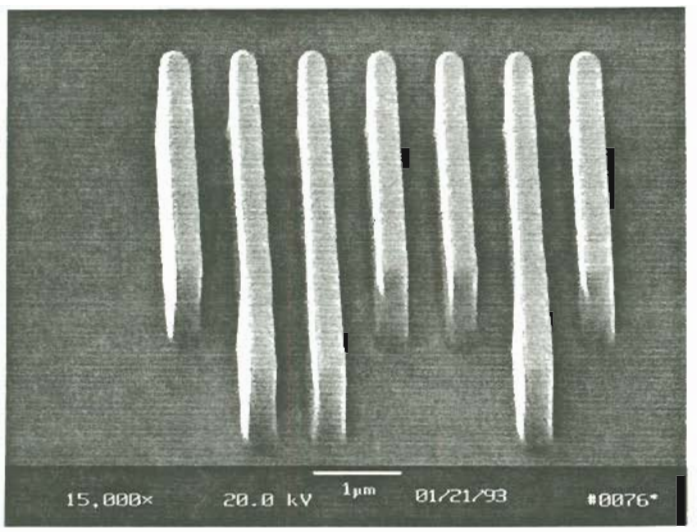

Off-Axis Illumination Quadrupole

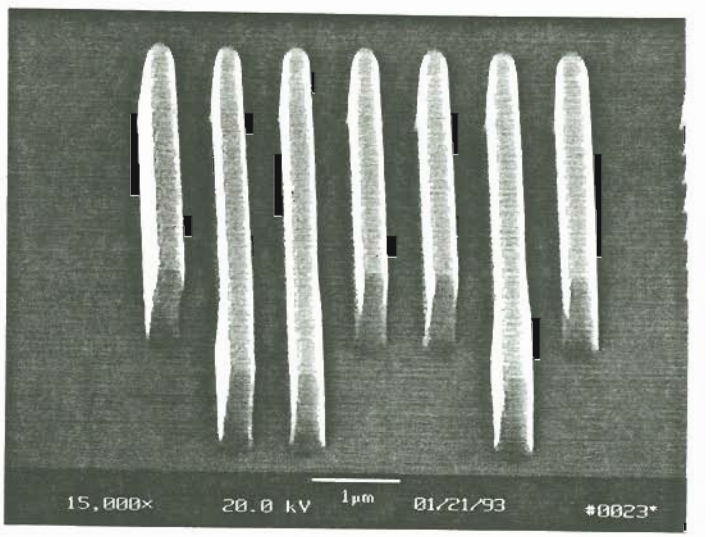

Partially coherent illumination
sigma =0.64

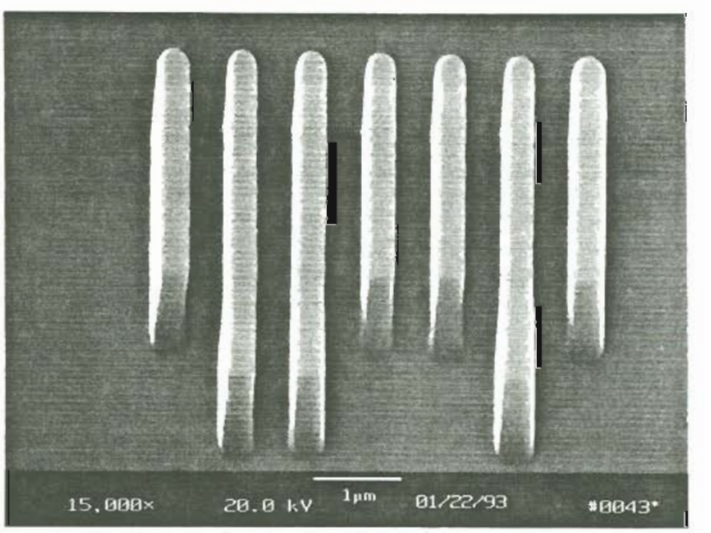

Off-Axis Illumination Annular

Figure 41. 0.00 micron Defocus condition for 0.40 micron linewidths.

+0.9μ Defocus
(wafer moved away from lens)

100 mj/cm2

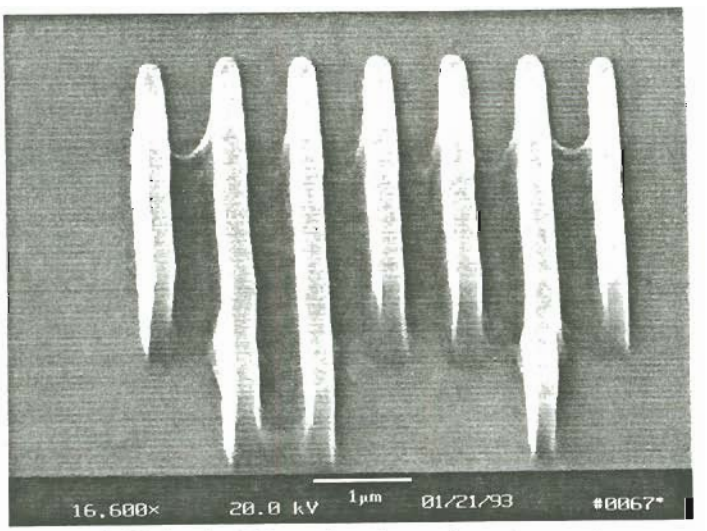

Off-Axis Illumination Quadrupole

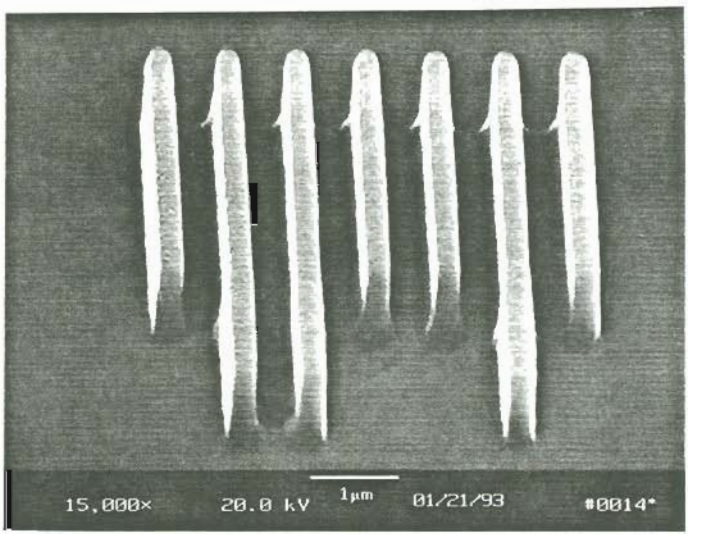

Partially coherent illumination
sigma =0.64

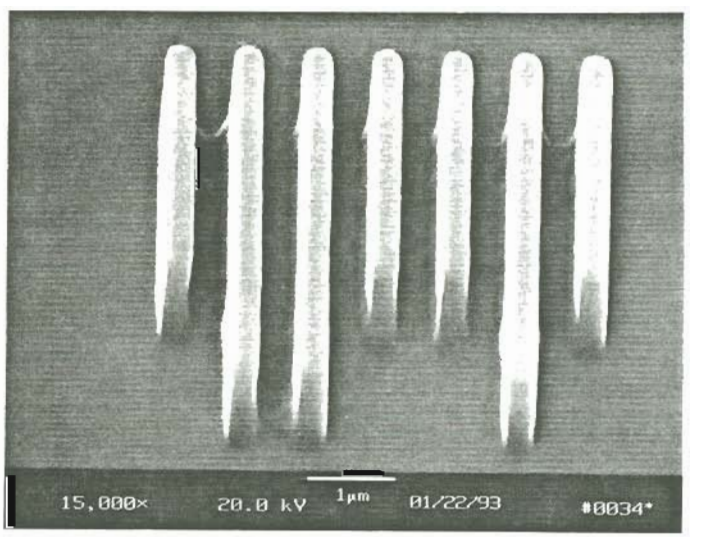

Off-Axis Illumination Annular

Figure 42. +0.90 micron Defocus condition for 0.40 micron linewidths.

-0.9μ Defocus
(wafer moved towards lens)

100 mj/cm2

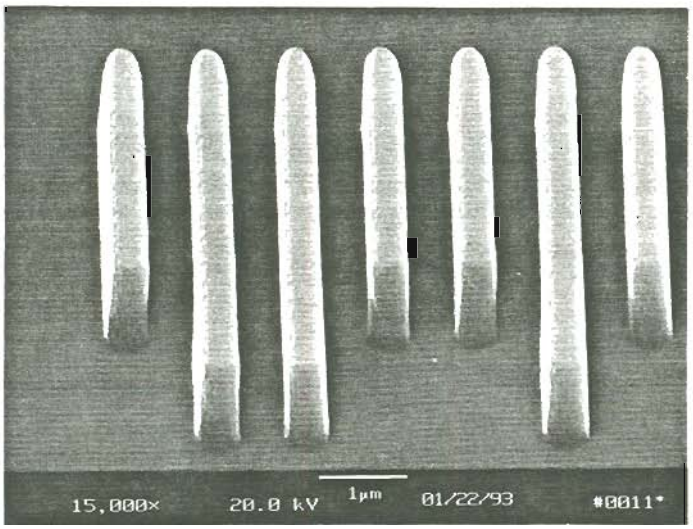

Off-Axis Illumination Quadrupole

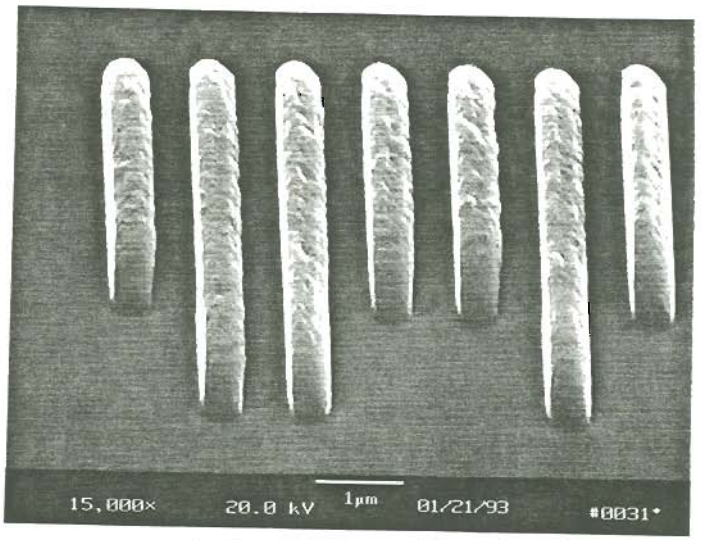

Partially coherent illumination
sigma =0.64

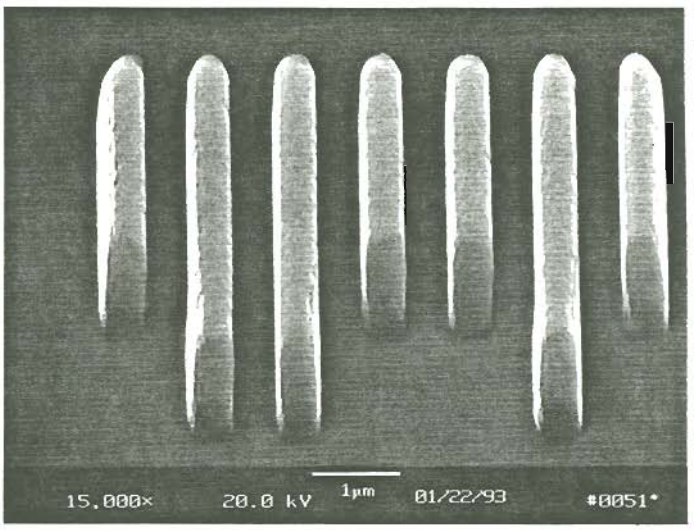

Off-Axis Illumination Annular

Figure 43. -0.90 micron Defocus condition for 0.50 micron linewidths.

0.0μ Defocus

100 mj/cm2

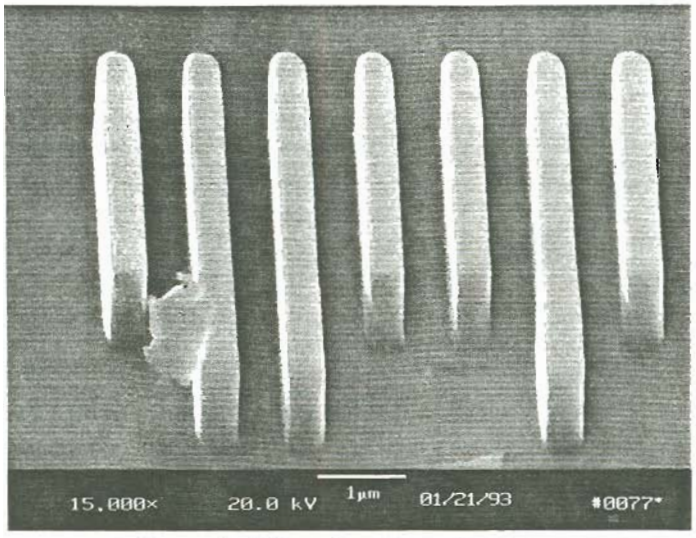

Off-Axis Illumination Quadrupole

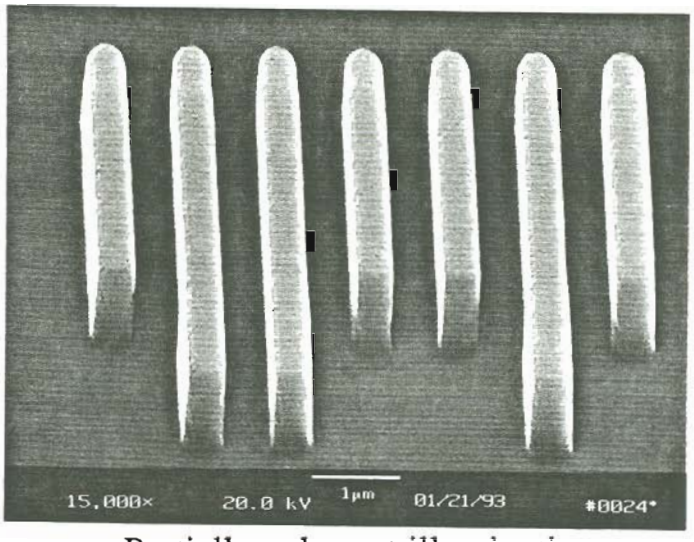

Partially coherent illumination
sigma =0.64

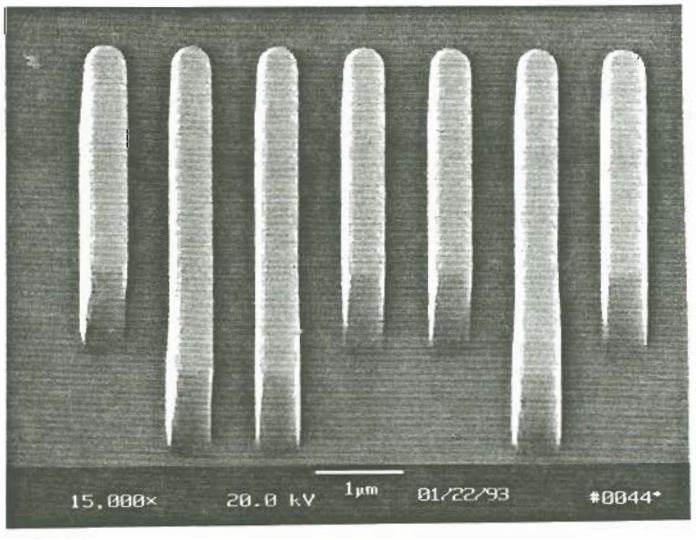

Off-Axis Illumination Annular

Figure 44. 0.00 micron Defocus condition for 0.50 micron linewidths.

+0.9μ Defocus
(wafer moved away from lens)

100 mj/cm2

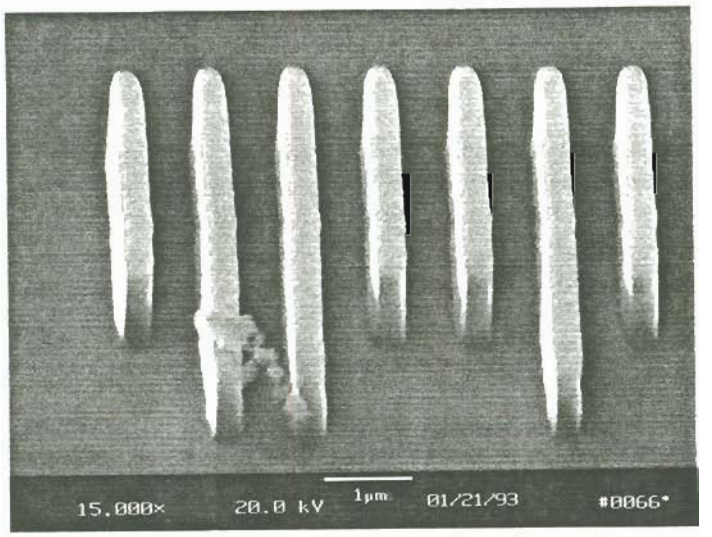

Off-Axis Illumination Quadrupole

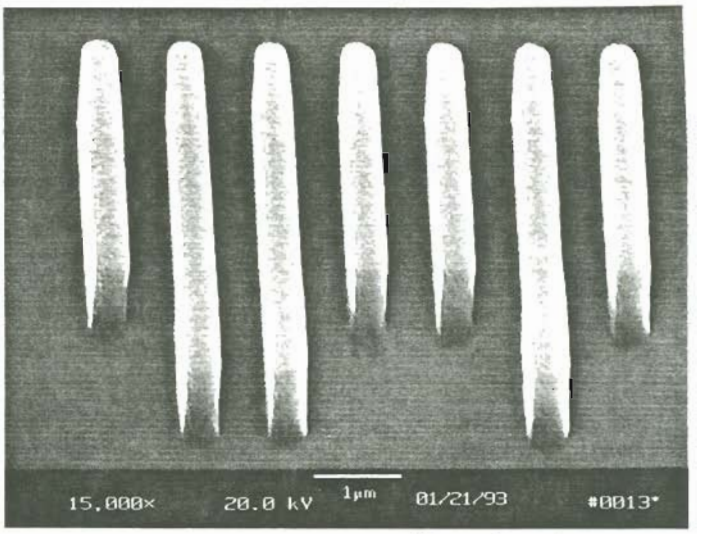

Partially coherent illumination
sigma =0.64

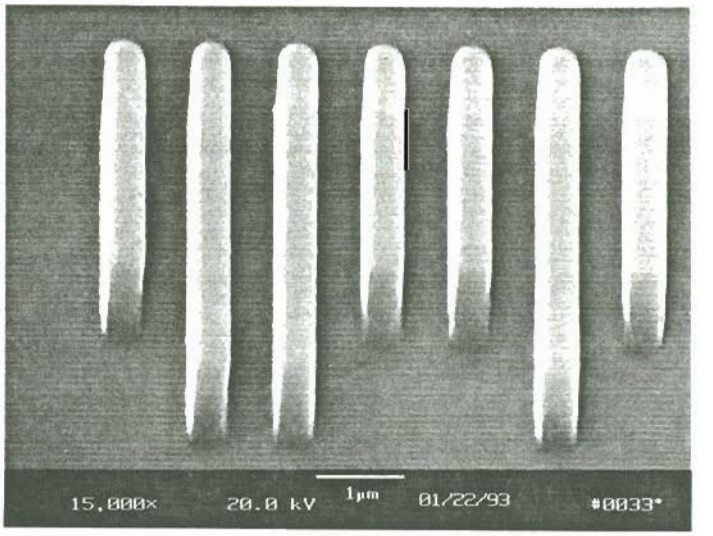

Off-Axis Illumination Annular

Figure 45. +0.90 micron Defocus condition for 0.50 micron linewidths.

H. Sub-resolution defocus proximity correction mask structures

The first solution to correct the degradation of the exterior features in the defocus mode with off-axis illumination was the use of a special modified outrigger structure on the reticle. Figure 46 shows the prototype structures evaluated here. These outrigger structures are designed to be sub-resolution for the optical system used here, which means they should not print. These subresolution structures are placed adjacent to the exterior features and are designed to protect them from the oblique scattered light in the defocus mode. While it was shown here that these structures did reduce the positive photoresist defocus proximity effect (figures 47-49), they tended to print as shown in figure 50. Further optimization of the design in regards to shape, size, and location is required to make this technique practical.

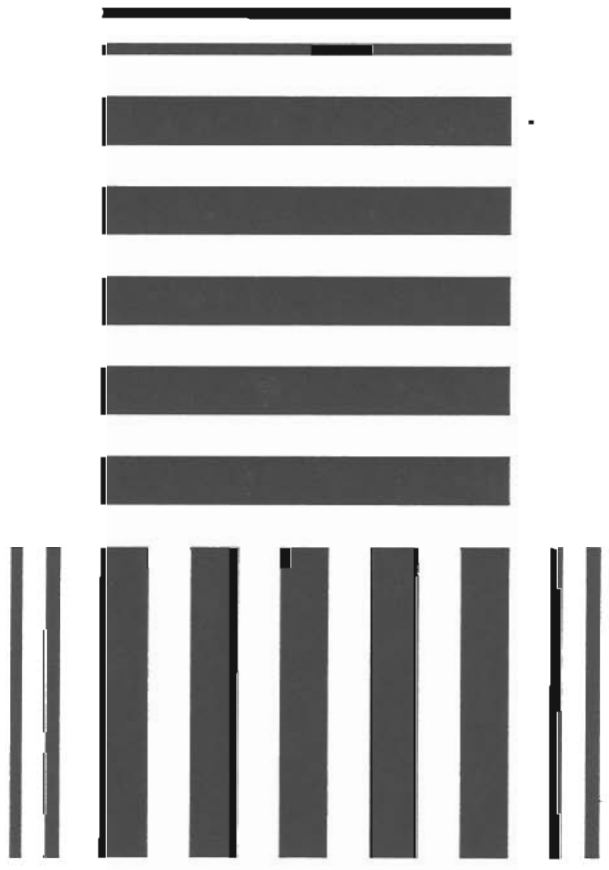

figure 46 Prototype resolution structure with 0.10μ sub resolution defocus proximity correctors

1. Critical dimension vs defocus curves

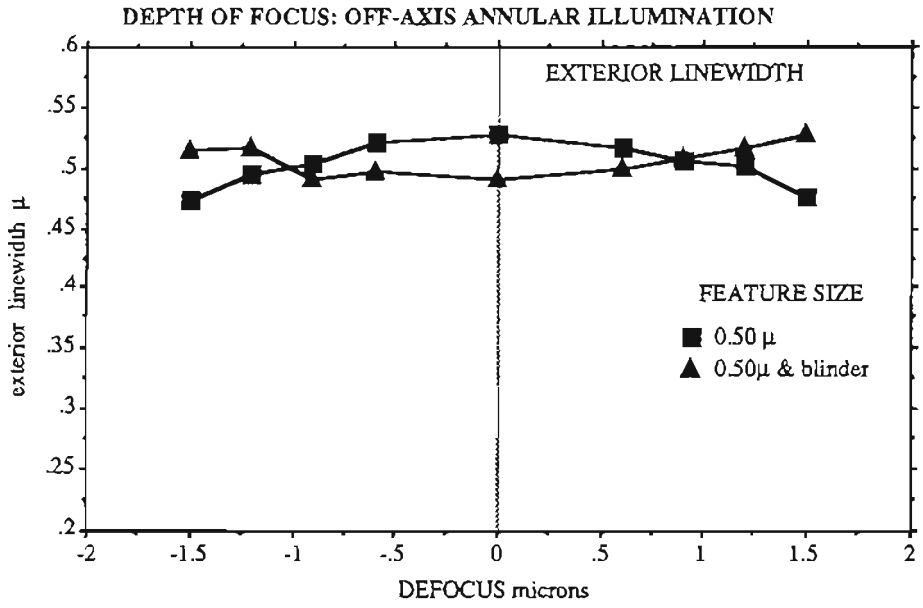

figure 47 Effect of sub-resolution structure on 0.50 micron linewidth depth of focus

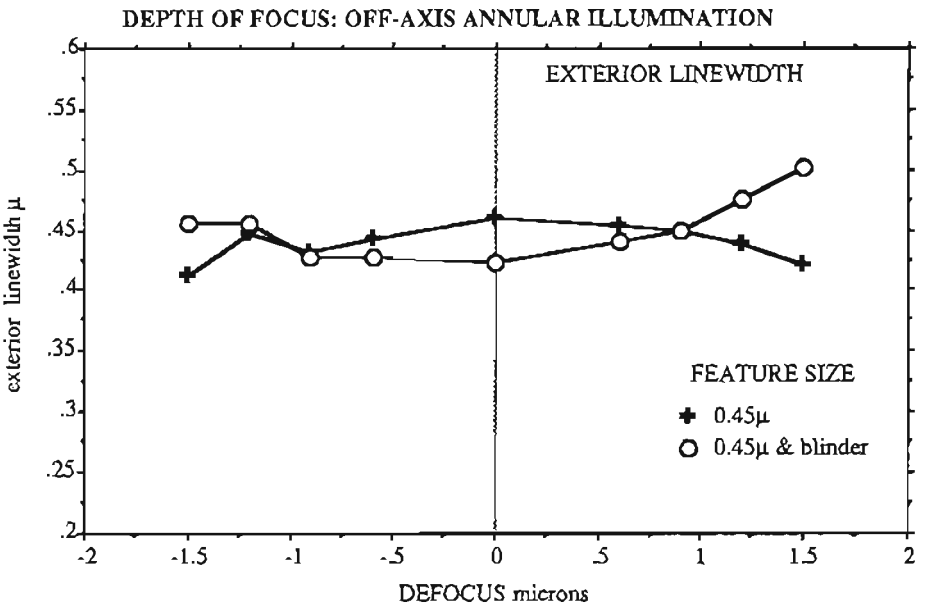

figure 48 Effect of sub-resolution structure on 0.45 micron linewidth depth of focus

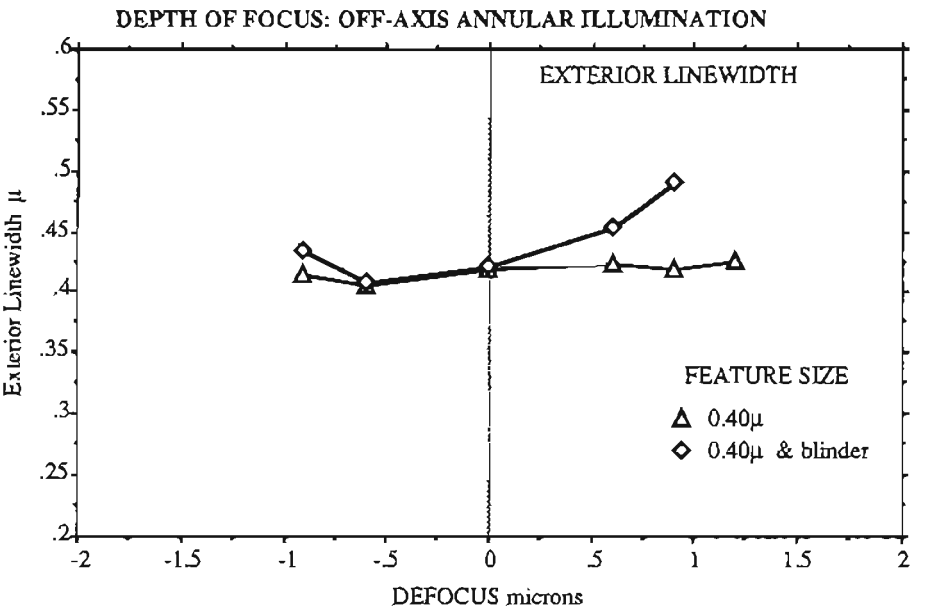

figure 49 Effect of sub-resolution structure on 0.40 micron linewidth depth of focus

2. Photoresist cross-section SEM micrographs of 0.45 micron linewidths with sub-resolution structures

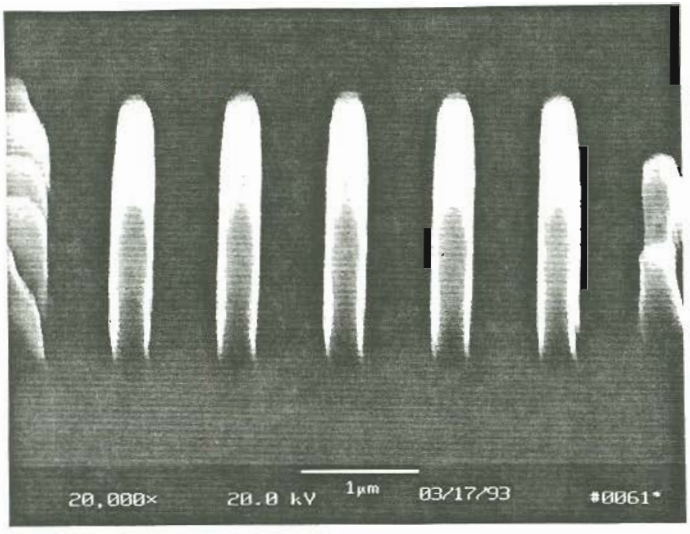

no sub-resolution
correction Defocus: -1.20μ

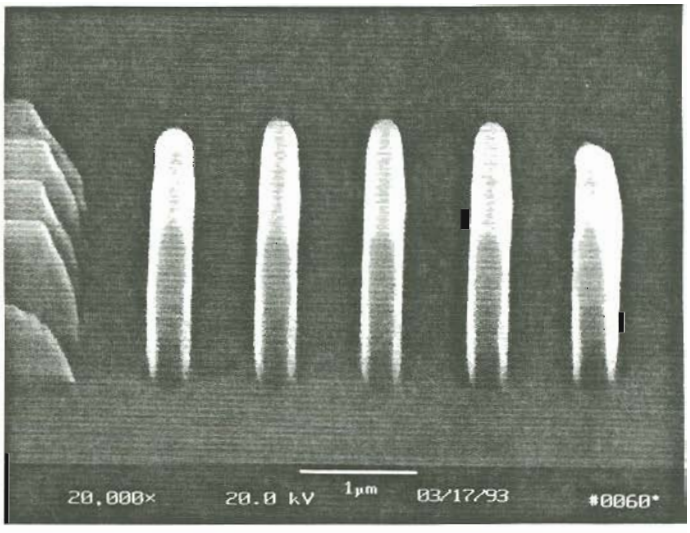

sub-resolution
correction Defocus: -1.20μ

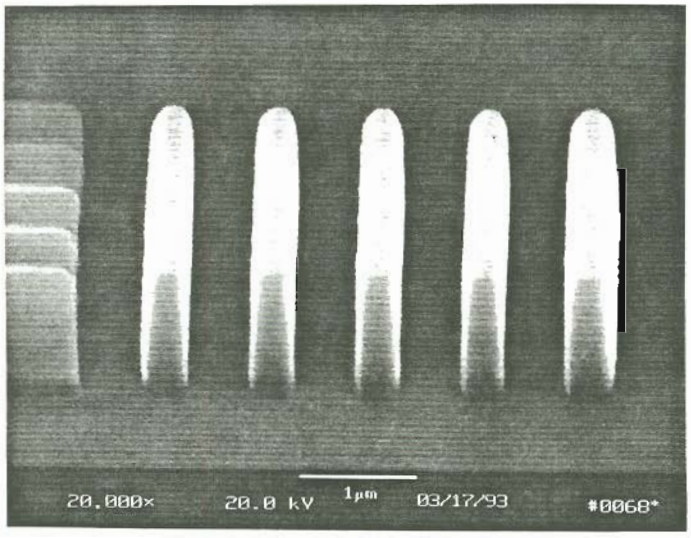

no sub-resolution
correction Defocus: 0.00μ

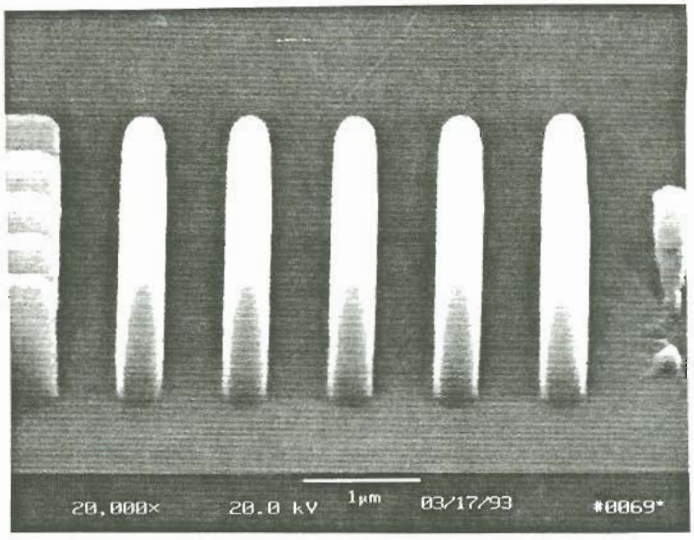

sub-resolution
correction Defocus: 0.00μ

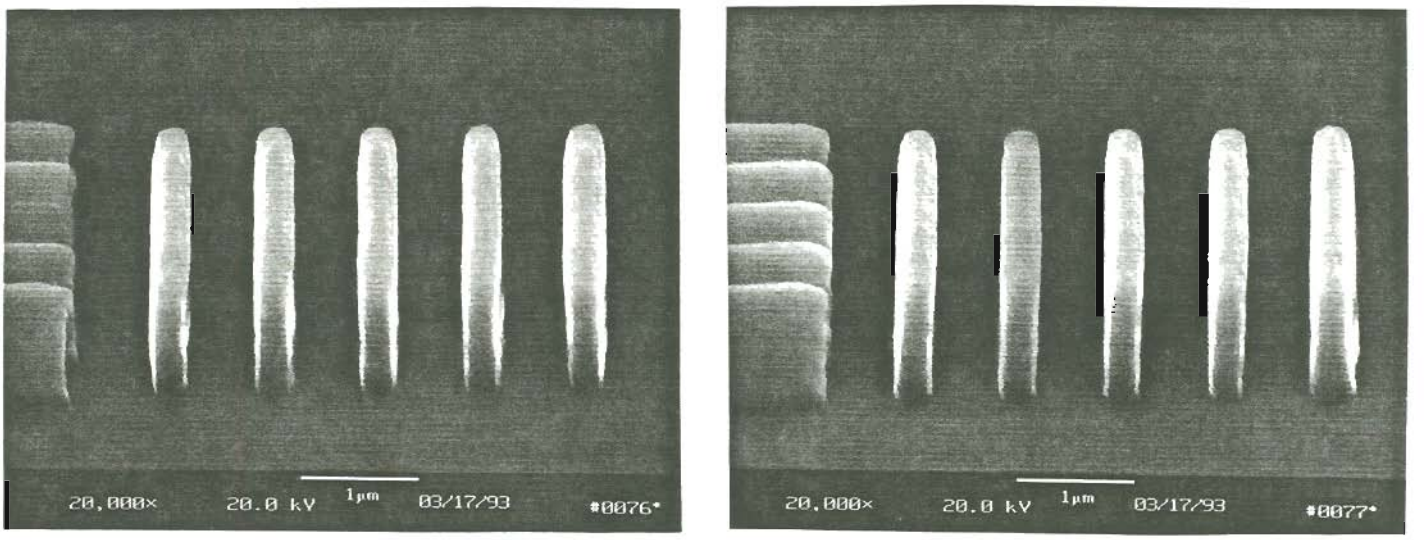

no sub-resolution correction Defocus: +1.20μ

sub-resolution correction Defocus: +1.20μ

figure 50 SEM micrographs of 0.45μ lines with and without sub-resolution correctors

H. "Super high contrast" photoresist process defocus proximity correction

1. Critical dimension vs defocus curves

Figures 51 through 56 show the effect of MicroSi WS365 contrast enhancement material CEM on the exterior linewidth degradation in the defocus mode with off-axis illumination. The positive photoresist exposure dose without the CEM was 150mj/cm2, while with the CEM overcoat the dose was 350mj/cm2. No improvement was seen on the feature sizes evaluated here using this material.

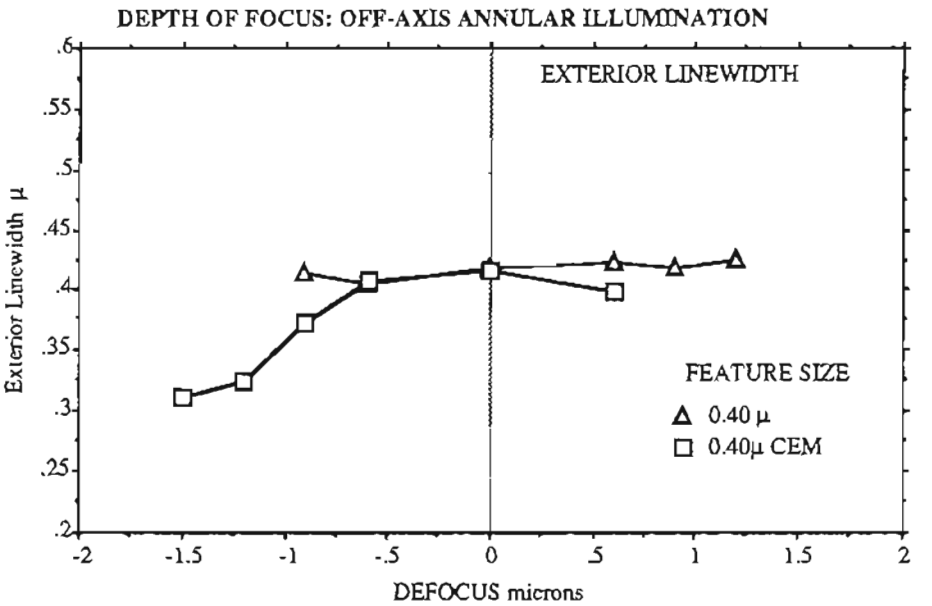

figure 51 Effect of contrast enhancement on 0.40µ exterior linewidth DOF for annular illumination.

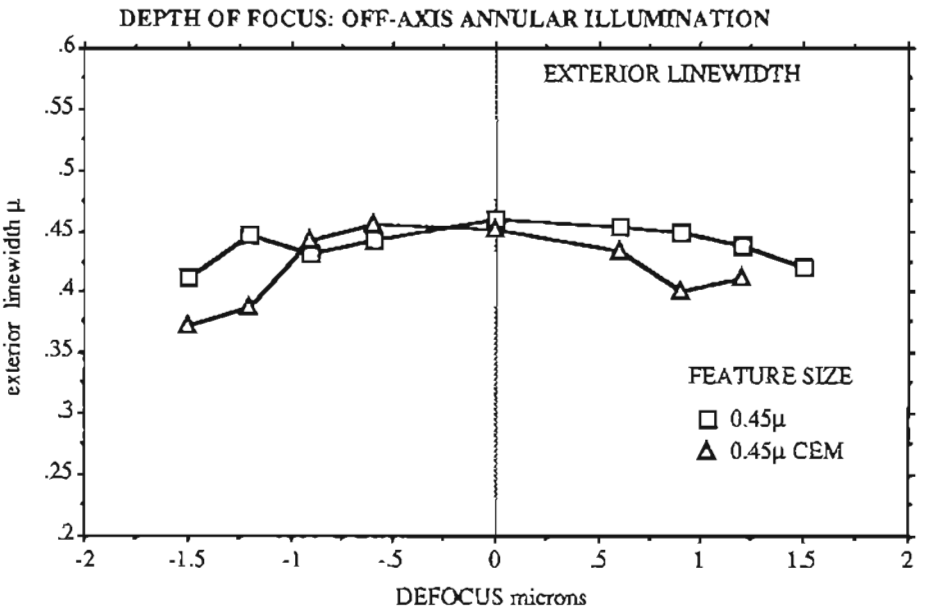

figure 52 Effect of contrast enhancement on 0.45µ exterior linewidth DOF for annular illumination.

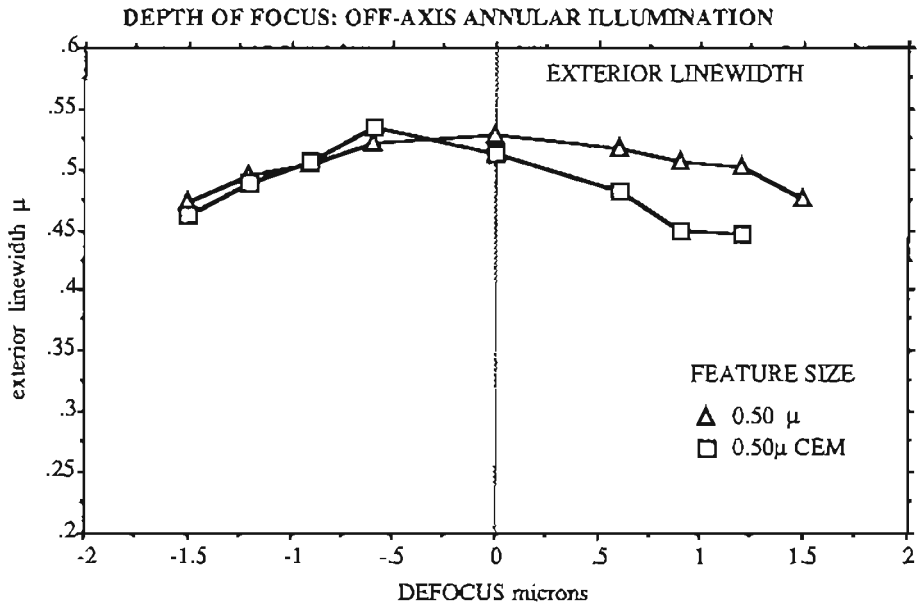

figure 53 Effect of contrast enhancement on 0.50μ exterior linewidth DOF for annular illumination.

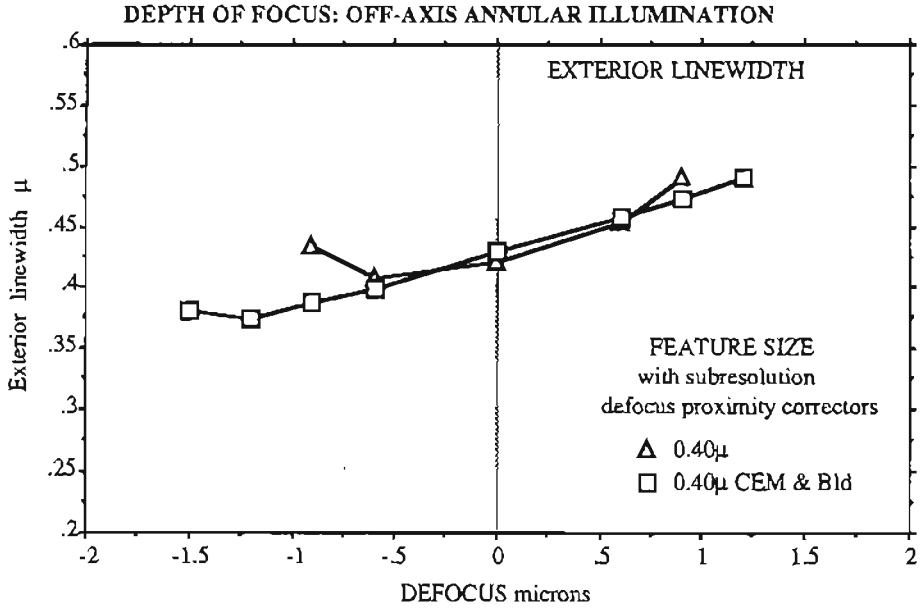

figure 54 Effect of contrast enhancement and sub-resolution correctors on 0.40μ exterior linewidth DOF for annular illumination.

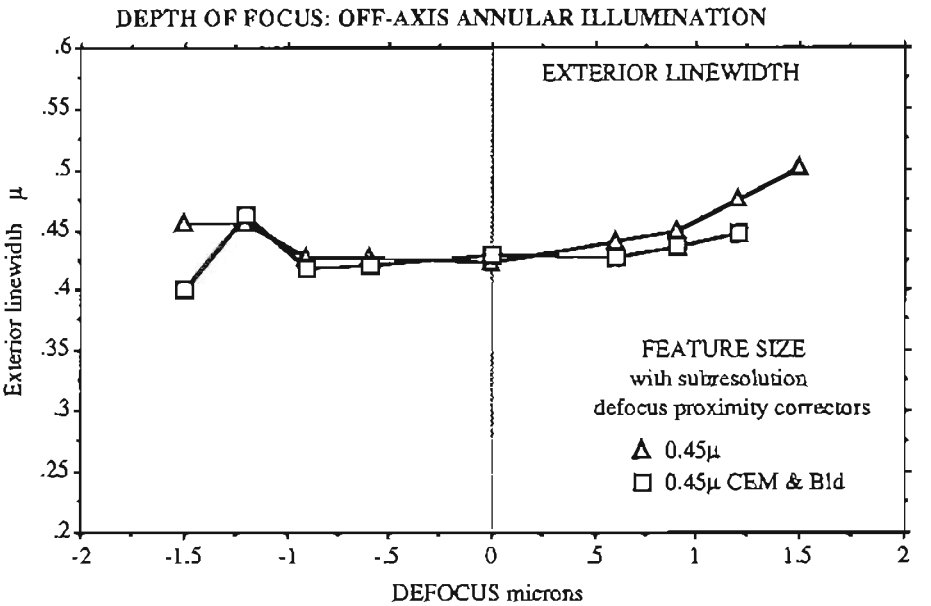

figure 55 Effect of contrast enhancement and sub-resolution correctors on 0.45μ exterior linewidth DOF for annular illumination.

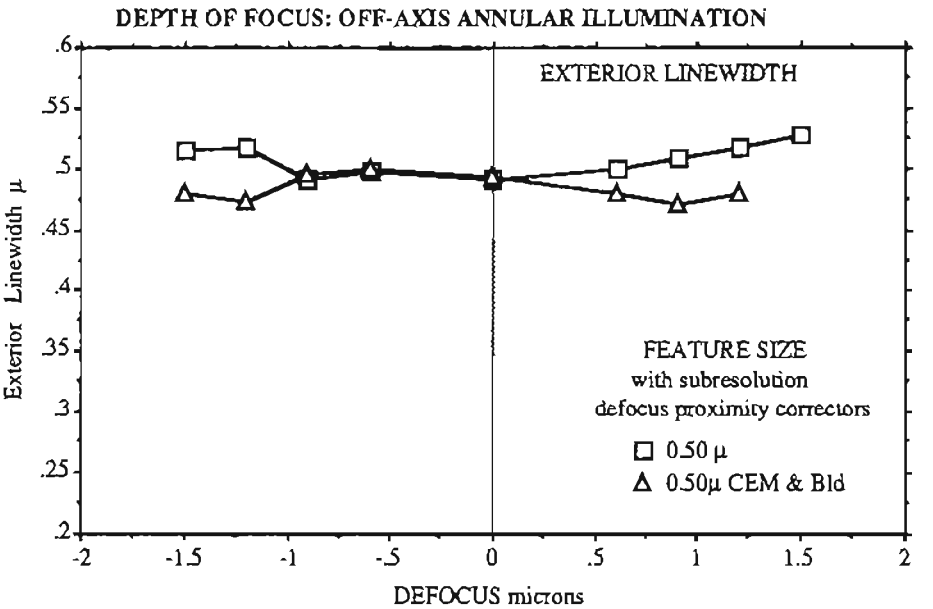

figure 56 Effect of contrast enhancement and sub-resolution correctors on 0.50μ exterior linewidth DOF for annular illumination.

2. Photoresist cross-section SEM micrographs of 0.40 micron lines with CEM with and without subresolution correctors

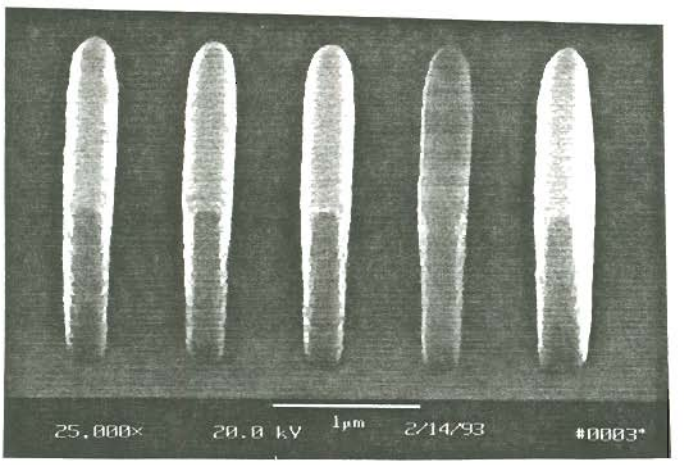

CEM without sub-resolution correction Defocus: -0.90μ

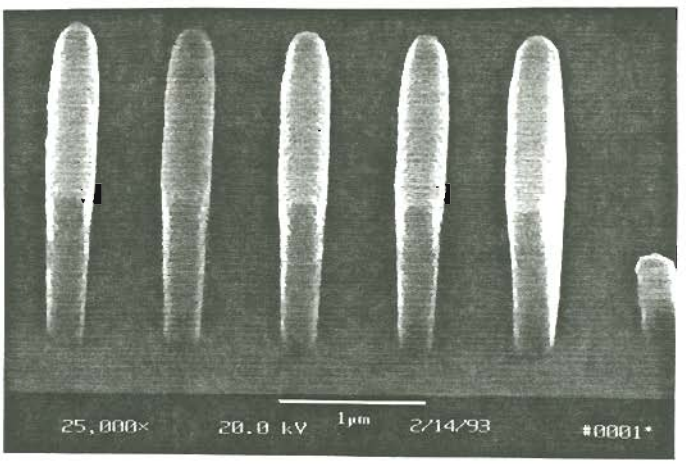

CEM with sub-resolution correction Defocus: -0.90μ

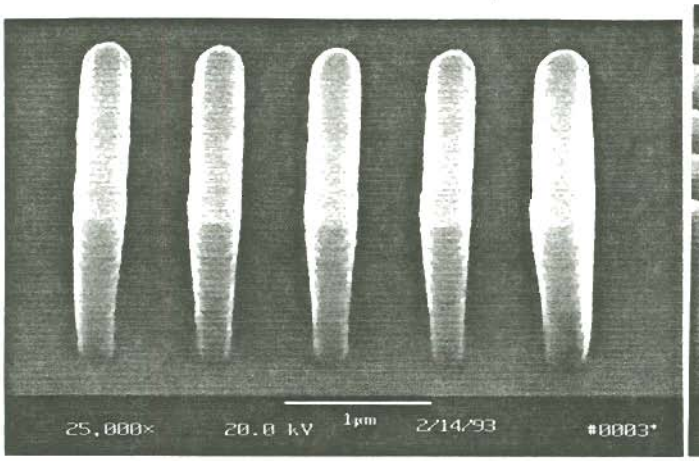

CEM without sub-resolution correction Defocus: 0.00μ

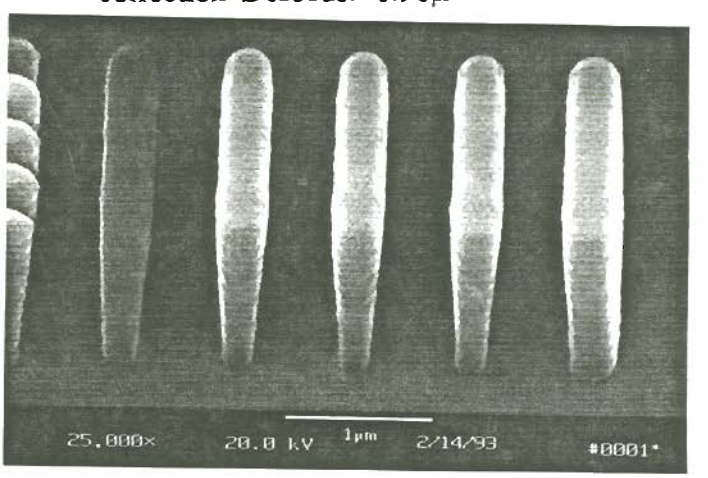

CEM with sub-resolution correction Defocus: 0.00μ

figure 57a SEM micrographs of 0.40μ pos. photoresist and CEM linewidths with and without sub-resolution correctors as exposed with quadrupole illumination.

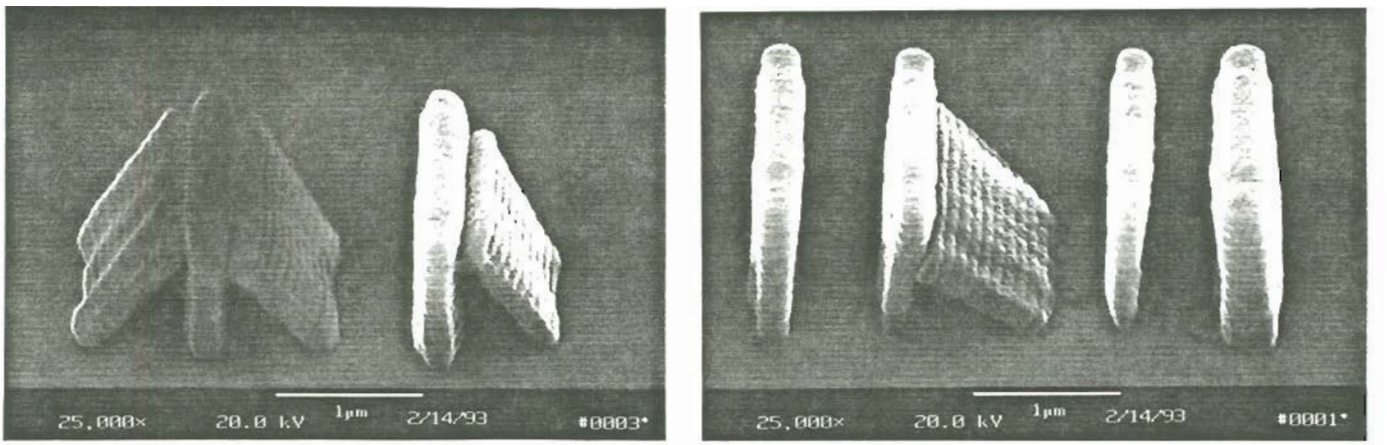

CEM without sub-resolution correction Defocus: +1.20μ

CEM with sub-resolution correction Defocus: +1.20μ

figure 57b SEM micrographs of 0.40μ pos. photoresist and CEM linewidths with and without sub-resolution correctors as exposed with quadrupole illumination.

It can be seen with the CD-defocus curves and SEM micrographs that the depth of focus with contrast enhancement processing offers no depth of focus improvement over standard processing for sub-half micron features. This was caused by the sub-half micron linewidths having retrograde sidewalls and falling over due to mechanical stress in the negative defocus mode. The retrograde sidewalls are believed to be caused by diffraction from the CEM edge, which has been discussed in detail by Brown and Mack at SPIE in 1988 [27]. The depth of focus was improved for features greater than 0.50 microns with the CEM, because the retrograde sidewall to photoresist width ratio is less and the lines remain up-right..

I. Anti-reflective coating photoresist process

Brewer Science, Inc. ARC-XLT organic spin on anti-reflective coating was applied to the silicon substrates prior to spin coating the photoresist. The reflectivity at 365nm was varied between 1.5% to 100% (no coating) by changing the coating thickness. The idea for this approach was obtained from the work of Fehrs etal [11]. They claimed that the off-axis illumination proximity effects could be caused by oblique reflected and scattered light from the substrate. They proposed the use

of an anti-reflective substrate coating to correct the problem. This approach was tried here without success as shown by the CD vs defocus curves in figures 58 through 60 for different substrate reflectivities. The different substrate reflectivities did slightly change the optimal exposure dose to produce a specific critical dimension target.

1. Critical dimension vs defocus curves

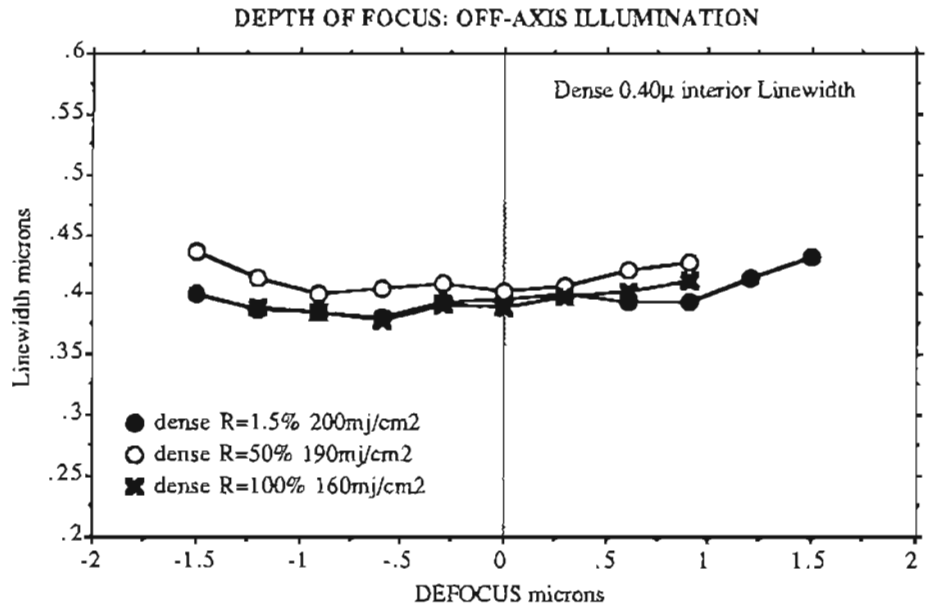

figure 58 Effect of bottom anti-reflective coating on 0.40 micron interior linewidth DOF for annular illumination.

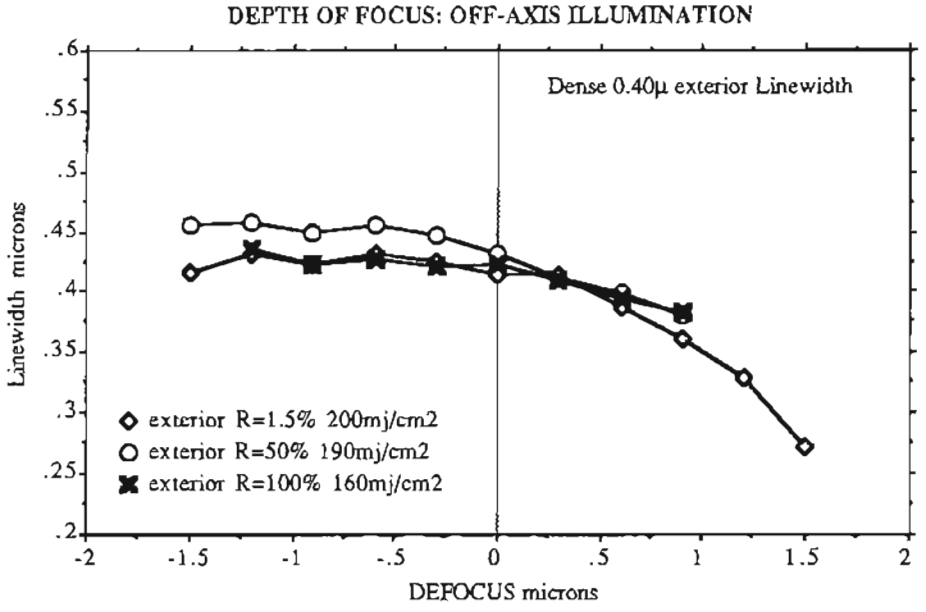

figure 59 Effect of bottom anti-reflective coating on 0.40 micron exterior linewidth DOF for annular illumination.

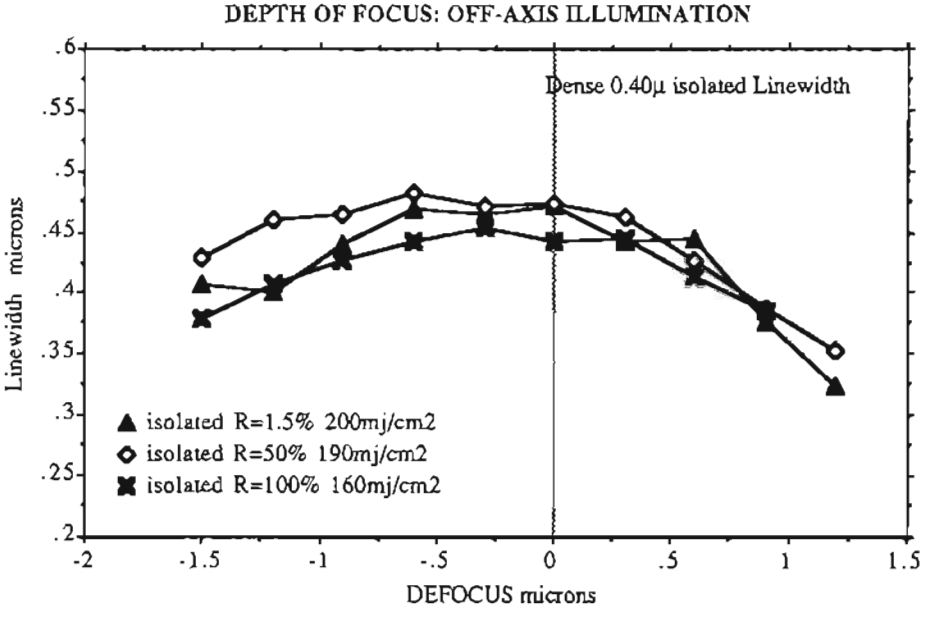

figure 60 Effect of bottom anti-reflective coating on 0.40 micron isolated linewidth DOF for annular illumination.

IV. SIMULATION RESULTS

Silvacos SOLID 3.1 was used to simulate the experimental results obtained here. The simulator was calibrated to the particular positive photoresist process used here. This was done by inputting a table of the photo active compound concentration and development rate into the job deck. The photo active compound concentration for each exposure dose was obtained using Dills[30] ABC parameters for the positive photoresist and the SOLID simulator. An experiment was run to determine the actual development rates in μ/min of the photoresist by measuring the photoresist thickness remaining for different development times for each exposure dose. The optical simulator also had to calibrated to actual exposure dose used for each illumination condition. This was done by inputting an intensity statement into the job deck. A sample SOLID job deck is in appendix 1.

There was a good correlation between the simulated linewidths and experimental for all defocus conditions with the different illumination conditions. The largest deviations were for dense linewidths with off-axis illumination , which may be caused by actual experimental error and inaccuracies in the illumination and photoresist process model. An optical simulator can never exactly predict a particular set of experimental data. An optimized simulation tool will have the same trend or change in a response parameter as the experimental data. This is because the experimental data has random errors or variations between different runs, while the simulator or model does not. This means that if the simulator were perfect it would accurately predict the average outcome of many replicated experimental trials.

A. Isolated linewidth critical dimension vs defocus curves

Figures 61 through 63 show the SOLID simulated isolated positive photoresist critical dimensions compared to the actual experimentally Hitachi SEM measured photoresist dimensions. Excellent correlation was achieved after the SOLID model was calibrated for the particular photoresist used here.

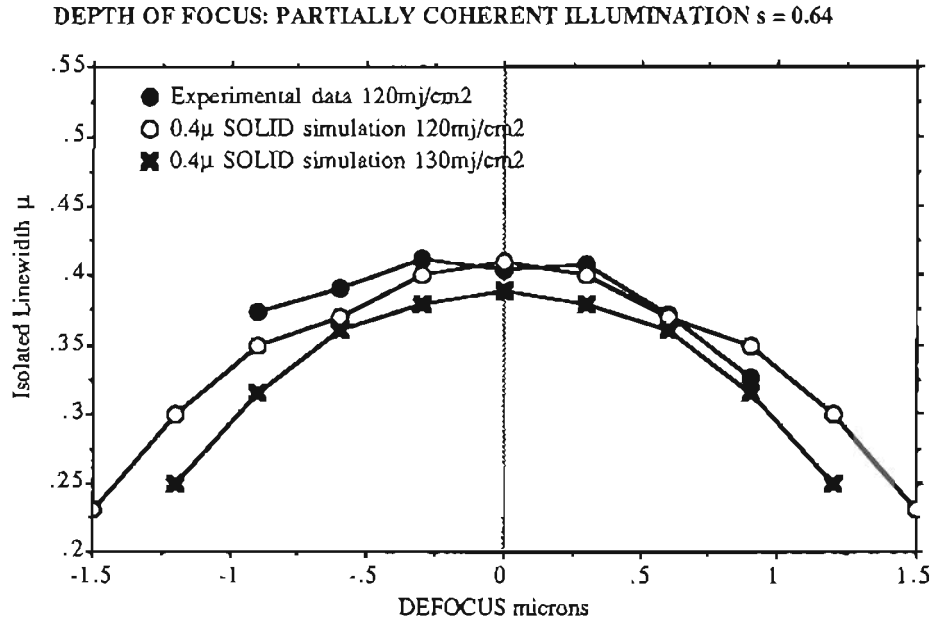

Figure 61. Experimental vs SOLID simulated DOF for isolated 0.4μ linewidths and partially coherent illumination .

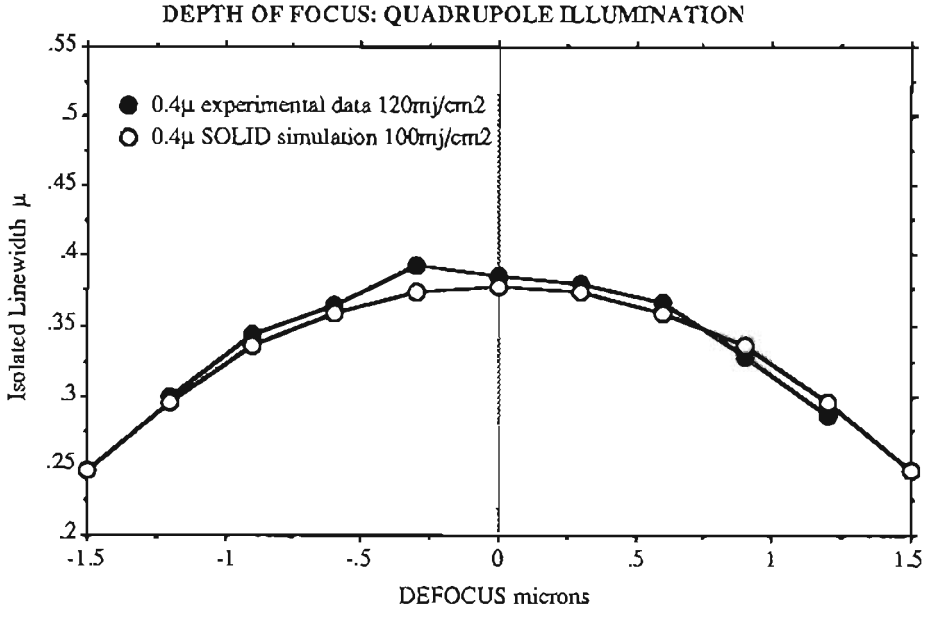

Figure 62. Experimental vs SOLID simulated DOF for isolated 0.4μ linewidths and quadrupole illumination .

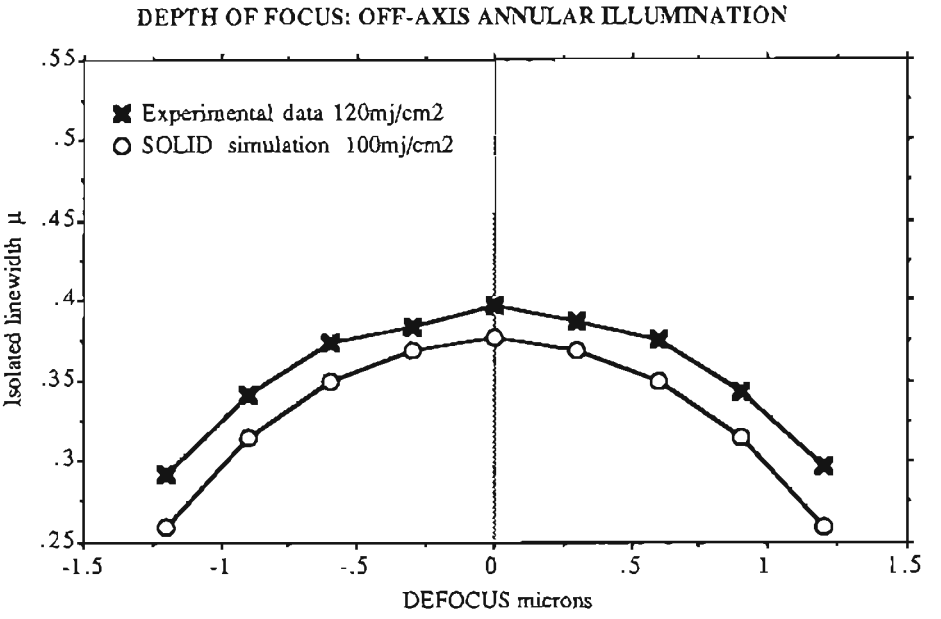

Figure 63. Experimental vs SOLID simulated DOF for isolated 0.4µ linewidths and annular illumination .

B. Dense linewidths (grating type features) critical dimension vs defocus curves

Figures 64 through 69 show the SOLID simulated dense positive photoresist critical dimensions compared to the actual experimentally Hitachi SEM measured photoresist dimensions. The SOLID model handled the defocus proximity effects with the off-axis illumination techniques fairly well as indicated by the defocus curved shown below for interior and exterior linewidths.

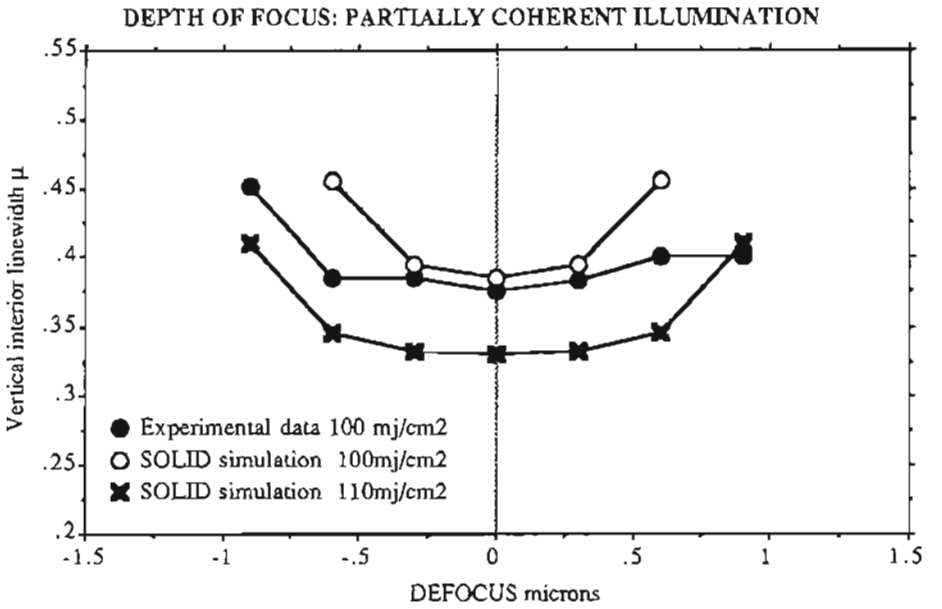

Figure 64. Experimental vs SOLID simulated DOF for dense vertical interior 0.4µ linewidths and partially coherent illumination (s=0.64).

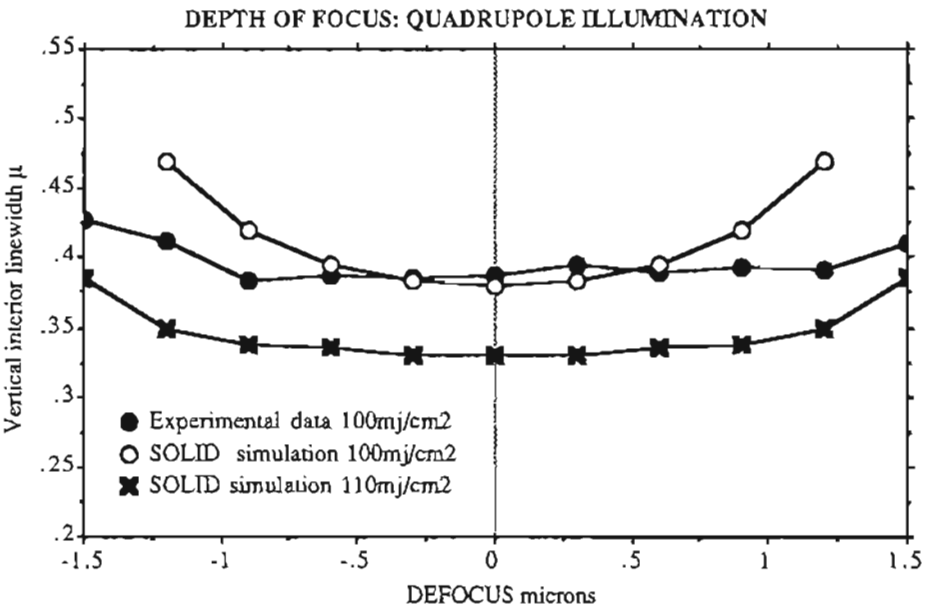

Figure 65. Experimental vs SOLID simulated DOF for dense vertical interior 0.4µ linewidths and quadrupole illumination. (s=0.26; offset s = 0.64)

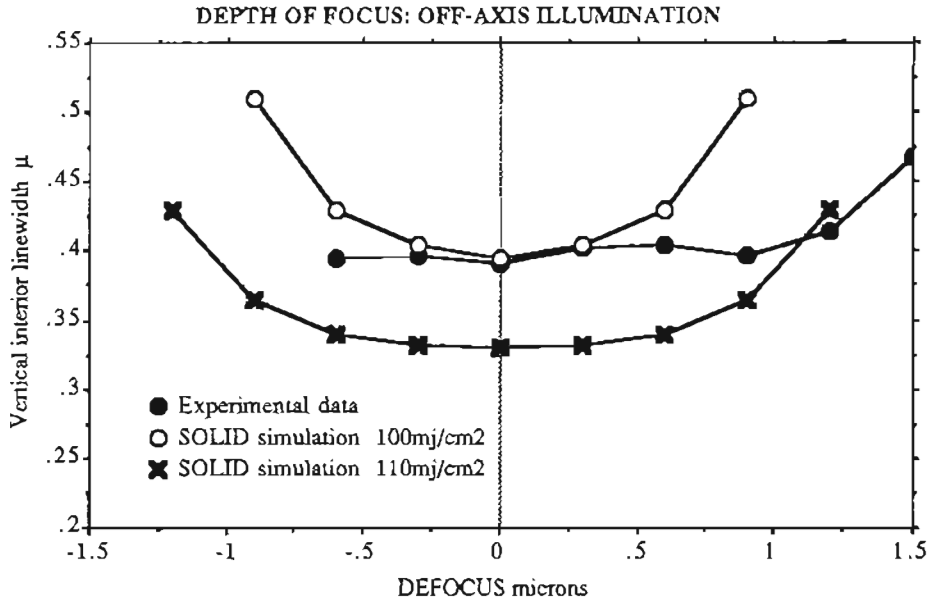

Figure 66. Experimental vs SOLID simulated DOF for dense vertical interior 0.4µ linewidths and annular illumination. (inner s=0.40; outer s = 0.70).

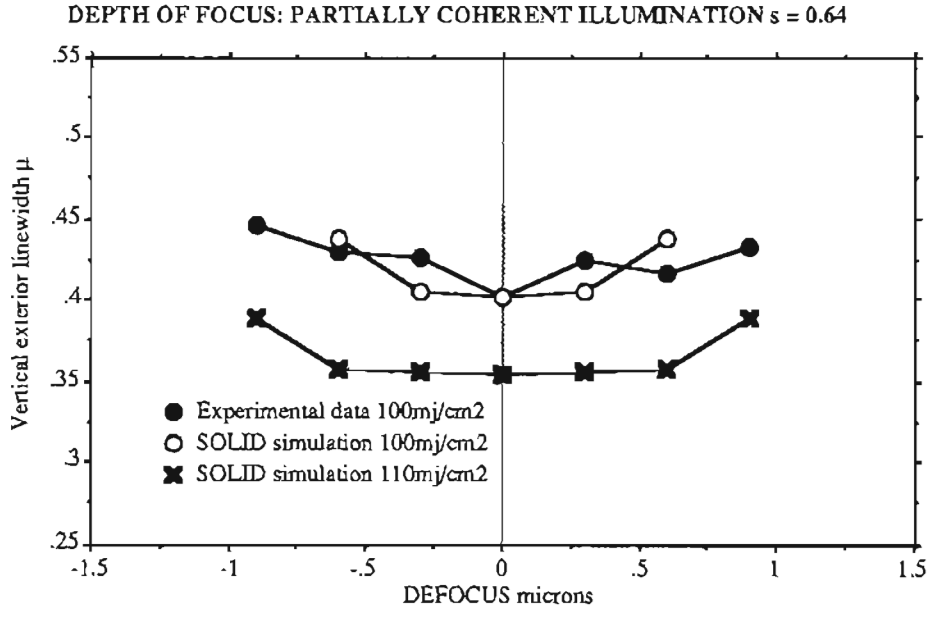

Figure 67. Experimental vs SOLID simulated DOF for dense vertical exterior 0.4µ linewidths and partially coherent illumination (s=0.64).

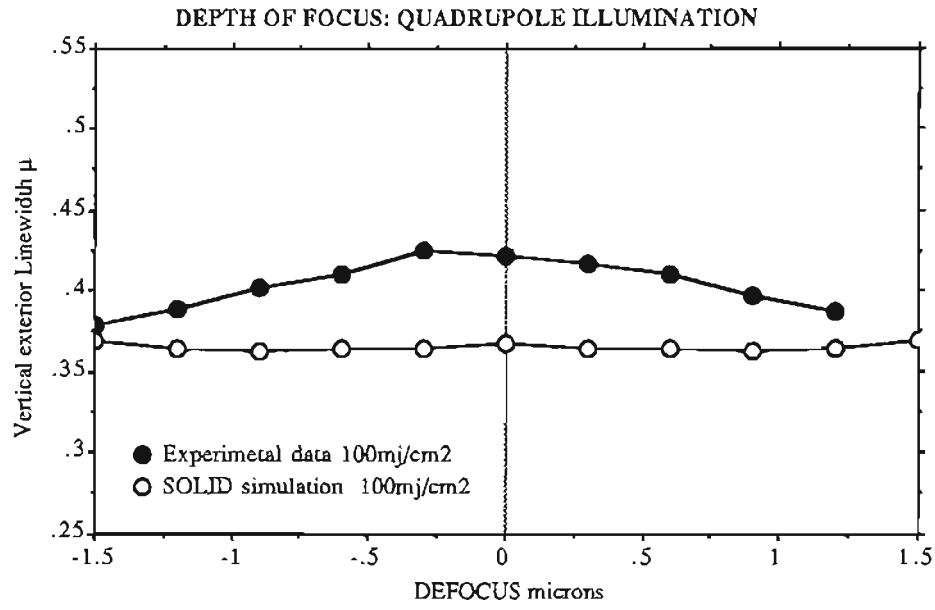

Figure 68. Experimental vs SOLID simulated DOF for dense vertical exterior 0.4µ linewidths and quadrupole illumination. (s=0.26; offset s = 0.64)

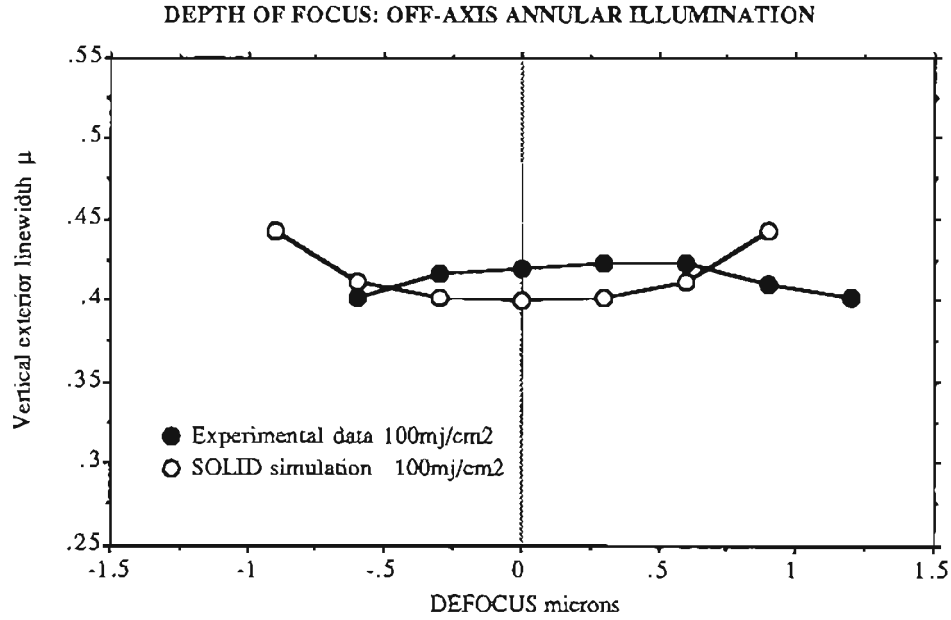

Figure 69. Experimental vs SOLID simulated DOF for dense vertical exterior 0.4µ linewidths and annular illumination. (inner s=0.40; outer s = 0.70).

C. Aerial image diagrams

Figures 70 through 72 show SOLID simulated aerial image intensity profiles for dense 0.40μ linewidths with partially coherent, quadrupole, and annular illumination at 0.0 and 1.5 micron focus conditions. The structure used was the same as the one illustrated in figure 12 with defocus proximity correction mask structures adjacent to the extreme left linewidth. The SOLID model predicts the increase in contrast for the off-axis illumination as shown by the larger aerial image intensity amplitude. The defocus proximity effect with the off-axis illumination techniques for the extreme left exterior linewidth is reduced using the correctors as shown by the increase in image contrast. The SOLID model predicts the highest contrast images and largest depth of focus is achieved with the quadrupole off-axis illuminator. This was verified with the experimental results presented in the body of this document.

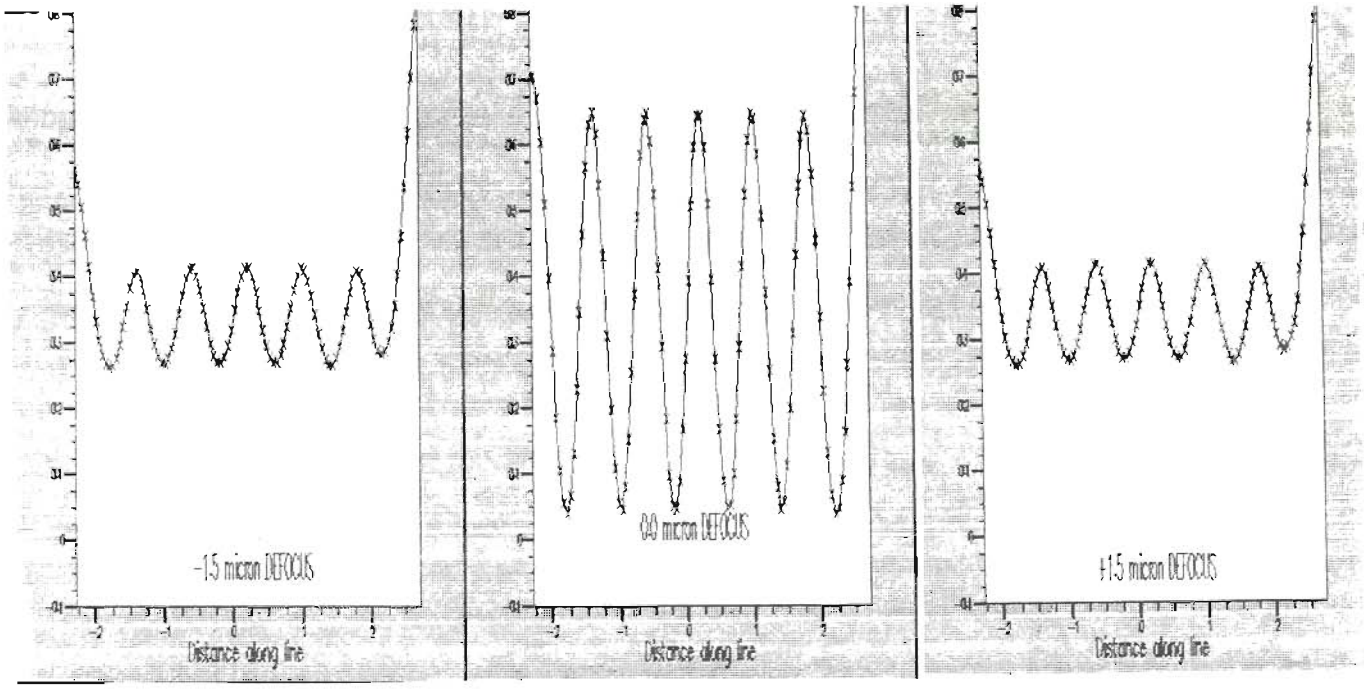

Figure 70. SOLID simulated aerial images for dense 0.4μ linewidths and partially coherent illumination.

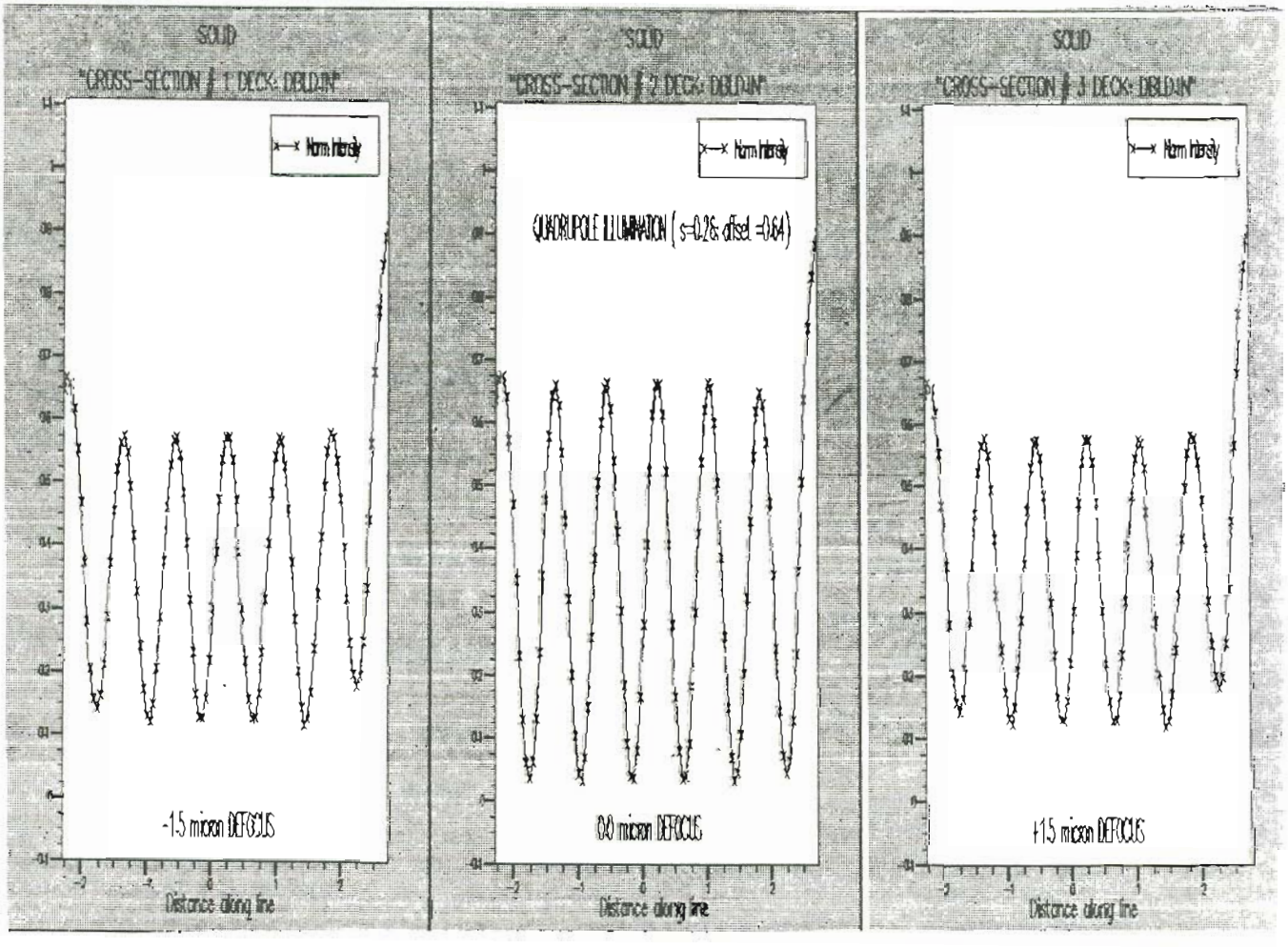

Figure 71. SOLID simulated aerial images for dense 0.4μ linewidths and quadrupole illumination.

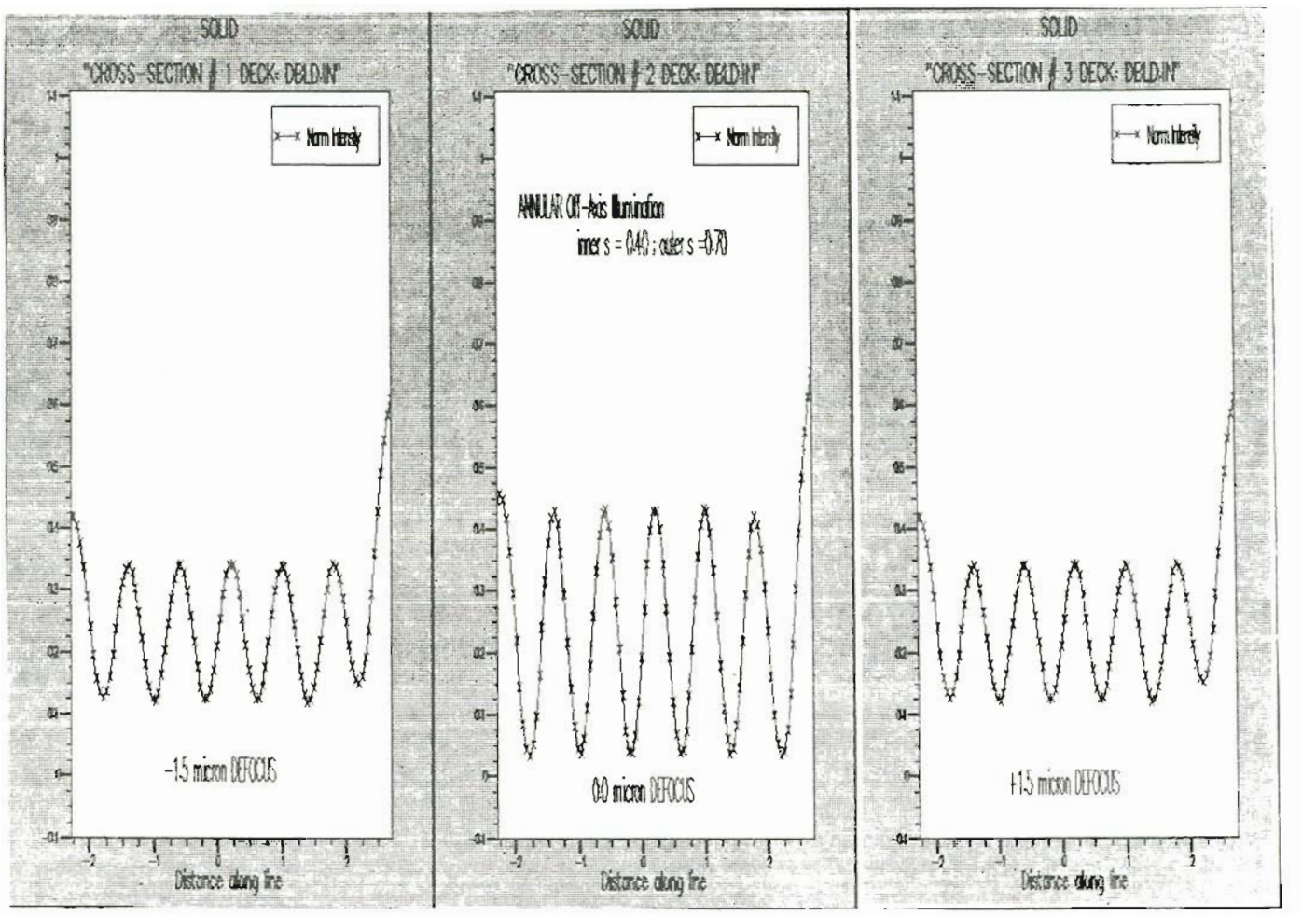

Figure 72. SOLID simulated aerial images for dense 0.4μ linewidths and annular illumination.

V. CONCLUSIONS

The results presented here show that significant gains in DOF can be achieved by using off-axis illumination. The defocus proximity effects are believed to be caused by scattered oblique rays from low resolution areas adjacent to high resolution areas. It was demonstrated that this effect can be reduced through the use of special reticle correction structures. Further design work is required to make these structures a practical solution. Silvacos optical simulator SOLID was found to be a valuable tool for evaluating the effect of these advanced off-axis illumination techniques. Excellent correlation to experiment results was achieved with the simulator calibrated to the actual process used.

The significant gains in process control with off-axis illumination through improvements in image quality, photoresist defocus thickness loss and depth of focus make it a requirement for sub-half micron processes. Off-axis annular is a better solution than quadrupole illumination for all feature types, because of its benefit to isolated and oblique (45º) features. Quadrupole illumination produces the highest image contrast and largest defocus improvement only for vertical and horizontally oriented features. To make off-axis illumination a viable solution for high volume manufacturing as an equipment upgrade to existing systems, the problem of decreased irradiance needs to be corrected. One promising solution to this problem has been reported by W.N. Partlo etal with GCA [25]. They developed an zoomable axicon system which moves the mercury arc lamps energy away from the optical axis into the desirable off-axis annular regions. Axicons are prism like optical components placed in the illumination light path, which convert the gaussian-like beam into a ring shaped beam.

APPENDIX

Sample SOLID 3.1 input job deck for SUN work station

This input deck can be used for each of the three illumination types evaluated here. each can be turned on by removing the # signs in front of each line statement. This input deck can generate aerial image 2D profiles with the "plot cross_section" statement, photoresist cross sections with the "plot layers" statement, CD vs defocus curves with the "plot smile" statement, and the reticle pattern and cross section area with the "plot mask" statement.

```
                    SOLID Input Deck: Offaxis.in
                       Steve Brainerd 2/9/93

#
reset image_mode /fsa
# next command will
# loop focus from -1.5 to +1.5 microns in 0.3 micron increments
loop /#i=-1.5,1.5 0.3
#
# standard partially coherent illumination
# define system=illumination /shape=circle /lambda=0.365 /sigma=0.64
# define system=illumination /tilt= 0.0,0.0 /intensity= 1.20
# This intensity is used to calibrate the simulators dose to the experimental
# exposure dose
#
# quadrupole illumination
# define system=illumination /shape=shrinc /radius=0.26 /offset=0.64
# define system=illumination /angle=45 /lambda=0.365 /sigma=0.70
# define system=illumination /tilt= 0.0,0.0 /intensity= 1.17
#
# annular illumination
# define system=illumination /shape=circle /lambda=0.365 /sigma=0.70
# define system=illumination /filter=0.00,0.57,0.00,0.00
# define system=illumination /tilt= 0.0,0.0 /intensity= 1.75
#
delete filter /all projection
define system=projection /shape= circle /NA=0.48 /flare=0.0
#
set defocus =#i
#
# define window for the dense features on this mask
# set window =-0.60,0.85,0.20,0.95
# define window for the isolated features on this mask
set window =-0.40,0.85,0.40,0.95
```

```
set image_points-100,3
delete mask_data /all
# input dense 0.40 micron equal line space pair mask pattern
# load data /mask_data /formatted /file=dense04.msk
# input isolated 0.40 micron line mask pattern
load data /mask_data /formatted /file=isolated04.msk
#
# Next command will
# set cross-section for aerial image simulation.
# The window for the simulation is a horizontal rectangle with
# "Y" coordinates 0.85um and 0.95um
# (contains 3 image points along the Y direction)
# and an "x" distance of 0.80um (with 100 points)
# cross-section goes through the center of this window at Y=0.90um
# and parallel to the X-axis.
#
preset aerial_image=cross_section /x_orientation=0.9
#
run image /log /no_table /evaluate
#
plot cross_section
#
#
delete layer /all
delete top_coating
#
define resist /sublayers=90 /interpolation=30
#
define resist /index=1.700,-0.0200 /thickness=1.1800 /a=0.7300 /b=0.0700
define resist /c=0.0170 /type=novolac /name=oir_POSRES
set layers = 1
define substrate /index=6.55,-2.705
#
# loop exposure dose
loop /#d=100.0,170.0 10.0
set dose =#d
run exposure /no_log
#
set diffusion_length-0.05
set thickness_loss=0.
run post_exposure_bake /no_log
#
select development_rate_model=user
# next a table of PAC concenration for a given dose and the corresponding
# experimentally determined development rates (Å/min) for this photoresist/
# exposure tool/developer system is input
load data /development_rate /file=POSRES.dat /log
#
# Set cross section area for photoresist 2D profile parallel to x axis
set cross_section=0.9 /x
#
set development_time =60.0,0.0,0
```

```
set smoothing= on
run development /2d
#
compute cd/fex
plot layers
#
endloop
endloop
plot smile
plot mask
#
exit
```

REFERENCES

1. H.H.Hopkins, "The concept of partial coherence in optics", Proc. Roy. Soc. A208 (1951). pp.263

2. E.H.Linfoot and E.Wolf (The Observatories, University of Cambridge), "Diffraction Images in Systems with an Annular Aperture", Proc. Phys. Soc., Vol. B66, 1953, pp.145

3. W.T.Welford (Imperial College London England), "Use of Annular Apertures to Increase Focal Depth", Journal of the Optical Society of America, Vol.50, No. 8, August 1960, pp.749

4. B.M.Watrasiewicz (Imperial College London England), "Image formation in microscopy at high numerical aperture", Optica Acta, Vol.12, No. 2, 1965, pp.167

5. P.K.Mondal (University of Calcutta, Calcutta, India), "Phase contrast microscopy in partially coherent light", Optica Acta, Vol.15, No. 1, 1968, pp.65

6. W.J.Baldwin and J.R.Meyer-Arendt, US Patent 3598471 (1971), "Optical Contrast Enhancement System"

7. D.J/Cronin etal (Technical Operations, Inc.), "Dynamic Coherent Optical System", Optical Engineering, Vol.12, March/April 1973, pp.50

8. D.J/Cronin etal (Aerodyne Research, Inc.), "Equivalence of Annular Source and Dynamic Coherent Phase Contrast Viewing Systems", Optical Engineering, Vol.15, May/June 1976, pp.276

9. P.D. Robertson etal (Data General Corp.), "Proximity effects and influences of non-uniform illumination in projection lithography", SPIE vol.334 Optical Microlithography- Technology for the Mid-1980s (1982) pp.37

10. G. Reynolds (Honeywell), "A Concept for High Resolution Optical Lithography System for Producing One-Half Micron Linewidths", SPIE vol.633 Optical Microlithography V (1986) pp.228

11. D.L.Fehrs etal.(TEK), " Illuminator Modification of an Optical Aligner", KTI Microelectronics seminar Interface '89 (1989), pp.217

12. S. Asai etal (Fujitsu), "Improving projection lithography image illumination by using sources far from the optical axis", J.Vac.Sci. Technol. B9 (6) Nov/Dec 1991 pp. 2788

13. H.Fukuda etal (Hitachi), "Spatial filtering for depth of focus and resolution enhancement in optical lithography", J.Vac.Sci. Technol. B9 (6) Nov/Dec 1991 pp. 3113

14. K.Kamon etal. (Mitsubishi) , "Photolithography System Using Annular Illumination", Jpn. J. Appl. Phys. Vol 30, (1991) pp. 3021

15. S.Matsuo etal. (NTT), "High Resolution System Using Oblique Incidence Illumination", IEDM 1991 Proceeding Digest, (1991), pp. 32.7.1

16. M.Noguchi etal. (Canon), "Subhalf Micron Lithography System with Phase-Shifting Effect", SPIE vol.1674 Optical/Laser Microlithography V (1992) pp.92

17. N. Shiraishi etal.(Nikon) , "New Imaging Technique for 64M-DRAM", SPIE vol.1674 Optical/Laser Microlithography V (1992) pp.741

18. K. Tounai etal. (NEC), "Resolution Improvement with Annular Illumination", SPIE vol.1674 Optical/Laser Microlithography V (1992) pp.753

19. N. Shiraishi etal.(Nikon) , "SHRINC: A New Imaging Technique for 64 Mbit DRAM", Microlithography World, Vol.1, No.3, July/Aug. 1992, pp.7

20. K.Matsumoto & T.Tsuruta (Nikon), "Issues and method of designing lenses for optical lithography", Optical Engineering, Vol. 31, No. 12, Dec. 1992, pp. 2657

21. M.Endo etal. (Matsushita), "Challenges in Excimer Lithography for 256M DRAM and beyond", IEEE IEDM 1992 Proceeding Digest, Dec 1992 ,pp. 3.1.1

22. H.Fukuda etal. (Hitachi), "Characterization of Super-Resolution Photolithography", IEEE IEDM 1992 Proceeding Digest, Dec 1992 ,pp. 3.2.1

23. K.Kamon etal. (Mitsubishi) , "Photolithography System Using Modified Illumination", Jpn. J. Appl. Phys. Vol 32, (January 1993) pp. 239-243

24. P.Luehrmann etal (ASM Lithography), "0.35 micron lithography with off-axis ilumination", SPIE vol. 1927 Optical/Laser Microlithography VI (1993), presented March 1993 Steve Brainerd was a co-author on this paper,

25. W.N.Partlo etal (GCA/Tropel), "Depth of Focus and Resolution Enhancement for i-line and deep-UV Lithography Using Annular Illumination", SPIE vol. 1927 Optical/Laser Microlithography VI (1993), presented March 1993

26. Ho-Young Kang etal (Samung), "A new methd of Tilted Illumination using grating Mask; ATOM (Advanced Tilted illumination On Mask)", SPIE vol. 1927 Optical/Laser Microlithography VI (1993), presented March 1993

27. M.M.OToole & A.R.Neureuther. (UC Berkeley), "Influence of partial coherence on projection printing", SPIE vol.174 Developments in Semiconductor Microlithography IV (1979) pp.22

28. M.Lacombat and G.M.Dubroeucq. (Thomson CSF), "Coherent illumination improves step and repeat printing on wafers", SPIE vol.174 Developments in Semiconductor Microlithography IV (1979) pp.28

29. T.Brown and C.Mack (GE), "Comparison of modeling and experimental results in contrast enhancement lithography", SPIE vol.920 Advances in Resist Technology and Processing (1988) pp.391

30. Dill (IBM), "Comparison of modeling and experimental results in contrast enhancement lithography", iEEE (1975) pp.391

31. B.Katz etal (ASM Lithography), "Definition of 0.5 micron Contacts for Advanced Integrated Circuit Production", KTI Microelectronics Seminar, Interface '90, (1990) pp. 147

32. J.W.Goodman, Introduction to Fourier Optics, McGraw-Hill, N.Y., (1968)

33. S.Olsen etal.,"Optimizing NA and Sigma for Sub-Half Micron Lithography", SPIE vol. 1927 Optical/Laser Microlithography VI (1993), presented March 1993

BIOGRAPHICAL SKETCH

Steven K. Brainerd was born in Englewood New Jersey on July 7, 1952. He received his B.S. degree in Photographic Science and Engineering from Rochester Institute of Technology in 1974. Steve is presently finishing his M.S.E.E. with emphasis on semiconductor processing from the Oregon Graduate Institute, where he has attended since 1990. He currently is a senior photolithographic engineer at Micron Semiconductor, Inc. working on sub-half micron photolithographic process development modules such as phase shift masks, off-axis illumination, negative i-line photoresist, optical simulation tools such as SOLID 3.1, and advanced positive photoresists. His interests include optical and photo processing applications for advanced microlithographic integrated circuit manufacture. Prior to joining Micron in June 1992, Mr. Brainerd held photographic process engineering positions at Bipolar Integrated Technology, Intel, and the photographic film industry. Mr. Brainerd co-authored two recent papers presented at the 1993 SPIE Optical Microlithography Seminar held in March on off-axis illumination and rim phase shifted spaces.

Publications:

1. "0.35 micron lithography using off-axis illumination", P.Luehrmann, P.vanOorschot, H.Jasper, S.Stalnaker, S.Brainerd, B.Rolfson, and L.Karklin, 1993 SPIE Optical Microlithography Proceedings, March 1993

2. "Response surface modeling of rim phase shifted masks", R.Holscher, B.Smith, and S.Brainerd, 1993 SPIE Optical Microlithography Proceedings, March 1993